TECHNICAL MEMORANDUM

536

Evaluation of revised parameterizations of sub-grid orographic drag

Andrew Orr

Research Department

November 2007

Abstract

CY31R1 of the IFS became operational on 12 September 2006, and included a Turbulent Orographic Form Drag (TOFD) scheme to compute form drag from sub-grid scale orography (SSO), a 'cutoff' or 'effective' mountain height in the computation of gravity wave drag, and a joint implicit calculation of momentum coefficients from the TOFD and SSO scheme. This technical memorandum evaluates these revised parameterizations by comparing their impact over the Himalayas and Rockies with control CY29R1 T511 and T95 winter and spring forecasts.

The more physically realistic cutoff mountain height reduced the excessive deceleration of flow over the Himalayas and Rockies, and generally over areas of significant orography. Through thermal wind balance this is associated with a reduction in temperature bias over the Himalayas. The TOFD scheme, which directly parameterises the drag and redistributes it vertically, typically resulted in an increase in the near-surface wind and was shown to reduce the predominately negative 10 m wind bias over orography. The joint implicit calculation of momentum coefficients introduced some degree of dependency into the coupled TOFD and SSO processes, and in doing so reduced the time step sensitivity that existed when the schemes were evaluated independently of each other.

However, when compared to the previous cycle, CY31R1 climate runs showed an increase in the winter positive zonal wind bias over winter northern hemisphere mid-latitudes, and a corresponding increase in the cold bias over the pole. This suggested that the reduction in gravity wave drag had been excessive (which had been apparent in the T95 results over the Rockies), and to remedy this the cutoff mountain height was doubled. This retuning was implemented operationally in CY32R2 on 5 June 2007.

1   Introduction

Accurate characterization of surface drag in Numerical Weather Prediction (NWP) models is crucial to correctly simulate flow deceleration. Contributions to surface drag when the flow is stably stratified come from both surface friction and orography. Moreover, the effects of sub-grid scale orography (SSO) are particularly important (e.g. Palmer et al., 1986). For SSO with horizontal scales less than 5000 m, small surface obstacles generate additional turbulence, or turbulent orographic form drag (TOFD). In the ECMWF Integrated Forecasting System (IFS) this was previously parameterised by an effective roughness length (EFRL), whereby the vegetative surface roughness length was enhanced to represent the additional contribution from the unresolved orography. For SSO with horizontal scales greater than 5000 m, low-level flow blocking (i.e. blocked flow drag) and the absorption and/or reflection of vertically propagating gravity waves (i.e. gravity wave drag) create additional drag. In the IFS this is parameterised by the Lott and Miller (1997) SSO scheme.

1.1   The turbulent orographic form drag scheme

Although the EFRL technique has been responsible for significant improvements in a number of NWP models, having the TOFD coupled to the vegetative roughness does create some difficulties. This is especially evident in mountainous terrain where the effective roughness length can reach values of the order of 100 m. Therefore, Beljaars et al. (2004a) developed a scheme based on earlier work by Wood et al. (2001) which directly parameterises the TOFD and distributes it vertically, allowing the vegetative roughness to be treated independently.

Single-column simulations showed that this new TOFD scheme works fairly well in the IFS (in conjunction

with a revised vegetation roughness table) (Beljaars et al., 2004a). Keil and Beljaars (2003) ran 48 hour T511 forecast experiments for two Mesoscale Alpine Programme (MAP) case studies over the Alps which showed that replacing the EFRL scheme with the TOFD scheme reduced the surface stress by up to 25% during the first 18 hours of the forecast. (Note that both TOFD and boundary layer friction contribute to the surface stress.) However, during this period considerable interaction between the TOFD and SSO scheme (Rontu, 2006) meant that the 10 m wind speed only slightly increased and the wind speed at 850 hPa was unaffected. Longer into the forecast the TOFD surface stress often exceeded that of the EFRL scheme. Additionally, the impact on model climatology was shown to be slightly beneficial.

1.2   The gravity wave drag scheme

In the Lott and Miller (1997) parameterization, the gravity wave drag, τ_{wave}, is given by the equation,

$$\tau_{wave} = \rho_H U_H N_H \frac{\sigma}{\mu} \frac{H^2}{4} GD, \tag{1}$$

where ρ_H, U_H and N_H are the density, velocity, and Brunt-Vaisala frequency averaged between μ and 2μ (where μ is the standard deviation of the SSO height). H and σ are the SSO height and slope respectively. G is a tuning coefficient, and directional terms are grouped together in D. If we take $H = 2\mu$ then essentially the full height of the SSO is used to calculate the drag. However, Brown (2004a) suggested that as a considerable proportion of the airflow impinging on the orography is likely to be blocked (i.e. blocked flow drag), it is more physically realistic to use an 'effective' or 'cutoff' mountain height in this calculation, that is the upper layer above the dividing streamline height where streamlines pass over the mountain. Here, equation (1) becomes

$$\tau_{wave} = \rho_H U_H N_H \frac{\sigma}{\mu} \frac{H_{eff}^2}{9} GD, \tag{2}$$

where $H_{eff} = 3\mu - Z_{blk}$. Note that the maximum possible value of H_{eff} is 3μ as this is the maximum height that the blocked layer depth can reach. Consequently, $H_{eff}^2/9$ is used rather than $H_{eff}^2/4$ so that equations (1) and (2) are both identical if $Z_{blk} = 0$. Brown (2004a) showed that this change resulted in a substantial reduction in the velocity deficit observed immediately downstream of the Himalayas in winter T95 24 hour forecasts. In a similar experiment at T511 he showed the forecast error was again reduced, though less so than at T95. These results are consistent with the findings of Brown (2004b), which showed that the IFS generated excessive parameterised orographic torques at low resolution during winter between 20°N and 50°N.

1.3   Joint implicit calculation of momentum tendency coefficients

Momentum tendencies from form drag, gravity wave drag, and low-level blocking can be significant over orography. And can result in quite large increments when the model time step is long (for example at climate resolution the time step is T=3600 s). Moreover, to some extent the processes are coupled, leading to a time step sensitivity in the IFS as each of the relative parameterization schemes evaluates its tendencies independently (Beljaars et al., 2004b). However, some degree of dependency can be introduced by solving the relevant momentum tendency coefficients in a joint implicit calculation.

The total (TOT) horizontal velocity tendency due to the dynamics (DYN), vertical diffusion (VDF), turbulent

orographic form drag (TOFD), and gravity wave drag (GWD) and blocked flow drag (BLK) is given by

$$\left(\frac{\partial u}{\partial t}\right)_{\text{TOT}} = \left(\frac{\partial u}{\partial t}\right)_{\text{GWD}} + \left(\frac{\partial u}{\partial t}\right)_{\text{BLK}} + \left(\frac{\partial u}{\partial t}\right)_{\text{DYN+VDF+TOFD}} = \alpha_{\text{u}} - \beta u^{n+1} + \left(\frac{\partial u}{\partial t}\right)_{\text{DYN+VDF+TOFD}}, \quad (3)$$

where α_{u} and β are the explicit gravity wave drag tendency coefficient and implicit blocked flow drag tendency coefficient respectively. A similar equation is apparent for the meridional velocity component. The tendency coefficients are then jointly implicitly computed in the vertical diffusion code with momentum tendency coefficients from the TOFD scheme. See Chapter 4 of the IFS documentation CY31R1 for further details and expressions for α_{u} and β (IFS CY31R1, 2007).

This technical memorandum evaluates these revised parameterizations (the TOFD scheme (TOFD), use of a cutoff mountain height (CO), and joint implicit calculation of momentum tendency coefficients (IMPVDF)), and in particular their impact over the Himalayas and the Rockies. A number of 10 day CY29R1 T511 L60 and T95 L60 experimental forecasts running from 12Z on each day of January 2005 (i.e. winter) and each day between 10 March to 10 April 2004 (i.e. spring) are employed. Further T95 L60 experiment forecasts ran from 12Z on 1, 6, 12, 18, 24, 30 of January 2001, 2002, 2003, 2004. These are detailed in Table 1.

Exper. ID	Description	Resolution	Dates	Data assim.
e019	control	T511 L60	20050101-20050131	y
epqi	TOFD	T511 L60	20050101-20050131	n
en09	CO	T511 L60	20050101-20050131	n
eppr	TOFD + CO	T511 L60	20050101-20050131	n
epi7	TOFD + CO + rev. coeff.	T511 L60	20050101-20050131	n
epql	control	T95 L60	20050101-20050131	n
eprb	TOFD + CO	T95 L60	20050101-20050131	n
en0a	control	T511 L60	20040310-20040410	n
eq7e	TOFD + CO	T511 L60	20040310-20040410	n
eq3d	TOFD + CO + T=300s	T95 L60	24 days Jan 2001-2004	n
eq3c	TOFD + CO + T=3600s	T95 L60	24 days Jan 2001-2004	n
eq3b	TOFD + CO + IMPVDF + T=300s	T95 L60	24 days Jan 2001-2004	n
eq39	TOFD + CO + IMPVDF + T=3600s	T95 L60	24 days Jan 2001-2004	n

Table 1: Summary of 10 day CY29R1 experimental forecasts. 'TOFD' is the Turbulent Orographic Form Drag scheme. 'CO' is the cutoff mountain technique. 'IMPVDF' is the joint implicit calculation.

Sections 2 and 3 details the impact of the TOFD scheme and cutoff mountain on the T511 winter and spring forecasts respectively. Section 4 details the impact on the T95 winter forecasts. Section 5 details the impact of the joint implicit calculation of momentum tendency coefficients.

1.4   Further re-tuning

The cutoff mountain (Eq. (2)) in combination with the TOFD scheme and the joint implicit calculation was implemented operationally in CY31R1 on 12 September 2006 (IFS CY31R1, 2007). Resulting T159 climate runs when compared to the previous cycle (CY30R1) showed a large increase in the winter positive zonal wind bias at upper levels between 40°N and 80°N, and a corresponding large cold bias developing over the winter pole (Holton, 1992). As there is considerable orography between 40°N and 80°N and the increase occured

during winter, this suggested that the reduction in gravity wave drag due to the implementation of the cutoff mountain was excessive at low resolution. To remedy this the effective mountain height H_{eff} in Eq. (2) was doubled, i.e.

$$\tau = \rho_H U_H N_H \frac{\sigma}{\mu} \frac{(2H_{eff})^2}{9} GD, \tag{4}$$

To evaluate this change a number of 10 day CY31R1 T511 L91 and T159 L91 experiments were run from 12Z on each day of 10 to 15 November 2006 (i.e. winter). These are detailed in Table 2, and the results compared to operational analysis are documented in section 6. This modification was implemented operationally in CY32R2 on 5 June 2007. The technical memorandum finishes with a conclusion in section 7.

Exper. ID	Description	Resolution	Date	Data assim.
euen	TOFD + CO	T511 L91	20061110-20061115	n
euev	TOFD + CO($2H_{eff}$)	T511 L91	20061110-20061115	n
eues	TOFD + CO	T159 L91	20061110-20061115	n
eueu	TOFD + CO($2H_{eff}$)	T159 L91	20061110-20061115	n
es2s	TOFD + CO	T799 L91	20060214-20060430	n

Table 2: Summary of 10 day CY31R1 experimental forecasts.

2 Evaluation of T511 wintertime forecasts

2.1 Control results

Experiment e019 was run at T511 for each day of January 2005 at 12Z to produce control CY29R1 winter forecasts.

Fig. 1 shows the e019 average vertically integrated zonal wind error (i.e. the difference from the analysis) (Pa s) for 24 hour (top) and 96 hour (bottom) forecasts. After 24 hours there is a velocity deficit of between -5000 and -15000 Pa s downstream of the Himalayas (approximately equal to a deceleration of around 1-2 m s^{-1} throughout the depth of the atmosphere). After 96 hours this deficit has strengthened and propagated east, with additional slowing apparent over the Tibetan Plateau. Further areas where the vertically integrated wind is significantly reduced relative to the analysis occur downstream of the Rockies, Andes, Taiwan, and Antarctic Peninsula.

2.1.1 Himalayas

Fig. 2 presents closer examination of the e019 control results for the Himalayan region of south-east Asia. Apparent to the south and north are areas of velocity surplus, perhaps in response to the velocity deficit.

Fig. 3 shows e019 T511 mean vertical error profiles of zonal velocity (left), meridional velocity (middle), and temperature (right), averaged over the Himalayas after 96 hours (also shown are equivalent T95 profiles, which are discussed in section 4). For levels below 400 hPa the error in zonal velocity is negligible. Above this height the error steadily increases, reaching a maximum of about -2 m s^{-1} at around 100 hPa. With the exception of levels above 100 hPa where it reaches around 1 m s^{-1}, the meridional velocity error is small throughout the depth of the atmosphere. For levels above 300 hPa the temperature error varies between 1 and -1 K. While at the surface it is around 0.5 K.

Fig. 4 shows the e019 mean zonal wind speed error, zonally averaged over the Himalayas for 24 hours (top) and 96 hours (bottom). The deficit at upper levels, which reaches up to -4 m s^{-1} after 96 hours, is confirmed. After 24 hours a relatively weak area of velocity surplus is shown directly above the Tibetan plateau. The velocity surplus to the south of the Himalayas (see Fig. 2) is confirmed, and occurs at around 200 hPa. This reaches a maximum of around 5 m s^{-1} after 96 hours. Fig. 5 presents the equivalent mean temperature error. An area of warming is situated to the north of the main velocity deficit region, and is probably a response to overly strong vertical wind shear as a further result of excessive drag, as governed by the thermal wind balance (Holton, 1992).

2.1.2 Rockies

Fig. 6 shows the equivalent of Fig. 2, but for the area of North America surrounding the Rockies. To the south and north are regions of velocity surplus relative to the analysis, again, perhaps in response to the velocity deficit region.

Fig. 7 shows the equivalent of Fig. 3, but averaged over the Rockies. At T511 the zonal velocity error is small throughout the depth of the atmosphere. At near-surface and at 300 hPa the meridional velocity error is respectively around -0.5 m s^{-1} and -1.5 m s^{-1}. The temperature error below 300 hPa is around -0.75 K, and above this height it is approximately zero.

Fig. 8 shows the equivalent of Fig. 4, but averaged over the Rockies. Around 200 hPa there is a velocity deficit

of 1-2 m s^{-1} after 24 hours. This increases after 96 hours, at which time areas of velocity surplus appear. Fig. 9 presents the equivalent mean temperature error, and confirms Fig. 7. After 96 hours a temperature deficit of between 1 and 2 K exists throughout much of the atmosphere.
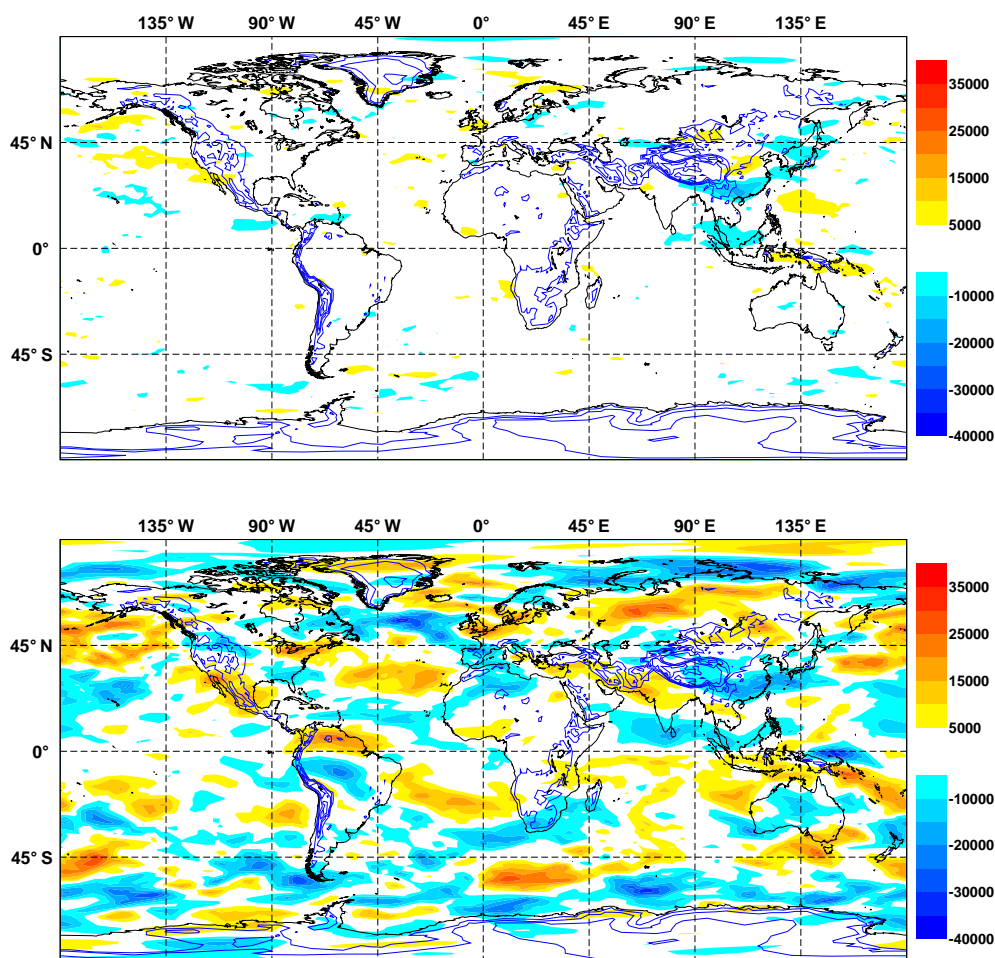
Figure 1: Experiment e019 average vertically integrated zonal wind error (Pa s) for 24 hour (top) and 96 hour (bottom) control T511 CY29R1 forecasts from 12Z on each day of January 2005. Also shown are contours of mean (T511) orography height from 1000 to 6000 m with a 1000 m interval.
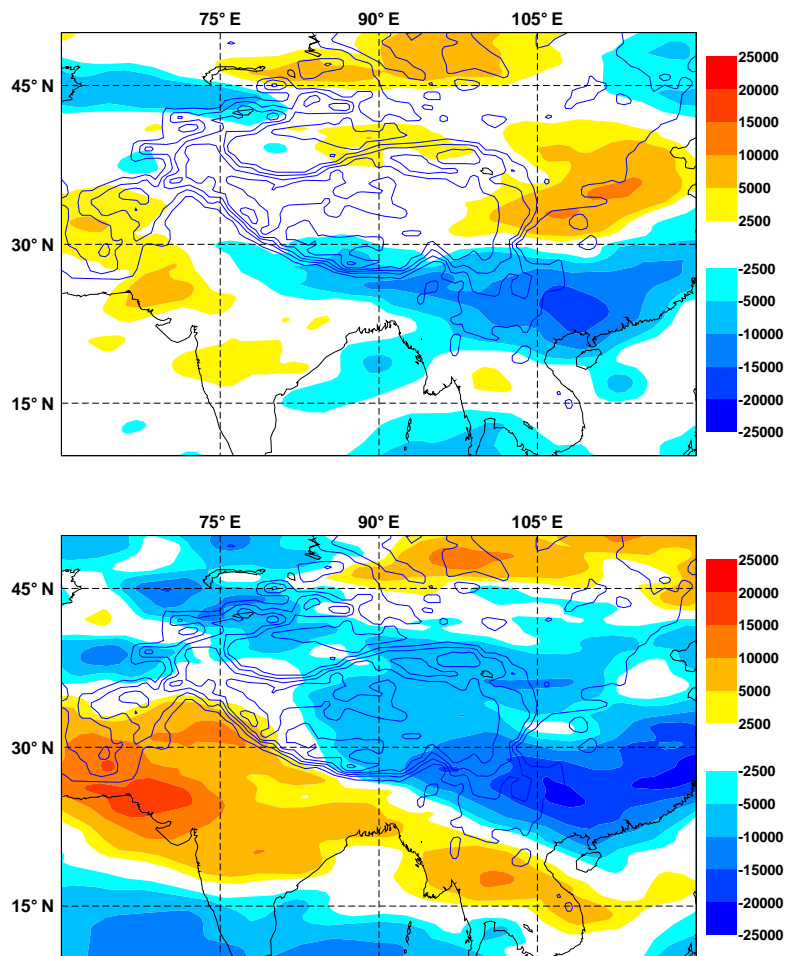
Figure 2: Experiment e019 average vertically integrated zonal wind error (Pa s) over the Himalayan region of south-east Asia for 24 hour (top) and 96 hour (bottom) control T511 CY29R1 forecasts from 12Z on each day of January 2005. Also shown are contours of mean (T511) orography height from 1000 to 6000 m with a 1000 m interval.
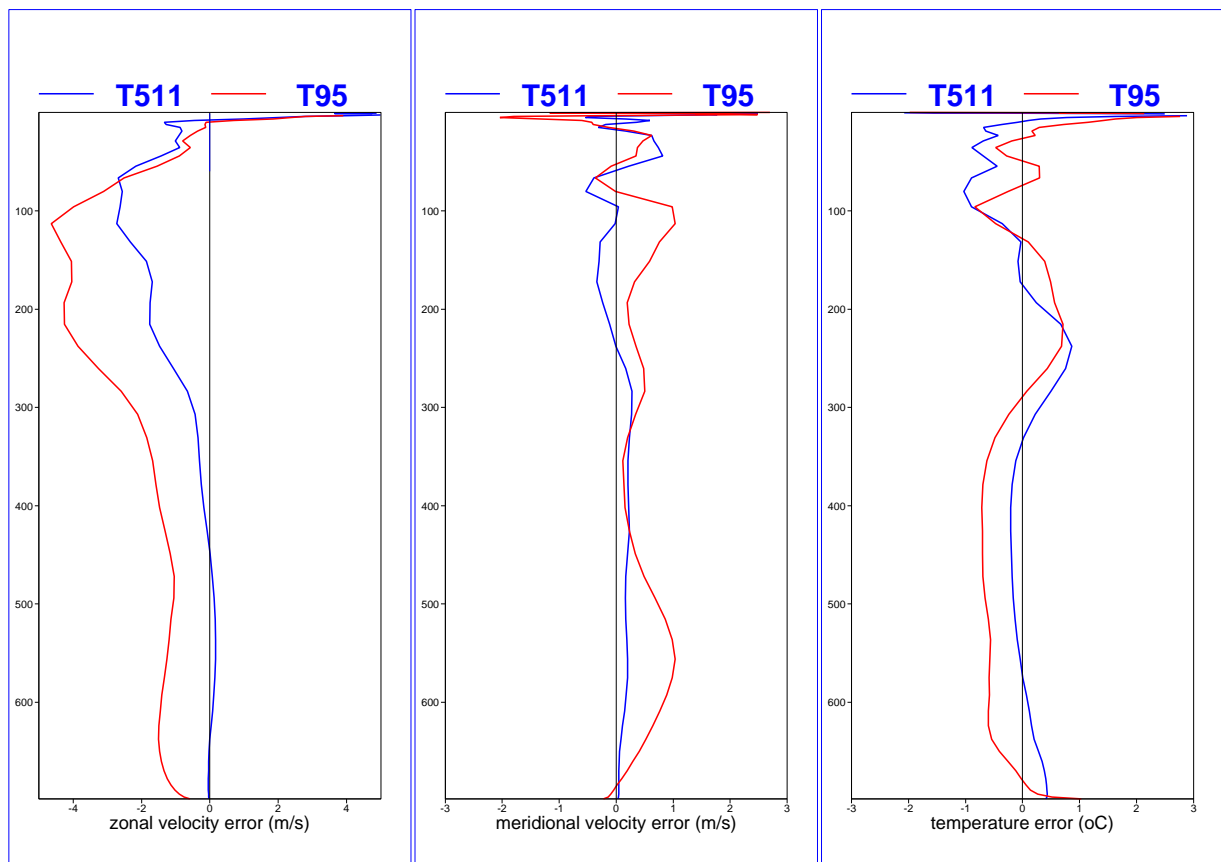
Figure 3: T511 (e019) and T95 (epql) mean vertical error profiles averaged over the Himalayas (26°N to 40°N and 75°E to 105°E) for 96 hour control CY29R1 forecasts from 12Z on each day of January 2005. Left panel: zonal velocity (m s⁻¹); middle panel: meridional velocity (m s⁻¹); right panel: temperature (K). Blue lines: T511 control error; red lines: T95 control error.
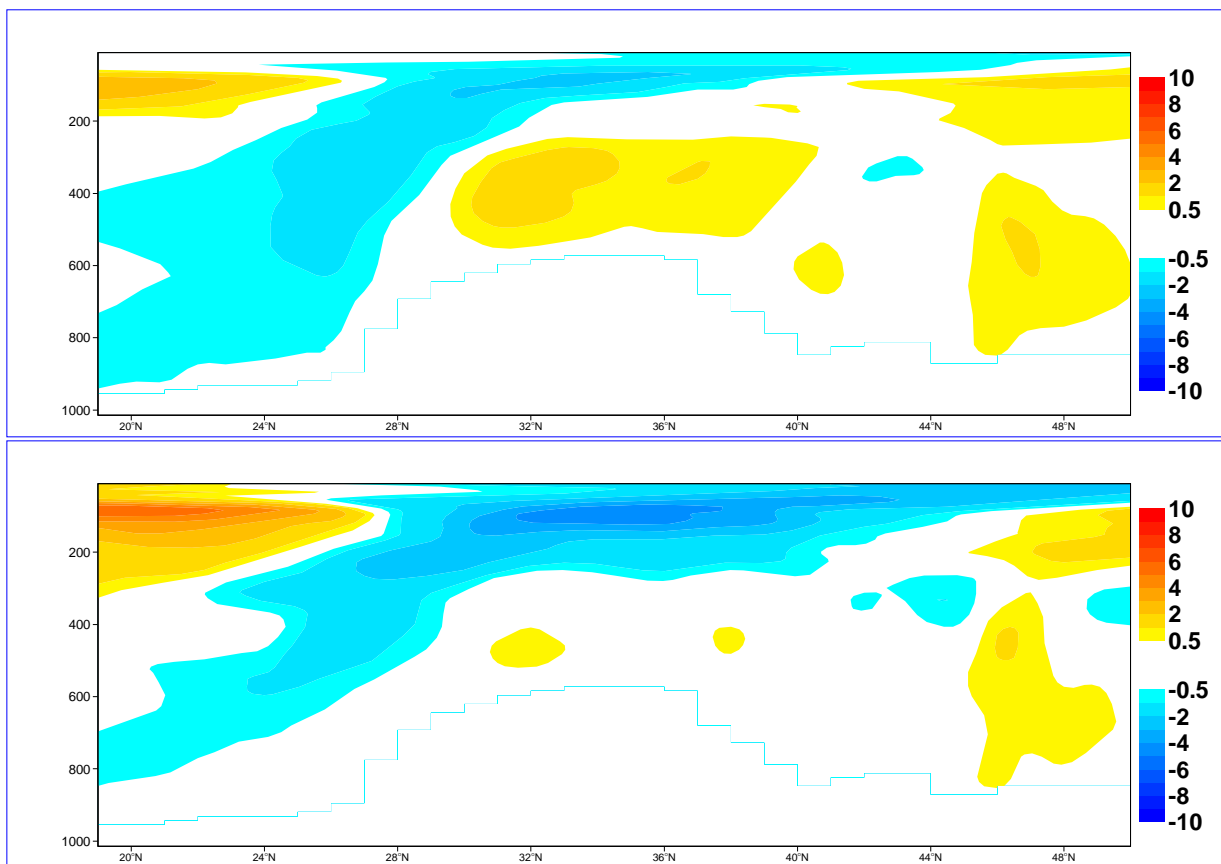
Figure 4: Experiment e019 mean zonal wind speed error (m s^{-1}) zonally averaged over the Himalayas between 75°E and 105°E for 24 hour (top) and 96 hour (bottom) control T511 CY29R1 forecasts from 12Z on each day of January 2005.
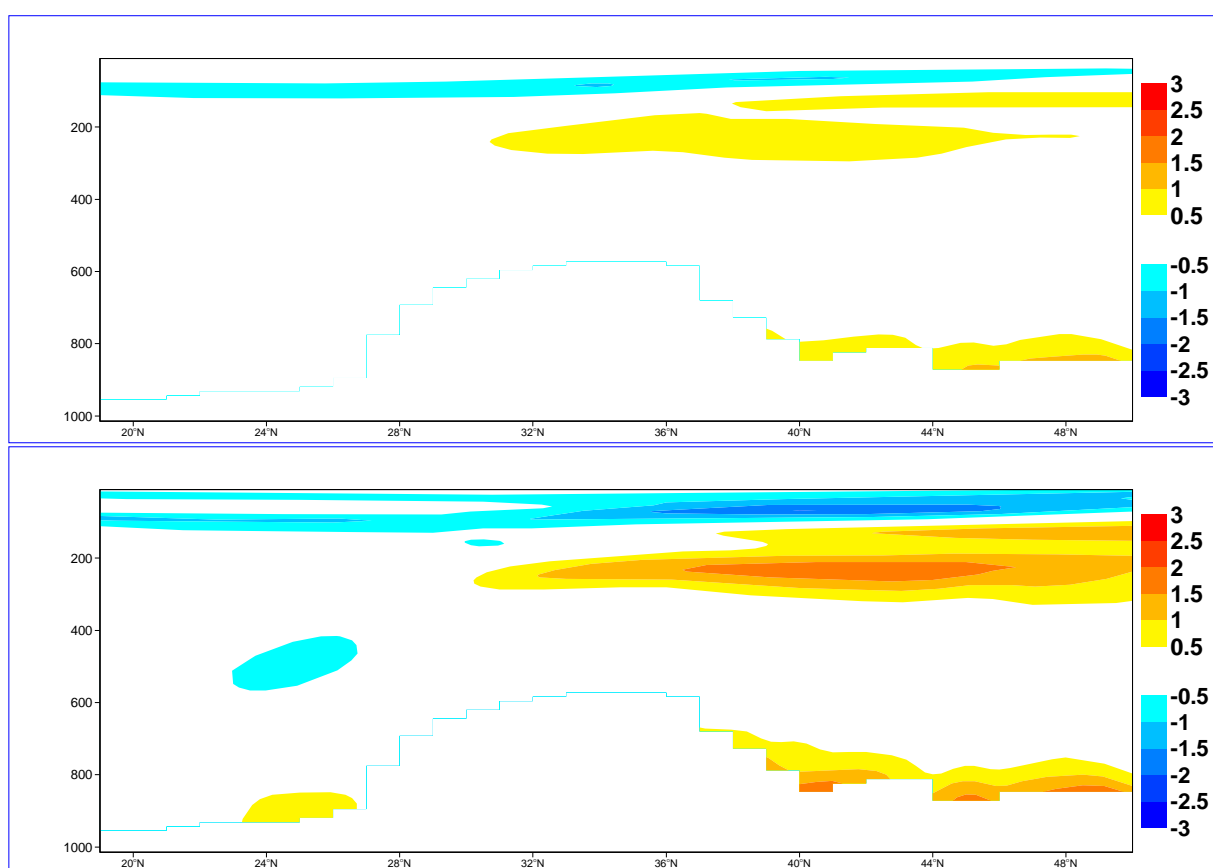
Figure 5: Experiment e019 mean temperature error (K) zonally averaged over the Himalayas between $75^{o}E$ and $105^{o}E$ for 24 hour (top) and 96 hour (bottom) control T511 CY29R1 forecasts from 12Z on each day of January 2005.
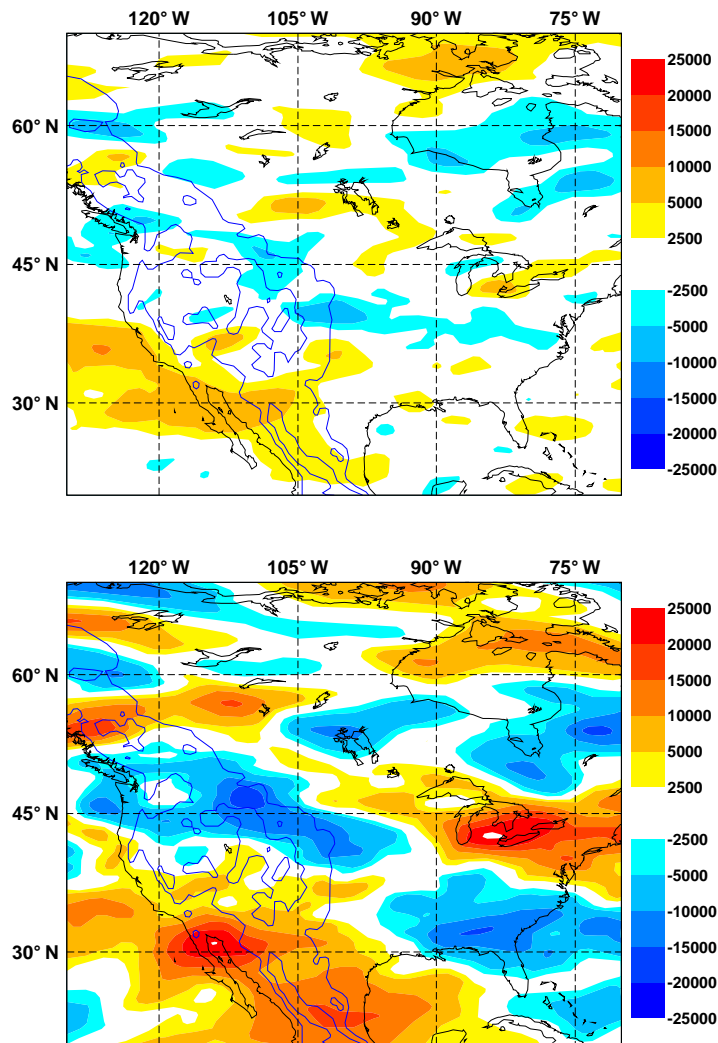
Figure 6: Experiment e019 average vertically integrated zonal wind error (Pa s) over North America for 24 hour (top) and 96 hour (bottom) control T511 CY29R1 forecasts from 12Z on each day of January 2005. Also shown are contours of mean (T511) orography height from 1000 to 6000 m with a 1000 m interval.
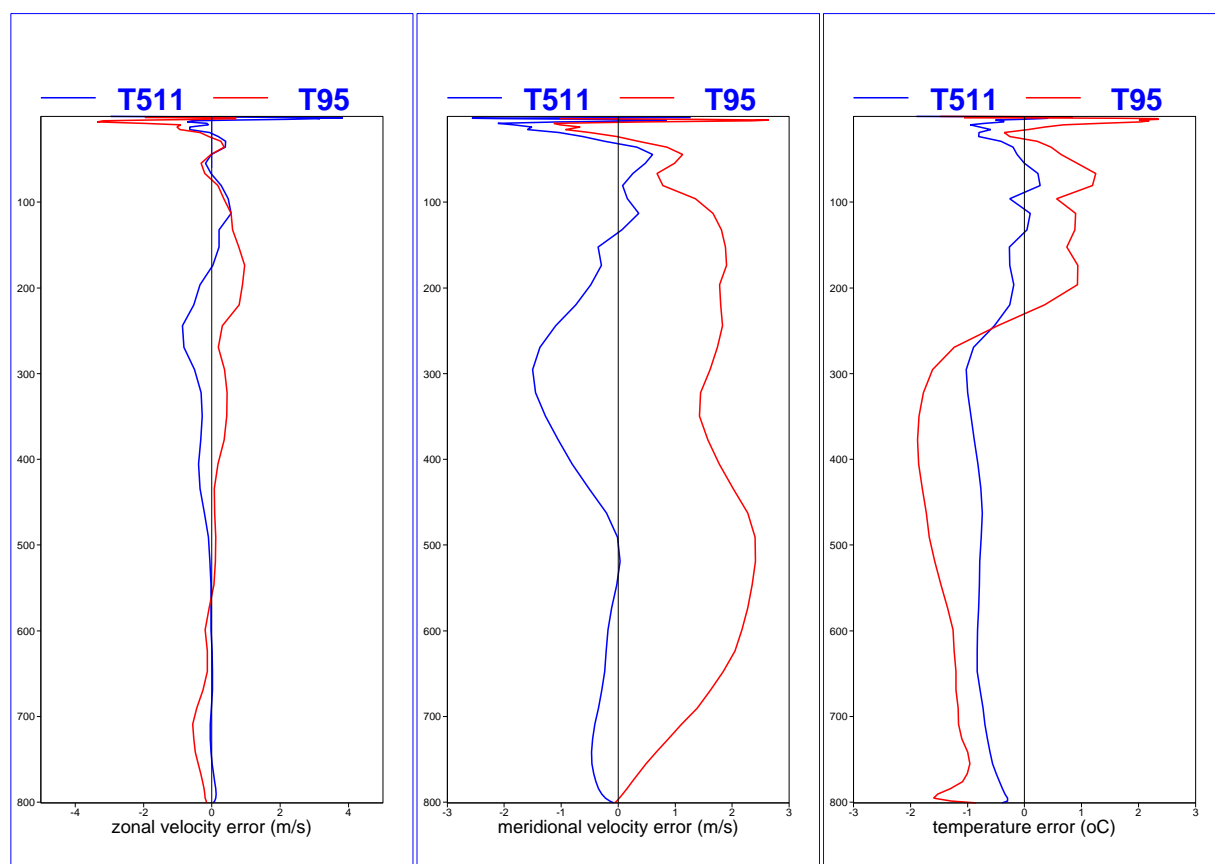
Figure 7: T511 (e019) and T95 (epql) mean vertical profiles averaged over the Rockies (34°N to 45°N and 112°W to 104°W) for 96 hour control CY29R1 forecasts from 12Z on each day of January 2005. Left panel: zonal velocity (m s⁻¹); middle panel: meridional velocity (m s⁻¹); right panel: temperature (K). Blue lines: T511 control error; red lines: T95 control error.
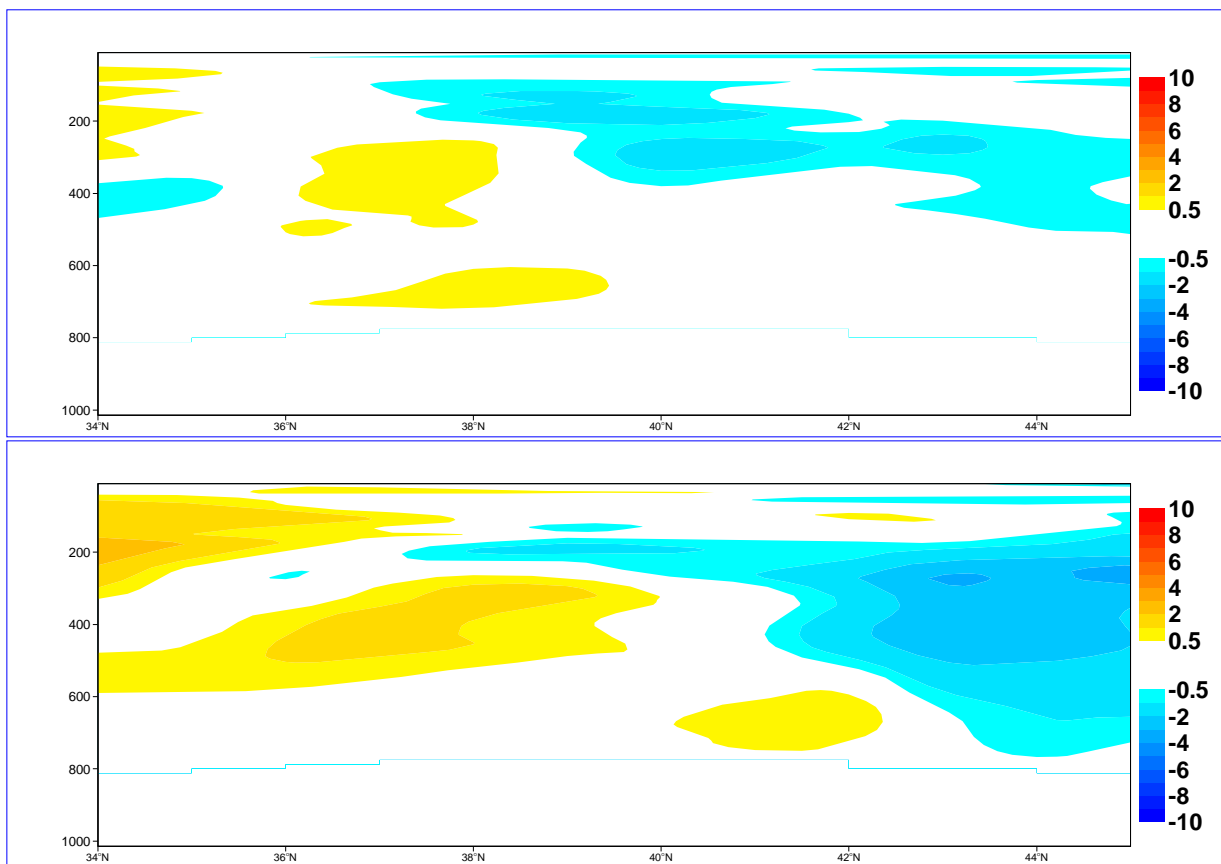
Figure 8: Experiment e019 mean zonal wind speed error (m s⁻¹) zonally averaged over the Rockies between 112^oW *and* 104^oW *for 24 hour (top) and 96 hour (bottom) control T511 CY29R1 forecasts from 12Z on each day of January 2005.*
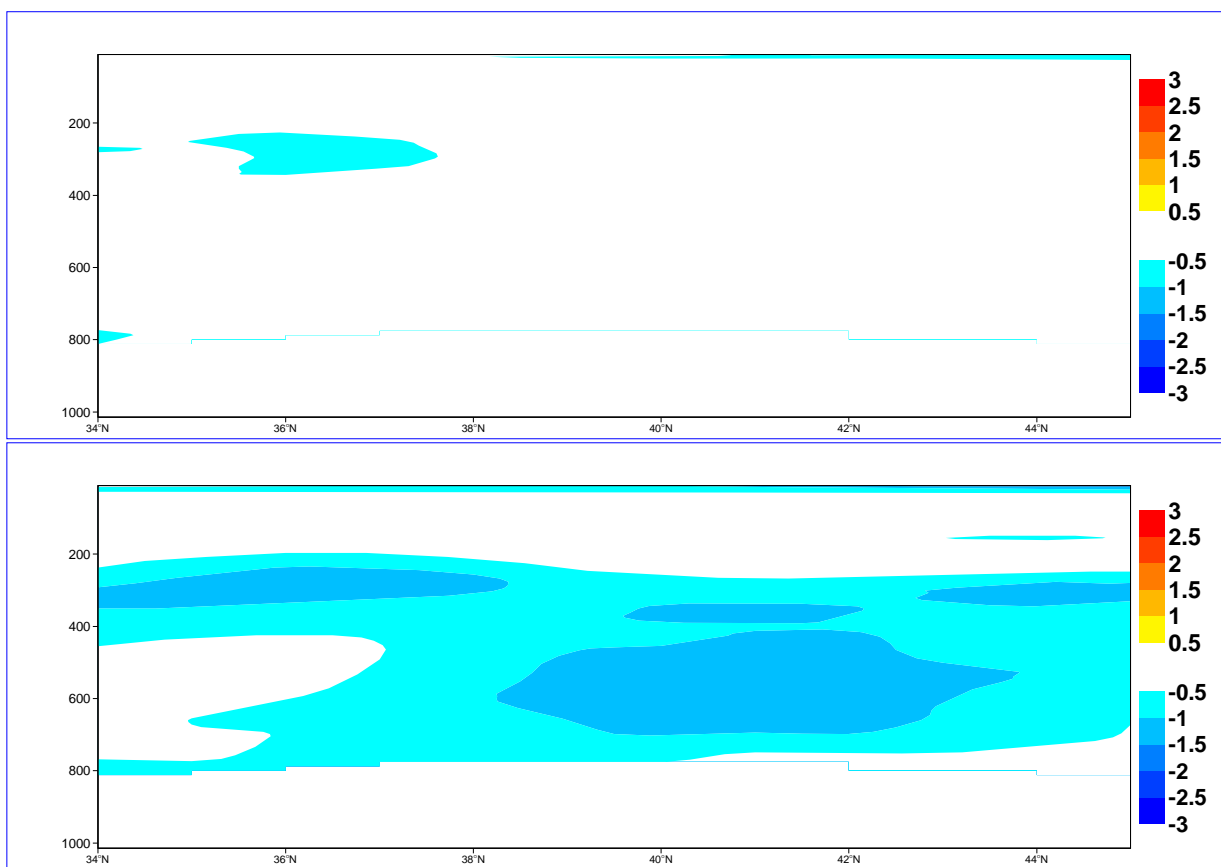
Figure 9: Experiment e019 mean temperature error (K) zonally averaged over the Rockies between 112^oW and 104^oW for 24 hour (top) and 96 hour (bottom) control CY29R1 forecasts from 12Z on each day of January 2005.

2.2   Evaluation of the turbulent orographic form drag scheme

Experiment epqi was run at T511 for each day of January 2005 at 12Z to produce CY29R1 winter forecasts with the TOFD scheme (see section 1.1).

2.2.1   Himalayas

Fig. 10 shows epqi average vertically integrated zonal wind difference fields for 96 hour forecasts. The top panel is the same as the bottom panel of Fig. 2, and shows the control error. The middle panel shows that the impact of the experiment relative to the control forecast is to slow flow upstream of the Himalayas. Over the Tibetan plateau there is a small region where the flow has speeded-up. The relatively small impact of the experiment is confirmed by the bottom panel. This shows the experiment error is similar to the control error. The velocity deficit region south-east of the Himalayas is unaffected.

Fig. 11 shows mean epqi vertical profiles of zonal velocity (left), meridional velocity (middle), and temperature (right) difference fields averaged over the Himalayas after 96 hours. The control errors (blue lines) are the same as those shown in Fig. 3. Here, the impact of the experiment relative to the control forecast (red line) is to reduce the zonal velocity by around 0.5 m s^{-1} between the surface and 300 hPa, resulting in a increase in the error relative to the analysis (green line). At around 100 hPa the experiment speeds-up the flow by around 0.5 m s^{-1} relative to the control, slightly reducing the large wind error here. This is probably in response to a reduction in gravity wave drag as a consequence of the reduced near-surface wind. Additionally, the experiment results in a slightly more southerly flow through the middle part of the atmosphere. With the exception of increasing the temperature error at the near surface level, the experimental impact on this parameter over the Himalayas is negligible.

Fig. 12 shows the mean zonal wind speed difference field, zonally averaged over the Himalayas for 96 hour forecasts. The top panel is the same as the bottom panel of Fig. 4, and shows the control error. The middle panel confirms that the impact of the TOFD scheme is to reduce/increase the near-surface/upper-level velocity. Fig. 13 presents a similar figure showing the mean temperature difference field. The small apparent cooling is consistent with a small reduction in gravity wave drag and a consequent slight weakening of the vertical wind shear.

Fig. 14 shows associated plots of mean surface stress, SSO stress (this is the combined stress due to gravity wave drag and low-level blocking, though has been labelled 'gravity wave stress' in the figure), and 850 hPa wind speed averaged over the Himalayas (also shown are equivalent results for the Rockies). Here, the impact of the experiment (labelled TOFD (Himalayas)) increases the surface stress from around 0.11 N m^{-2} to 0.18 N m^{-2}, as evident in the reduction of the 850 hPa wind speed (and the slowing of the near-surface zonal flow in Figs. 11 and 12). There is some compensation from the SSO stress which decreases from around 0.3 to 0.25 N m^{-2} (as evident in the speed up of the zonal flow at upper-level).

2.2.2   Rockies

Fig. 15 presents the equivalent of Fig. 10, but for the Rockies. The impact of the TOFD scheme is predominately neutral, showing only a small reduction in velocity downstream of the Rockies at around 50°N.

Fig. 16 shows the equivalent of Fig. 11, but for the Rockies. With the exception of a small increase in zonal wind speed and temperature at near-surface level, the impact of the experiment here is negligible. Note that the area over which these mean profiles are calculated is south of 50°N.

The minimal impact of the experiment is confirmed by Fig. 17.

Examining Fig. 14 shows that, unlike over the Himalayas where the surface stress increased considerably with the TOFD scheme, over the Rockies it decreased from around 0.15 to 0.12 N m^{-2}. This has little impact on the 850 hPa wind speed (as evident in the small acceleration of the near-surface zonal flow shown in Fig. 16). In response the SSO stress compensated by increasing slightly. Note that with the control experiment the surface stress over the Rockies exceeds that over the Himalayas. However, on implementing the TOFD scheme this reverses and the surface stress over the Himalayas exceeds that over the Rockies. SSO stress over the Himalayas exceeds that over the Rockies regardless of control or experiment.

eo19-eo19 an: T511 Jan2005 average T+96h vertically integrated zonal wind error (Pa s) (level 1 to 60)

epqi-eo19: T511 Jan2005 average T+96h vertically integrated zonal wind error (Pa s) (level 1 to 60)

epqi-eo19 an: T511 Jan2005 average T+96h vertically integrated zonal wind error (Pa s) (level 1 to 60)
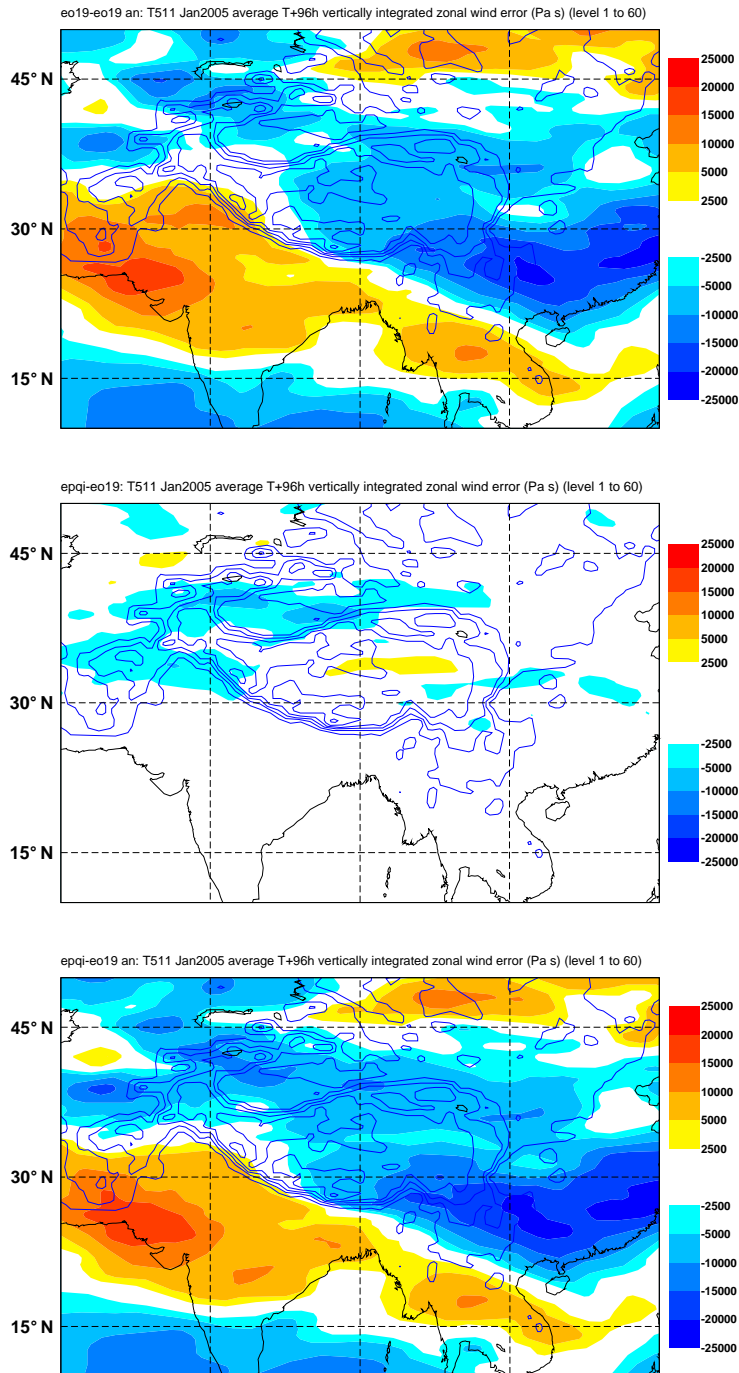
Figure 10: Experiment epqi average vertically integrated zonal wind difference fields (Pa s) over the Himalayan region of south-east Asia for 96 hour T511 CY29R1 forecasts from 12Z on each day of January 2005 with the TOFD scheme. Top panel: control error; middle panel: impact of experiment; bottom panel: experiment error. Also shown are contours of mean (T511) orography height from 1000 to 6000 m with a 1000 m interval.
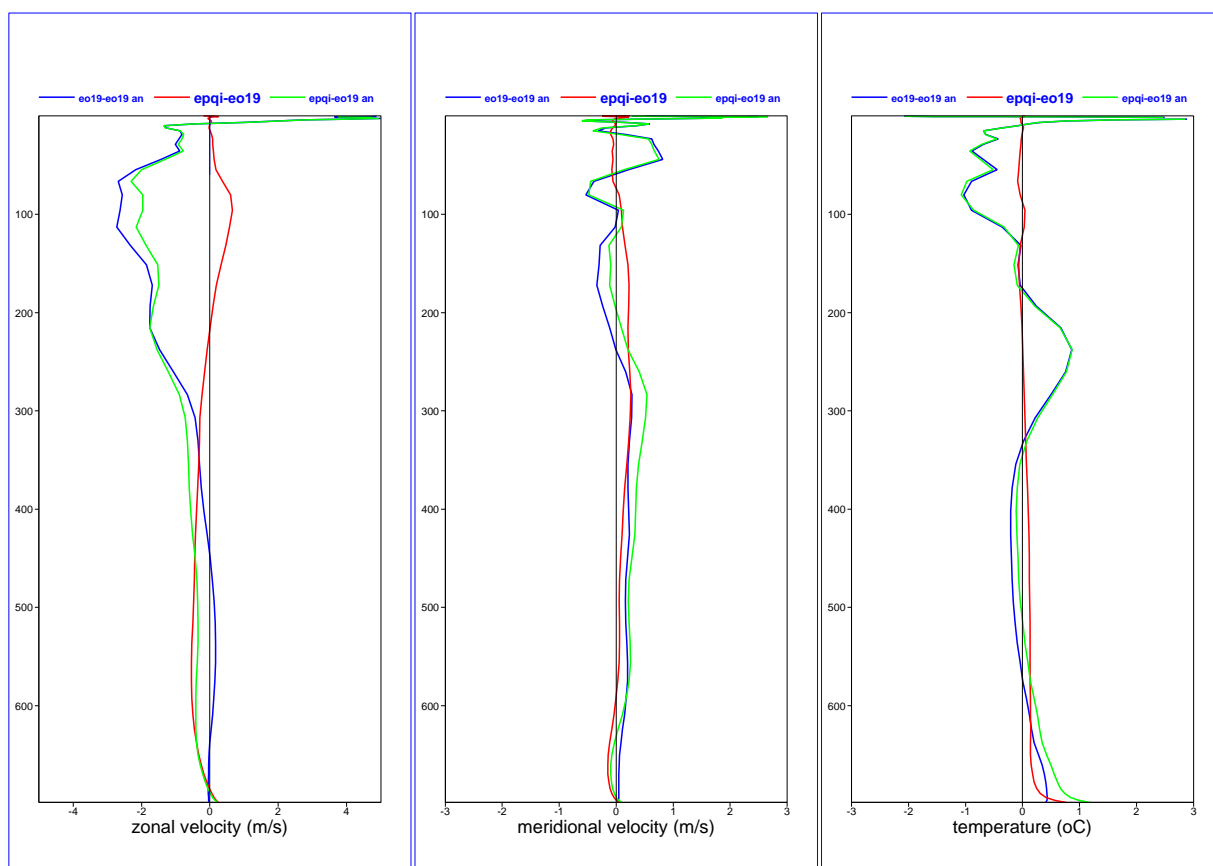
Figure 11: Experiment epqi vertical profiles of difference fields averaged over the Himalayas (26ºN to 40ºN and 75ºE to 105ºE) for 96 hour T511 CY29R1 forecasts from 12Z on each day of January 2005 with the TOFD scheme. Left panel: zonal velocity (m s^{-1}); middle panel: meridional velocity (m s^{-1}); right panel: temperature (K). Blue lines: control error; red lines: impact of experiment; green lines: experiment error.
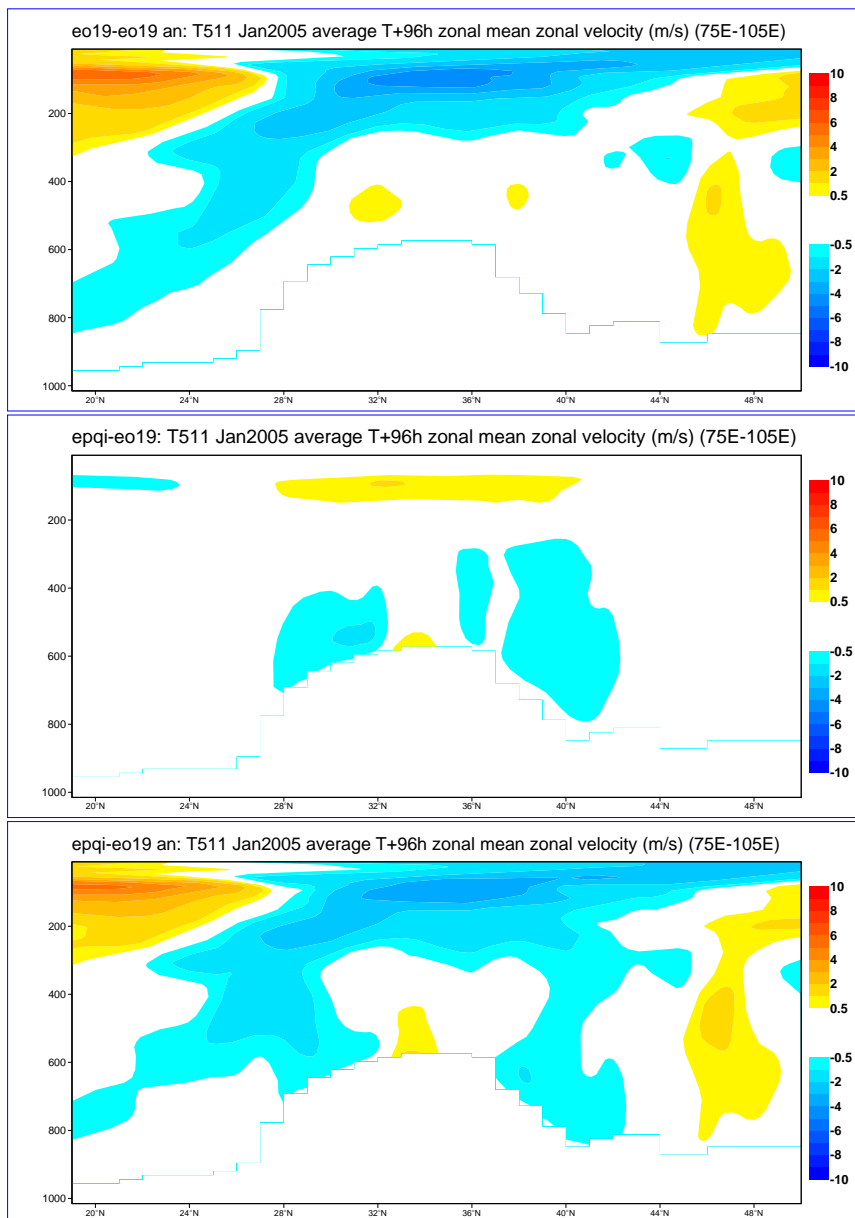
Figure 12: Experiment epqi mean zonal wind speed difference field (m s^{-1}) zonally averaged over the Himalayas between 75ºE and 105ºE for 96 hour T511 CY29R1 forecasts from 12Z on each day of January 2005 with the TOFD scheme. Top panel: control error; middle panel: impact of experiment; bottom panel: experiment error.
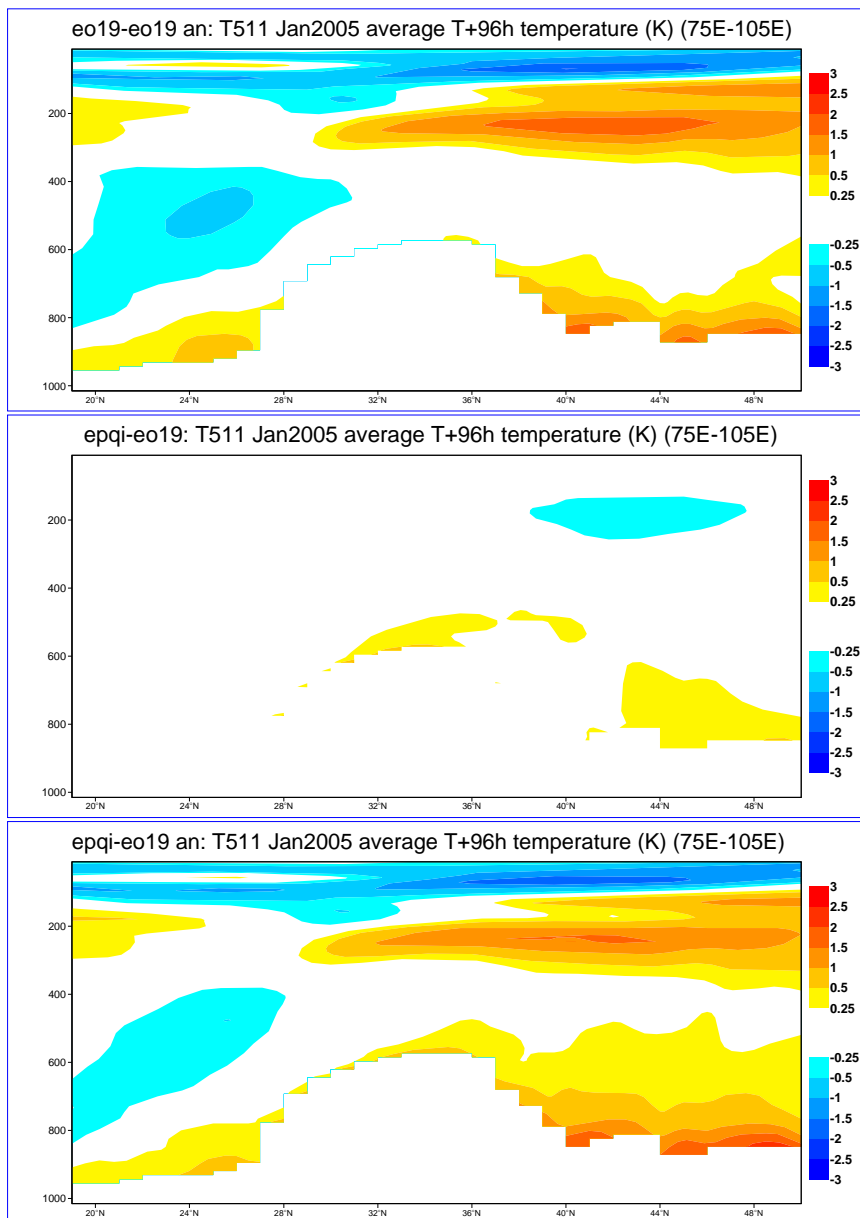
Figure 13: Experiment epqi mean temperature difference field (K) zonally averaged over the Himalayas between 75°E and 105°E for 96 hour T511 CY29R1 forecasts from 12Z on each day of January 2005 with the TOFD scheme. Top panel: control error; middle panel: impact of experiment; bottom panel: experiment error.
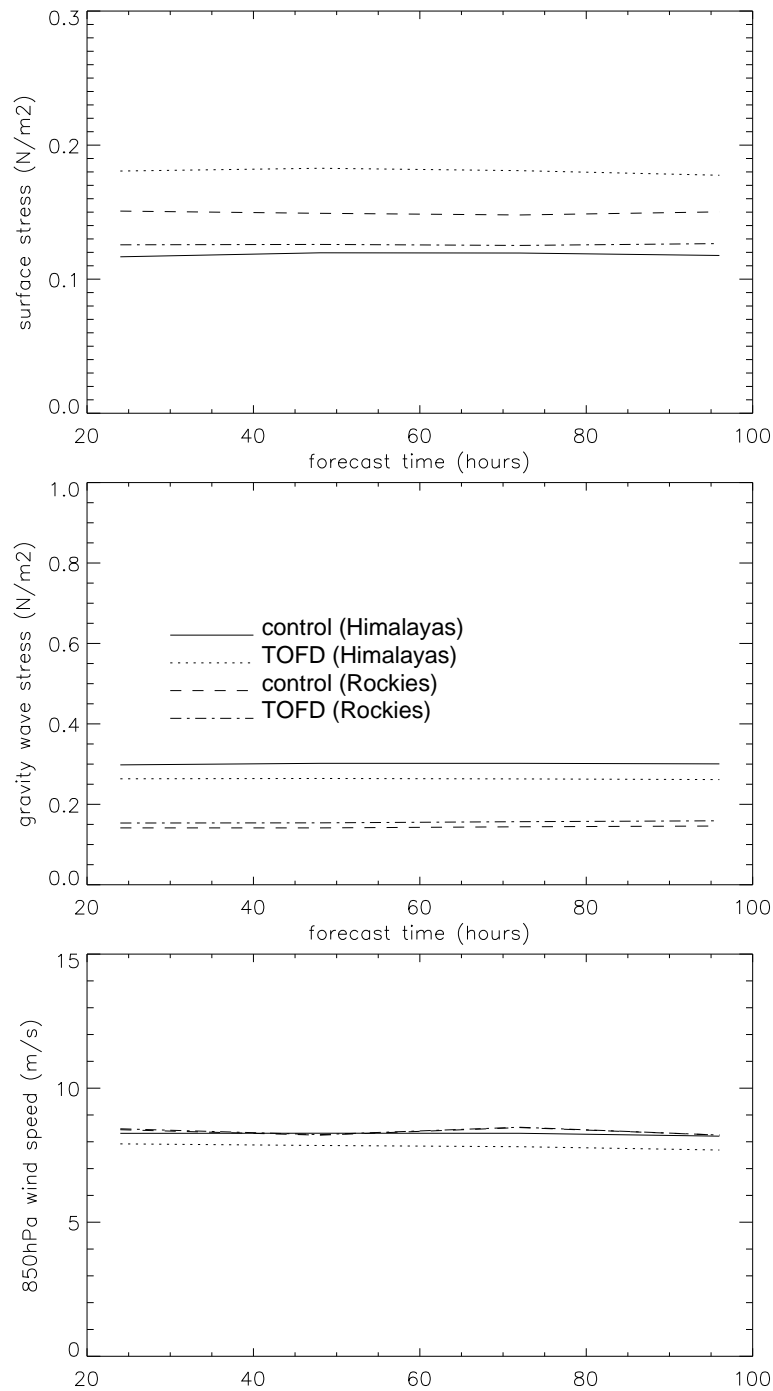
Figure 14: Sensitivity to forecast time of experiment epqf (and control eo19) surface stress (N m^{-2}; top panel), SSO stress (N m^{-2}; middle panel, labelled 'gravity wave stress') , and 850 hPa wind speed (m s^{-1}; bottom panel) averaged over the Himalayas (26°N to 40°N and 75°E to 105°E) and the Rockies (34°N to 45°N and 112°W to 104°W) from CY29R1 forecasts from 12Z on each day of January 2005 with the TOFD scheme.
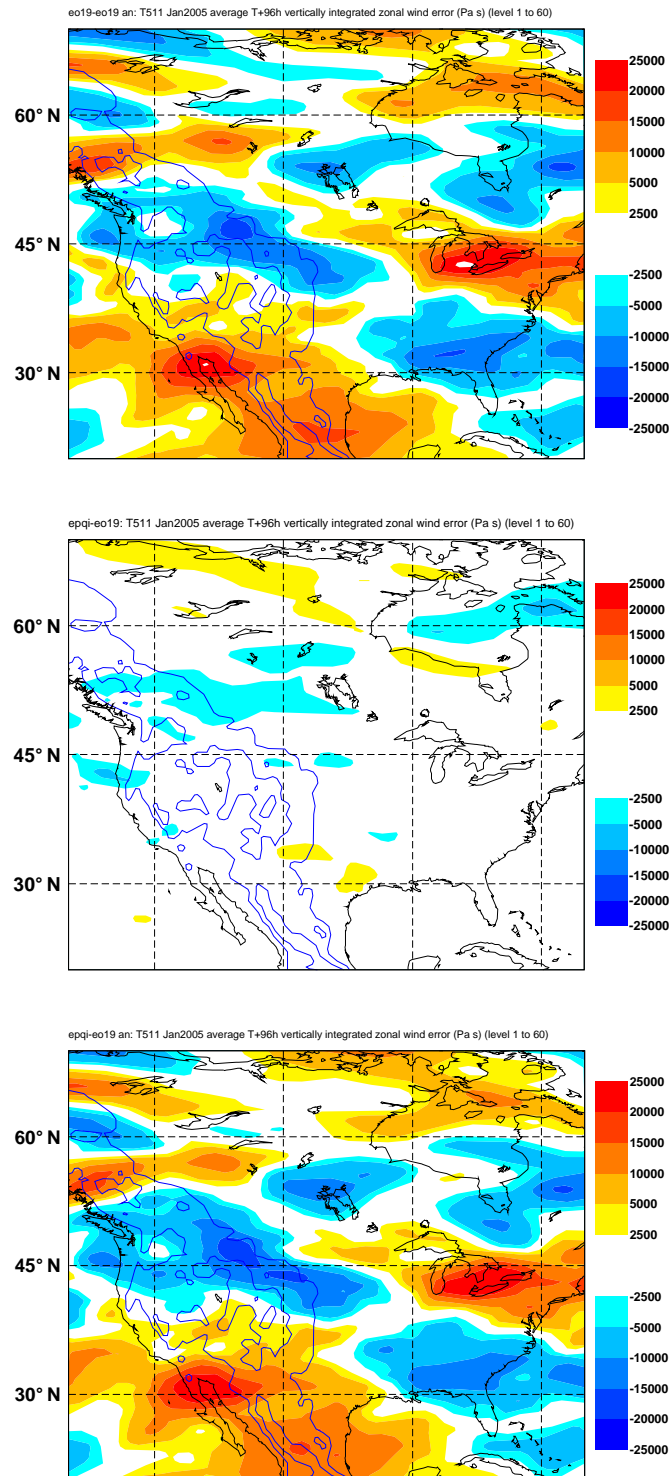
Figure 15: *Experiment epqi average vertically integrated zonal wind difference fields (Pa s) over North America for 96 hour T511 CY29R1 forecasts from 12Z on each day of January 2005 with the TOFD scheme. Top panel: control error; middle panel: experiment impact; bottom panel: experiment impact. Also shown are contours of mean (T511) orography height from 1000 to 6000 m with a 1000 m interval.*
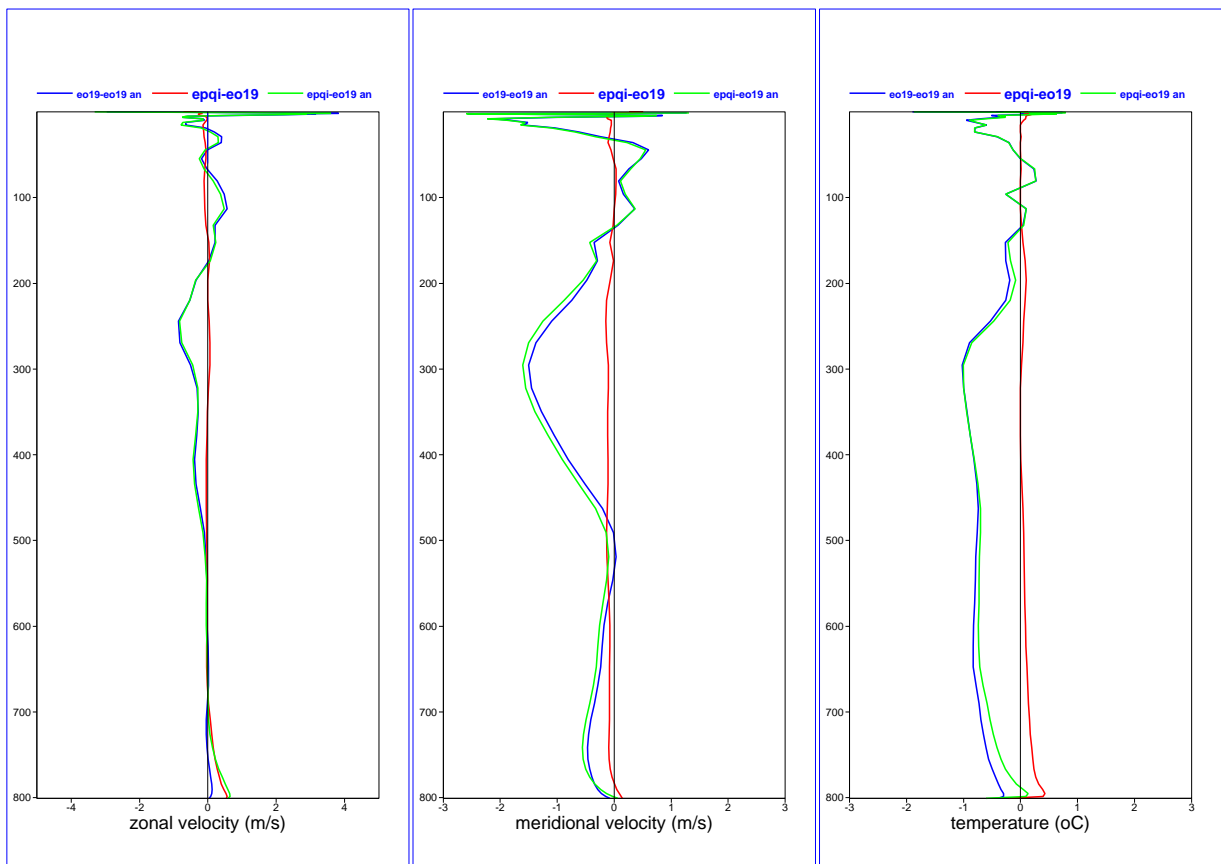
Figure 16: Experiment epqi vertical profiles of difference fields averaged over the Rockies (34ºN to 45ºN and 112ºW to 104ºW) for 96 hour T511 CY29R1 forecasts from 12Z on each day of January 2005 with the TOFD scheme. Left panel: zonal velocity (m s^{-1}); middle panel: meridional velocity (m s^{-1}); right panel: temperature (K). Blue lines: control error; red lines: impact of experiment; green lines: experiment error.
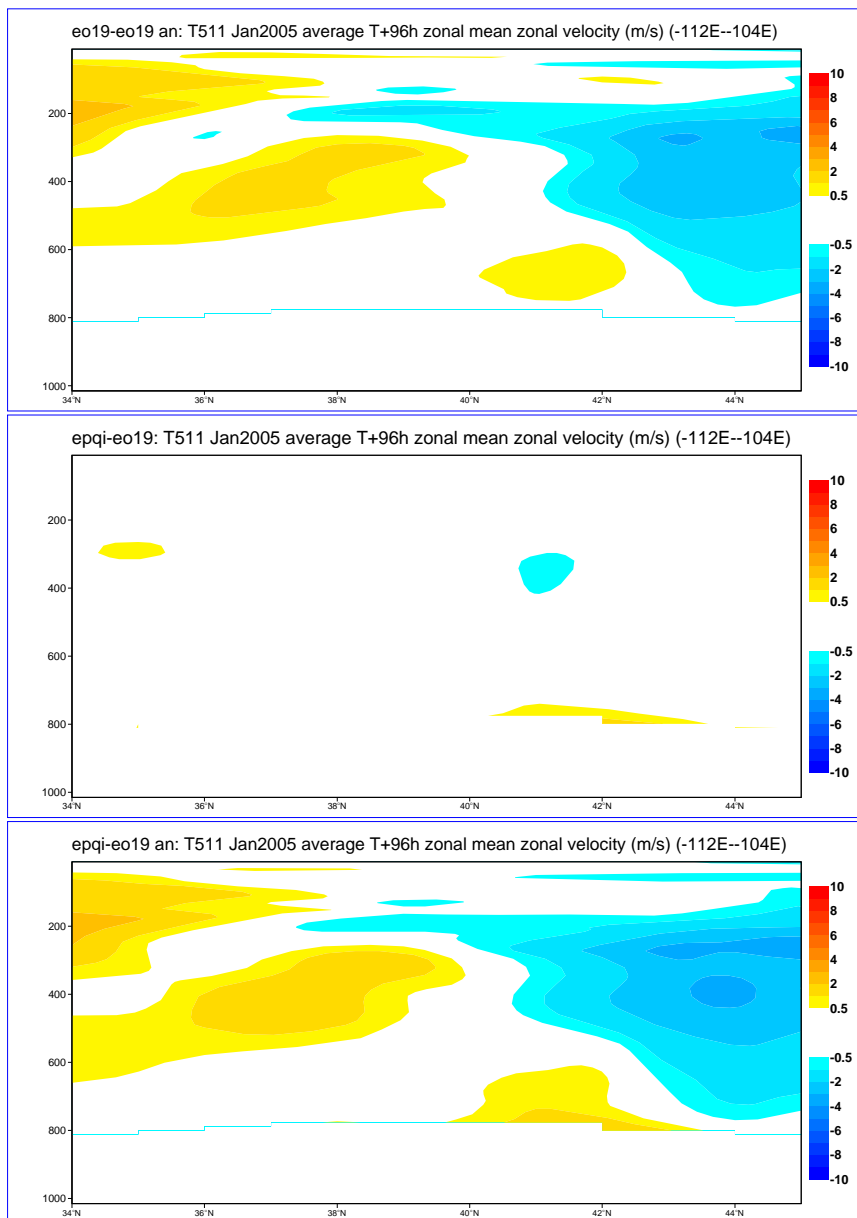
Figure 17: Experiment epqi zonal wind speed difference field (m s^{-1}) zonally averaged over the Rockies between 112^oW and 104^oW for 96 hour T511 CY29R1 forecasts from 12Z on each day of January 2005 with the TOFD scheme. Top panel: control error; middle panel: impact of experiment; bottom panel: experiment error.

2.3   Evaluation of the cutoff mountain technique

Experiment en09 was ran at T511 for each day of January 2005 at 12Z to produce CY29R1 winter forecasts with the gravity wave scheme using the cutoff mountain technique (see section 1.2).

2.3.1   Himalayas

Fig. 18 shows en09 average vertically integrated zonal wind difference fields for 96 hour forecasts. The impact of the experiment (middle panel) is to speed up the flow relative to the control. This is reflected in a reduction in the error (bottom panel) over and downwind of the Himalayas and Tibetan plateau. However, the speed up increases the velocity surplus to the south-west.

Fig. 19 shows that the impact of the experiment is to increase the velocity of the zonal flow throughout much of the depth of the atmosphere, peaking at around 100 hPa with a velocity speed up of around 4 m s^{-1}. At around this height a northerly component of just less than 1 m s^{-1} is produced, resulting in an increase in error here. Below this height the impact is negligible. Temperature error was broadly reduced at upper levels.

Fig. 20 confirms a strong velocity speed up at around 100 hPa over the orography, and a weaker increase throughout the rest of the atmosphere. Fig. 21 confirms the impact of the experiment on temperature, with pronounced cooling over and to the north of the Himalayas between 300 and 100 hPa. To the south is a smaller region of warming. The net effect of this heating would be to increase the meridional temperature gradient, which is consistent with thermal wind balance through a reduction in vertical wind shear as a result of the decreased drag. This results in a significant reduction in temperature bias.

Fig. 22 shows, as expected, that the impact of the cutoff mountain reduces the SSO stress by just over a third. The surface stress responds by increasing slightly. The 850 hPa wind speed is largely unaffected.

2.3.2   Rockies

Fig. 23 shows that the impact of the experiment is smaller over the Rockies than the Himalayas in terms of average vertically integrated zonal wind error in 96 hour forecasts. Some localised regions of velocity speed up are apparent (middle panel). The impact of this is to reduce the error over velocity deficit regions, but increase it over regions of velocity excess.

The much smaller impact the experiment has on zonal flow over the Rockies is confirmed by Fig. 24. Any impact on the zonal flow is confined to levels around 100 hPa. This is perhaps partly due to the area chosen for the averaging procedure including regions of both increasing and decreasing flow. There is an additional small negative meridional velocity increase throughout the entire depth of the atmosphere, which increases the error. Effects on temperature are negligible.

Fig. 22 shows that the impact of the cutoff mountain is to reduce the SSO stress over the Rockies by around a third (the same reduction as over the Himalayas). The surface stress increased slightly in response.

eo19-eo19 an: T511 Jan2005 average T+96h vertically integrated zonal wind error (Pa s) (level 1 to 60)

en09-eo19: T511 Jan2005 average T+96h vertically integrated zonal wind error (Pa s) (level 1 to 60)

en09-eo19 an: T511 Jan2005 average T+96h vertically integrated zonal wind error (Pa s) (level 1 to 60)
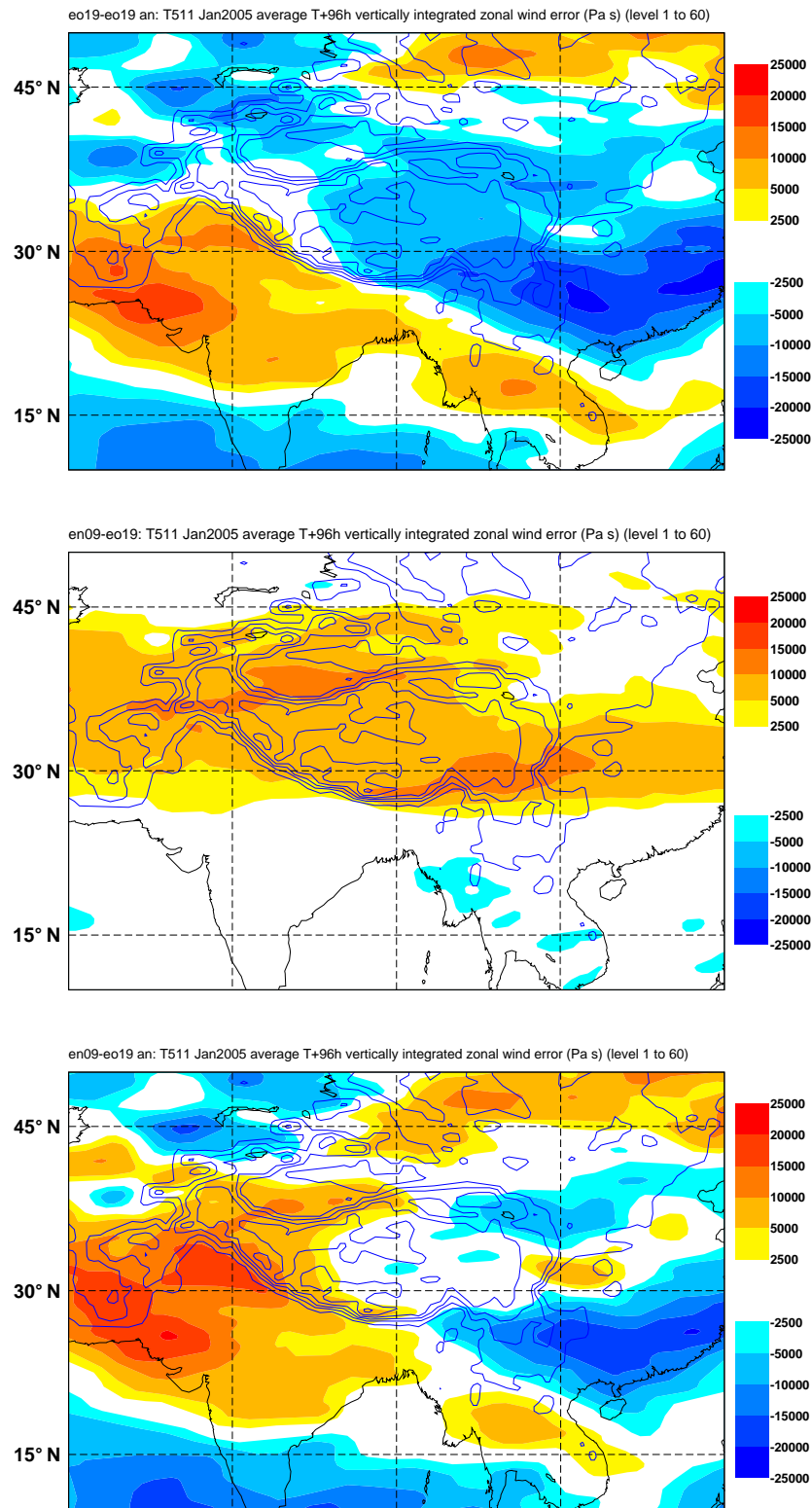
Figure 18: Experiment en09 average vertically integrated zonal wind difference fields (Pa s) over the Himalayan region of south-east Asia for 96 hour T511 CY29R1 forecasts from 12Z on each day of January 2005 using the cutoff mountain technique. Top panel: control error; middle panel: impact of experiment; bottom panel: experiment error. Also shown are contours of mean (T511) orography height from 1000 to 6000 m with a 1000 m interval.
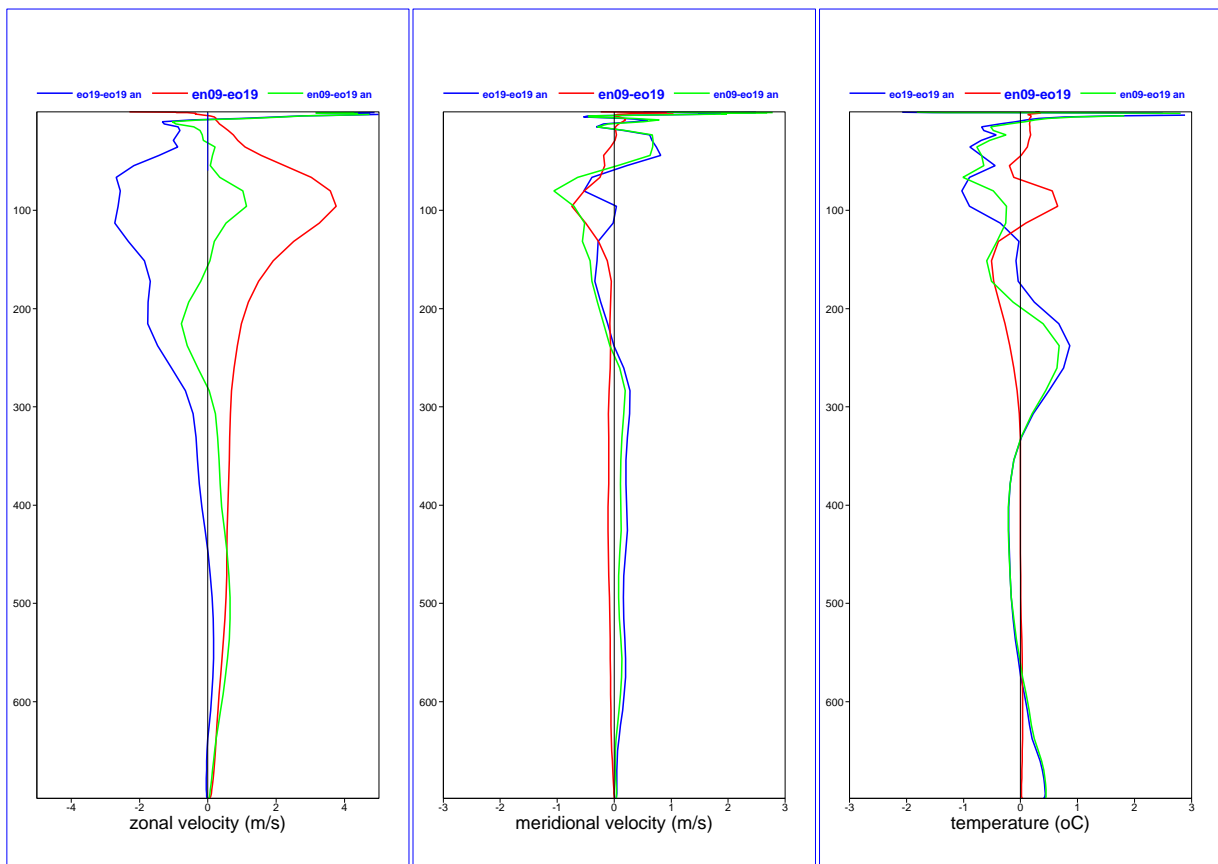
Figure 19: Experiment en09 vertical profiles of difference fields averaged over the Himalayas (26ºN to 40ºN and 75ºE to 105ºE) for 96 hour T511 CY29R1 forecasts from 12Z on each day of January 2005 using the cutoff mountain technique. Left panel: zonal velocity (m s^{-1}); middle panel: meridional velocity (m s^{-1}); right panel: temperature (K). Blue lines: control error; red lines: impact of experiment; green lines: experiment error.
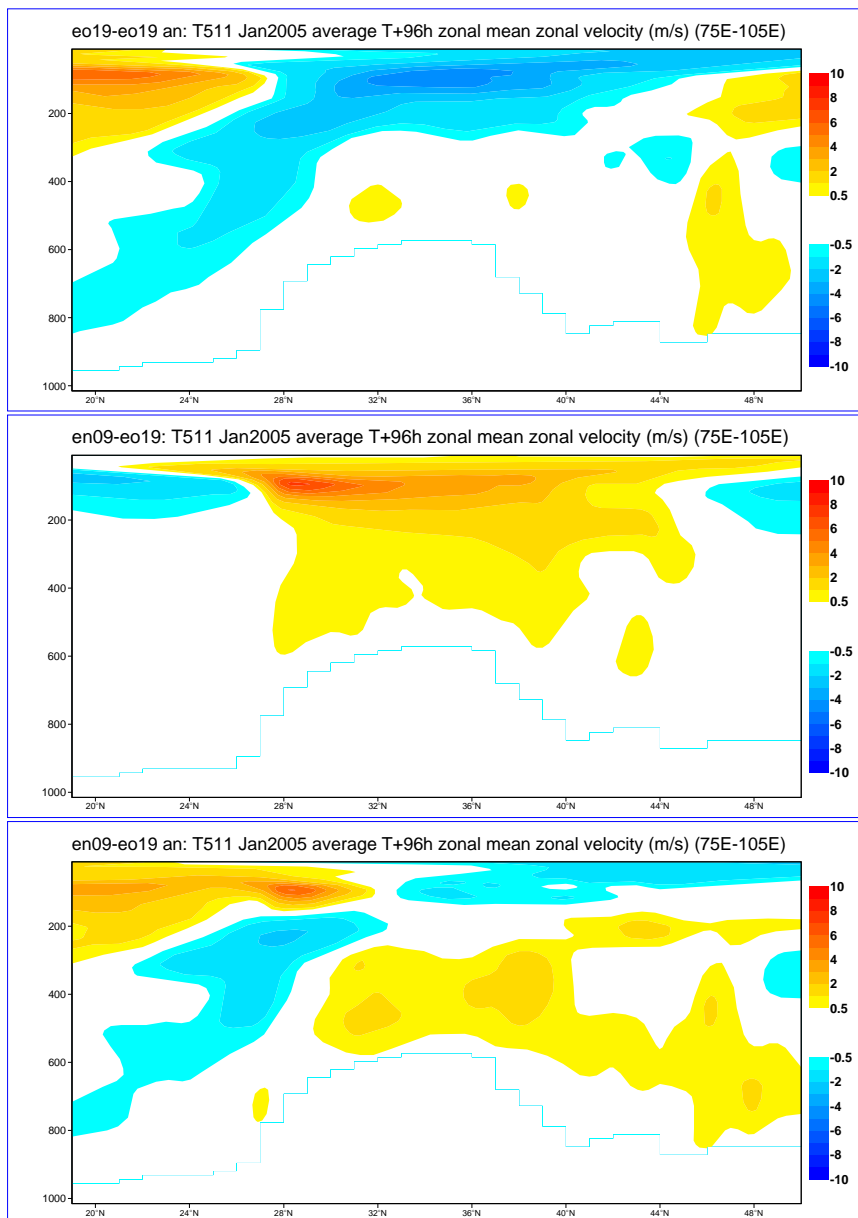
Figure 20: Experiment en09 mean zonal wind speed difference field (m s^{-1}) zonally averaged between 75°E and 105°E for 96 hour T511 CY29R1 forecasts from 12Z on each day of January 2005 using the cutoff mountain technique. Top panel: impact of experiment; bottom panel: experiment error.
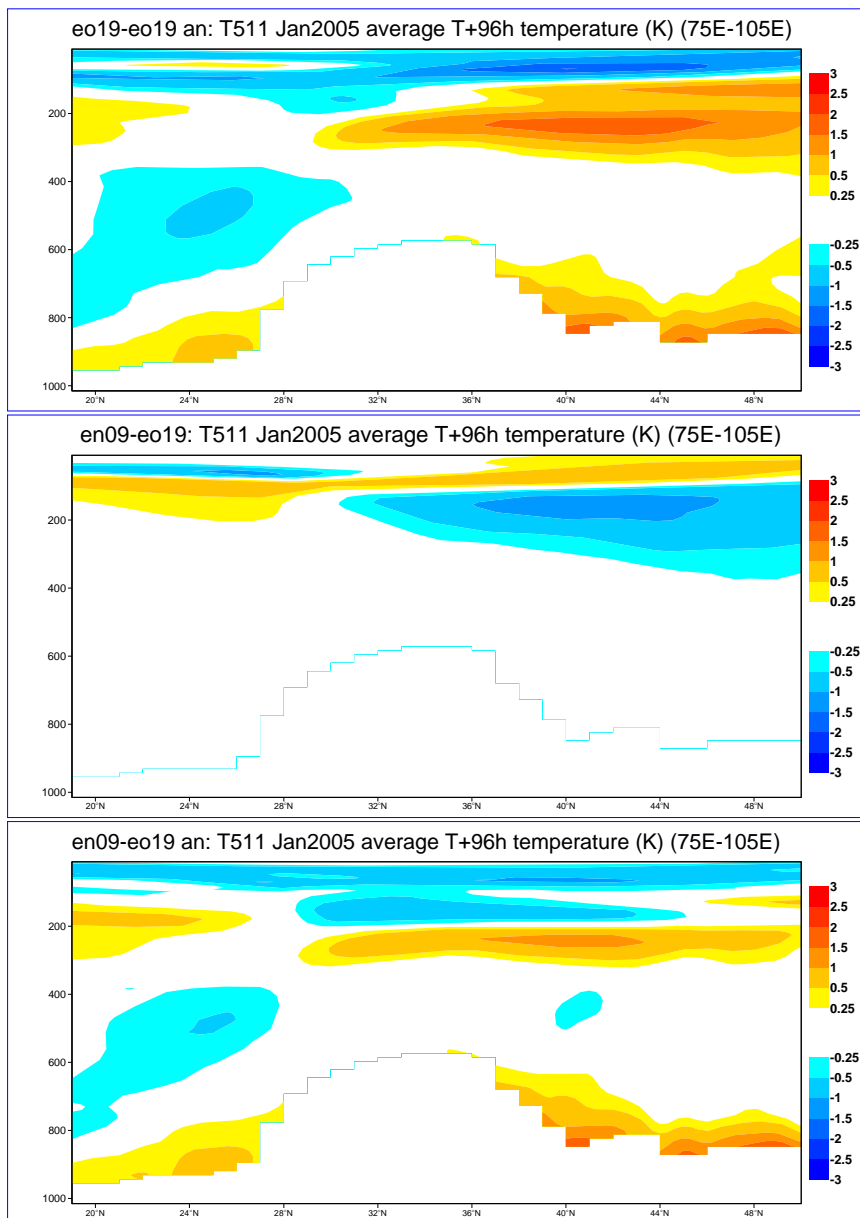
Figure 21: Experiment en09 mean temperature difference field (K) zonally averaged between 75°E and 105°E for 96 hour T511 CY29R1 forecasts from 12Z on each day of January 2005 using the cutoff mountain technique. Top panel: impact of experiment; bottom panel: experiment error.
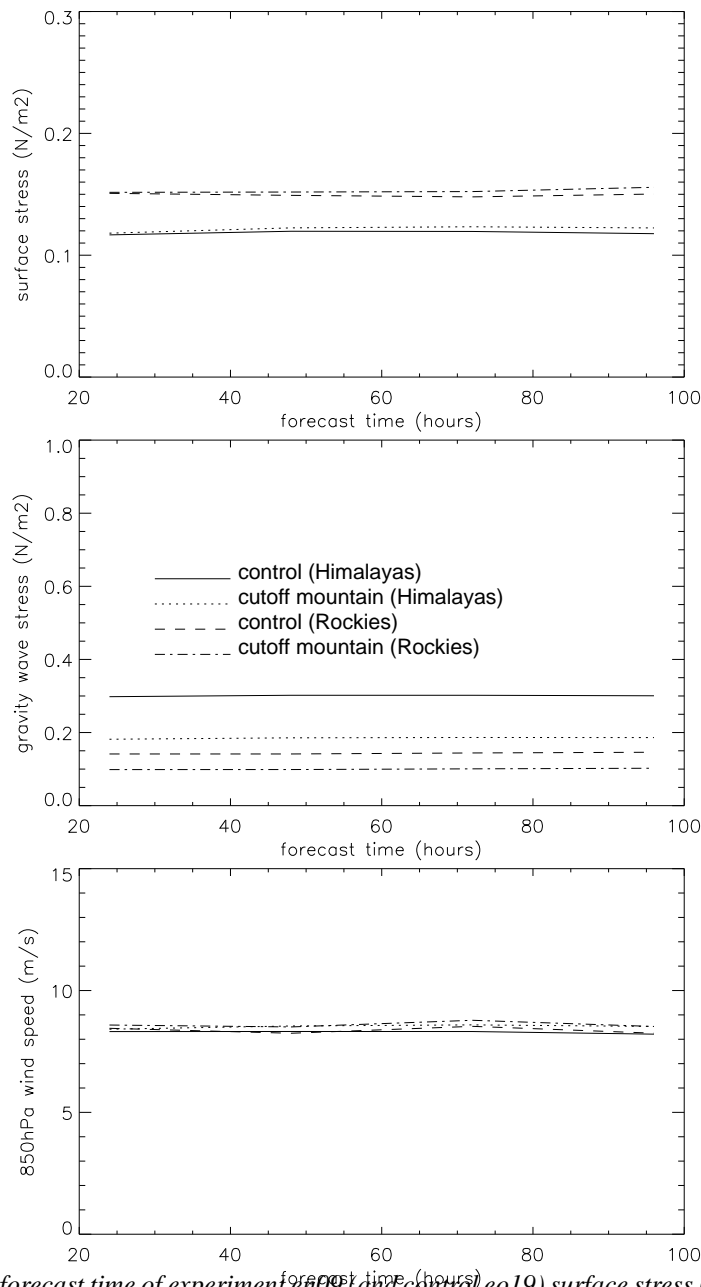
Figure 22: Sensitivity to forecast time of experiment en09 (and control eo19) surface stress (N m⁻²; top panel), SSO stress (N m⁻²; middle panel, labelled 'gravity wave stress'), and 850 hPa wind speed (m s⁻¹;bottom panel) averaged over the Himalayas (26ºN to 40ºN and 75ºE to 105ºE) and the Rockies (34ºN to 45ºN and 112ºW to 104ºW) from T511 CY29R1 forecasts from 12Z on each day of January 2005 using the cutoff mountain technique.
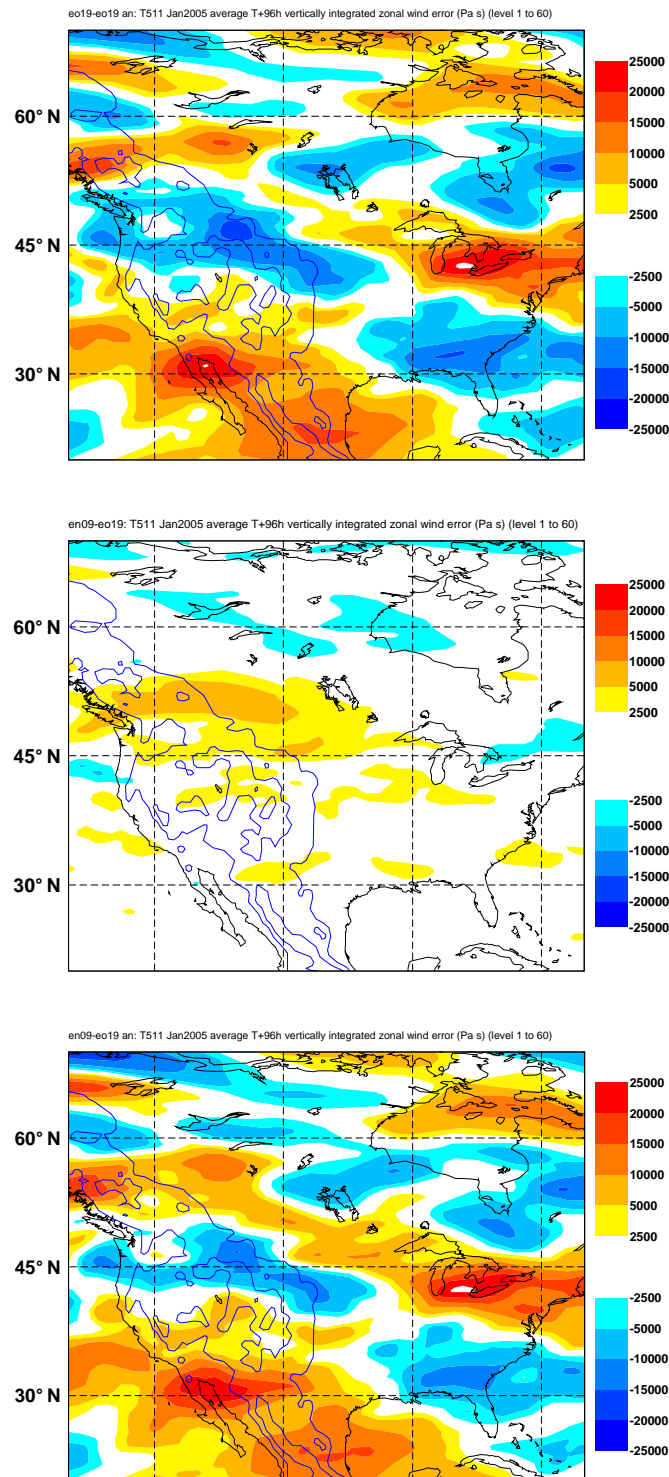
Figure 23: Experiment en09 average vertically integrated zonal wind difference fields (Pa s) over North America for 96 hour T511 CY29R1 forecasts from 12Z on each day of January 2005 using the cutoff mountain technique. Top panel: control error; middle panel: experiment impact; bottom panel: experiment impact. Also shown are contours of mean (T511) orography height from 1000 to 6000 m with a 1000 m interval.
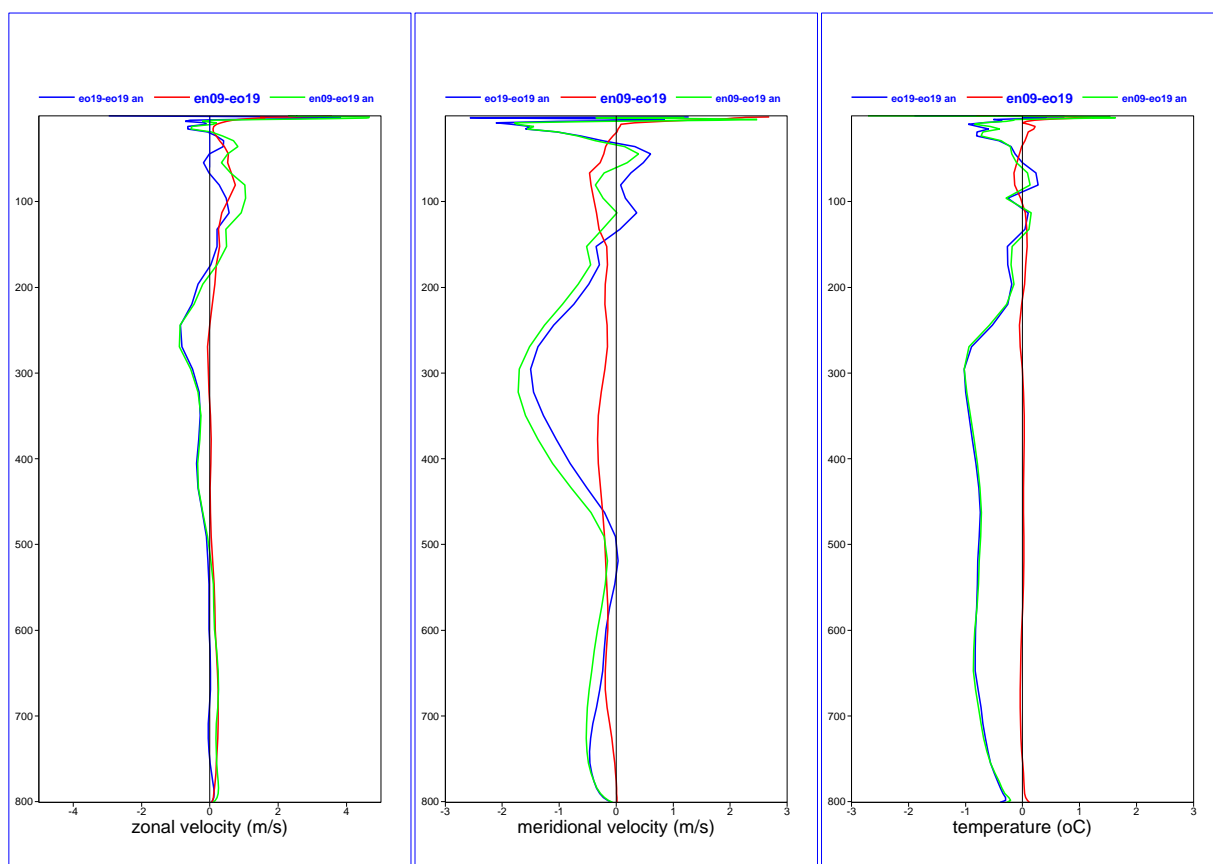
Figure 24: Experiment en09 vertical profiles of difference fields averaged over the Rockies (34ºN to 45ºN and 112ºW to 104ºW) for 96 hour T511 CY29R1 forecasts from 12Z on each day of January 2005 using the cutoff mountain technique. Left panel: zonal velocity (m s^{-1}); middle panel: meridional velocity (m s^{-1}); right panel: temperature (K). Blue lines: control error; red lines: impact of experiment; green lines: experiment error.
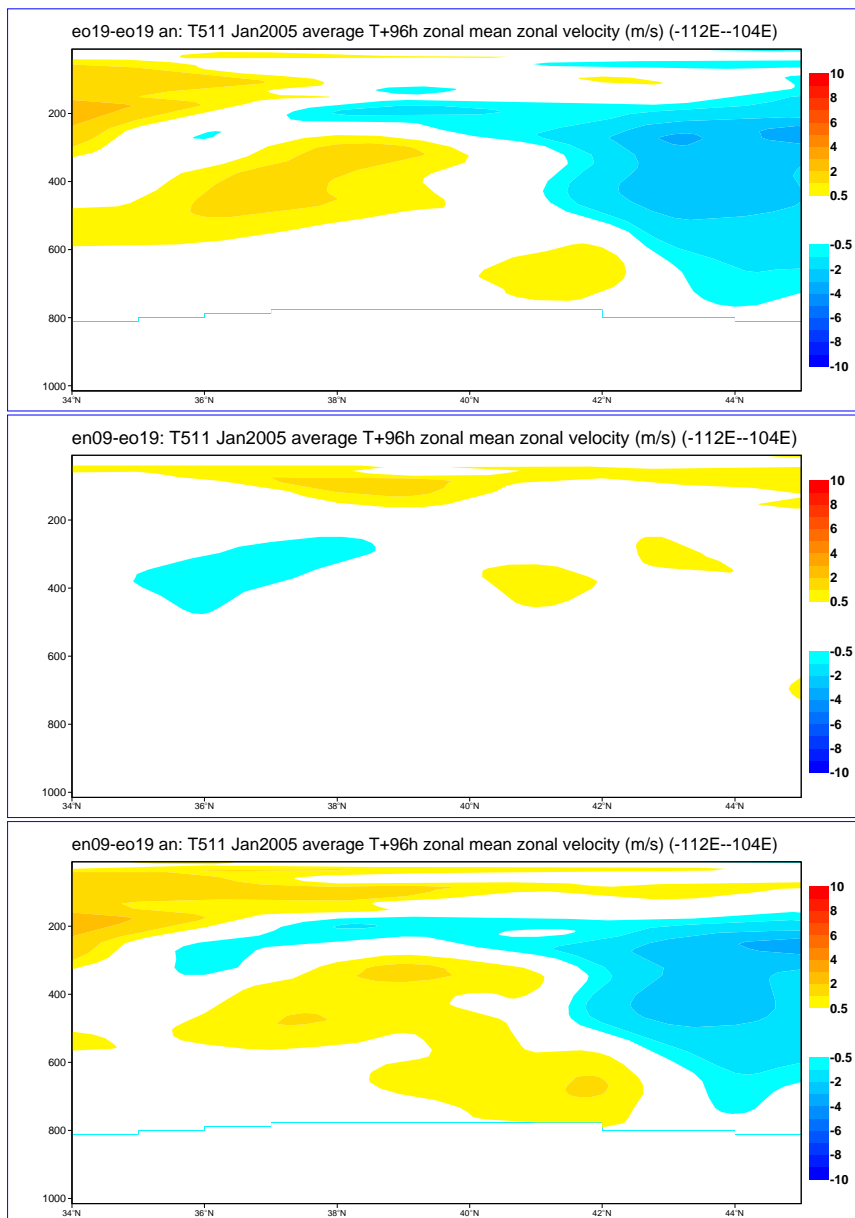
Figure 25: Experiment en09 zonal wind speed difference fields (m s^{-1}) zonally averaged between 112°W and 104°W for 96 hour T511 CY29R1 forecasts from 12Z on each day of January 2005 using a cutoff mountain. Top panel: control error; middle panel: impact of experiment; bottom panel: experiment error.

2.4 Evaluation of the cutoff mountain technique in combination with the turbulent orographic form drag scheme

Experiment eppr was ran at T511 for each day of January 2005 at 12Z to produce CY29R1 winter forecasts with the TOFD scheme in combination with the cutoff mountain technique.

2.4.1 Himalayas

Fig. 26 shows the average vertically integrated zonal wind error for 96 hour forecasts. The middle panel shows that the flow speed up is slightly less increased than when the cutoff mountain is implemented by itself (Fig. 18). This is confirmed by the bottom panel which shows a slightly smaller reduction in the velocity deficit over and downwind of the Himalayas and Tibetan plateau (although also a slightly smaller increase in error to the south-west). Note that the large velocity deficit region to the south-east is still present.

Fig. 27 indicates that at near-surface and mid-level the negative zonal wind error apparent with the TOFD scheme (Fig. 11) and the positive zonal wind error apparent with the cutoff mountain (Fig. 19) have largely cancelled each other out. The impact of the TOFD scheme (i.e. slight decrease in zonal velocity incident to the orography, reducing the gravity wave stress) means that the TOFD scheme in combination with the cutoff mountain results in a slightly stronger speed-up at upper levels than the case of the cutoff mountain by itself. The impact of the experiment on meridional velocity and temperature mirrors the response due to the TOFD scheme at low level and the response due to the cutoff mountain at upper levels.

Fig. 28 confirms that the impact of the experiment is to increase the zonal flow at upper-levels (middle panel), reducing the error (bottom panel). Additionally, as shown by Fig. 27, the excessive slowing at low-level that occurs under the TOFD scheme (Fig. 12) is reduced.

Fig. 29 shows the impact of the experiment on zonally averaged mean temperature. The middle panel shows a pronounced cooling over and to the north of the Himalayas between 300 and 100 hPa (see also Fig. 27) and a thin region of warming above this, resulting in a reduction in temperature bias.

Fig. 30 confirms that the impact of the experiment reduces the SSO stress more than the cutoff mountain only (Fig. 22). To compensate the surface stress increased slightly more than in the case of the experiment with the TOFD scheme only. The 850 hPa wind speed is reduced, as was also evident with the TOFD scheme only.

2.4.2 Rockies

Fig. 31 shows that the impact of the experiment is smaller over the Rockies than the Himalayas in terms of average vertically integrated zonal wind error in 96 hour forecasts. Some localised regions of velocity speed up are apparent (middle panel). One region just north of 30°N increases the already present velocity surplus.

The small impact the experiment has on zonal flow over the Rockies is confirmed by Fig. 32. At upper levels the response is similar to the cutoff mountain only, while at near-surface and mid-level it is similar to that of the TOFD scheme only. As with both the cutoff mountain only and TOFD scheme only there is a small negative meridional velocity difference throughout the entire depth of the atmosphere, which increases the wind error. A small reduction in the negative temperature bias at low-level occurs.

Fig. 33 confirms that the overall impact over the Rockies is small and confined to upper and near-surface levels.

Fig. 30 shows that the experiment results in a slightly smaller reduction in SSO stress than for the case of the cutoff mountain only (Fig. 22). This is due to the effect of the TOFD scheme increasing the near-surface

velocity, and therefore the gravity wave drag. The increase in near-surface velocity is evident in the small increase in 850 hPa wind speed.
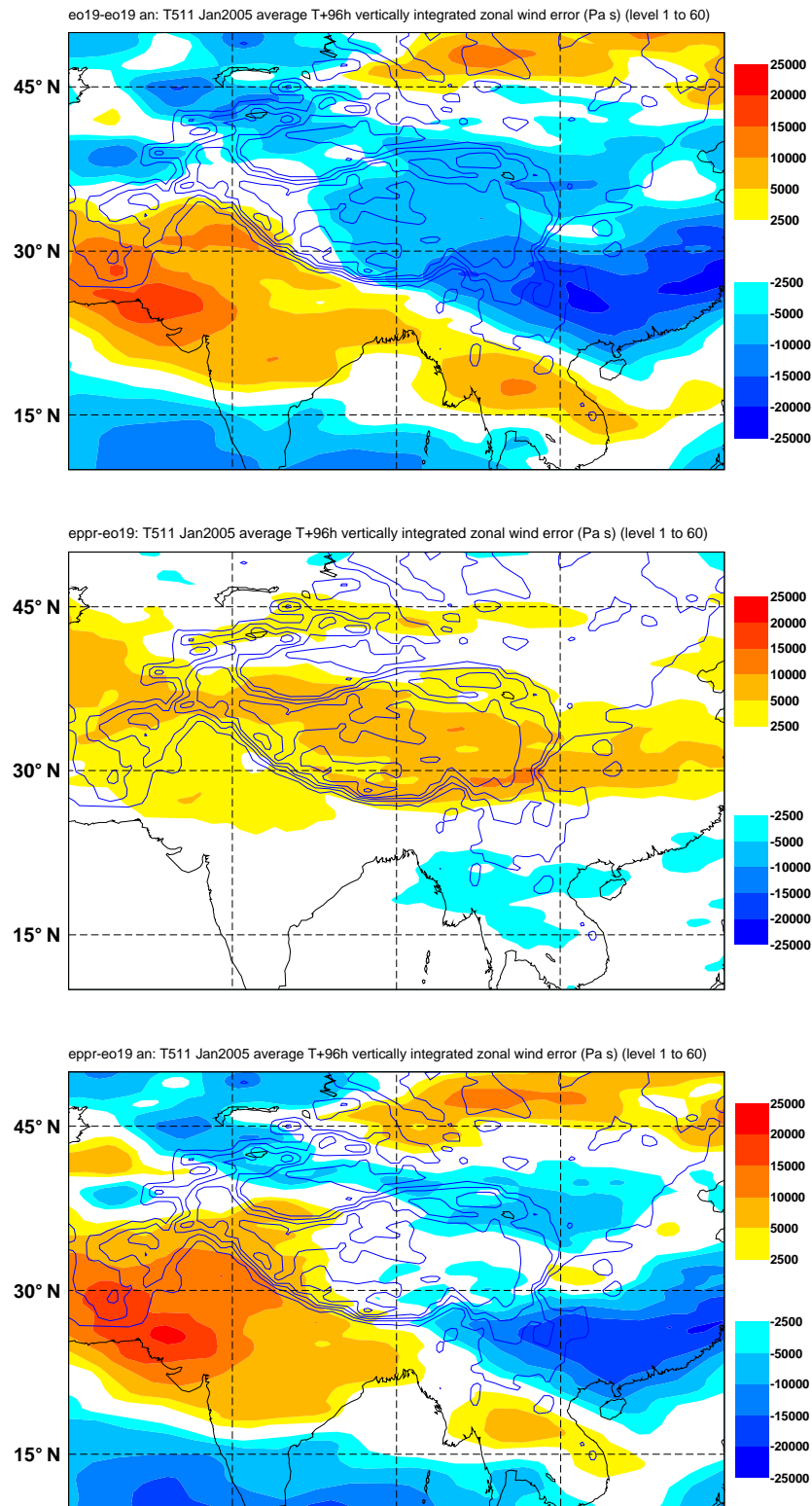
Figure 26: Experiment eppr average vertically integrated zonal wind difference fields (Pa s) over the Himalayan region of south-east Asia for 96 hour T511 CY29R1 forecasts from 12Z on each day of January 2005 using the cutoff mountain technique in combination with the TOFD scheme. Top panel: control error; middle panel: impact of experiment; bottom panel: experiment error. Also shown are contours of mean (T511) orography height from 1000 to 6000 m with a 1000 m interval.
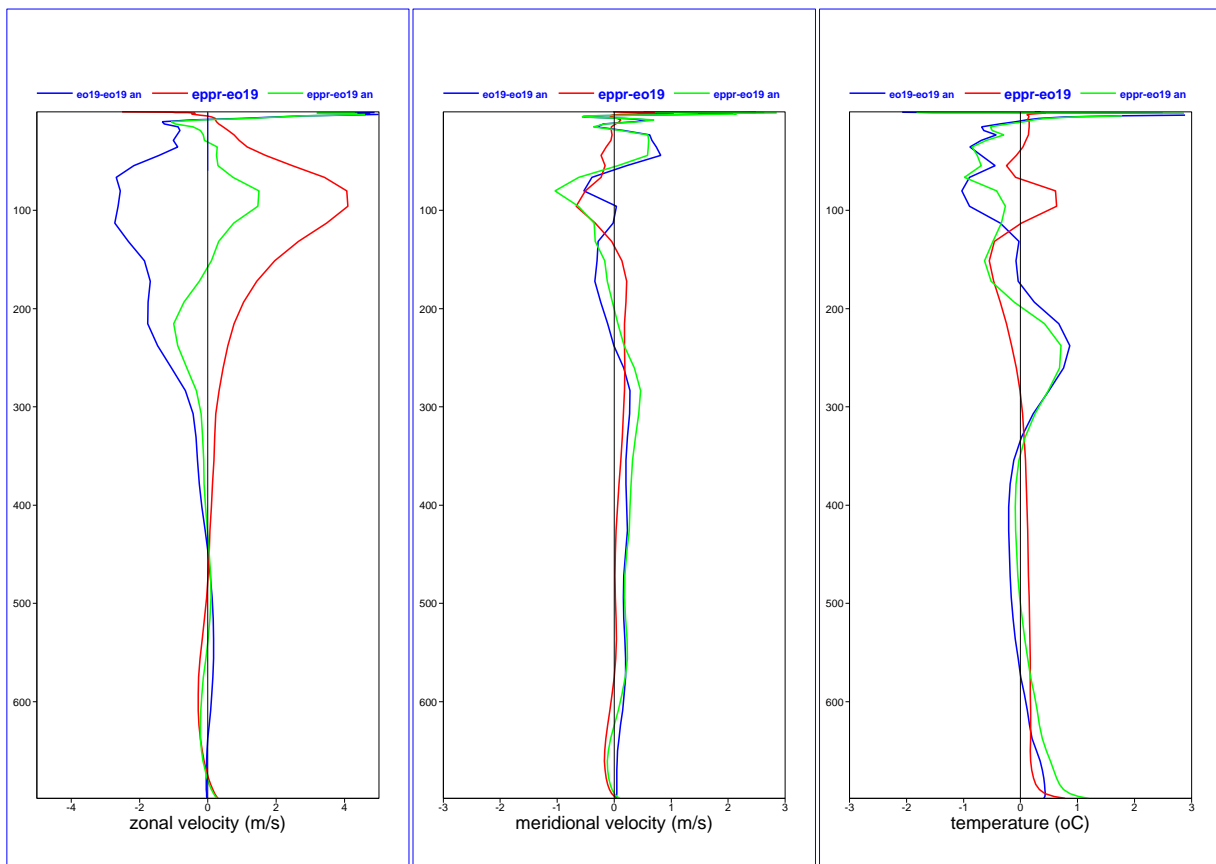
Figure 27: Experiment eppr vertical profiles of difference fields averaged over the Himalayas (26ºN to 40ºN and 75ºE to 105ºE) for 96 hour T511 CY29R1 forecasts from 12Z on each day of January 2005 using the cutoff mountain technique in combination with the TOFD scheme. Left panel: zonal velocity (m s^{-1}); middle panel: meridional velocity (m s^{-1}); right panel: temperature (K). Blue lines: control error; red lines: impact of experiment; green lines: experiment error.
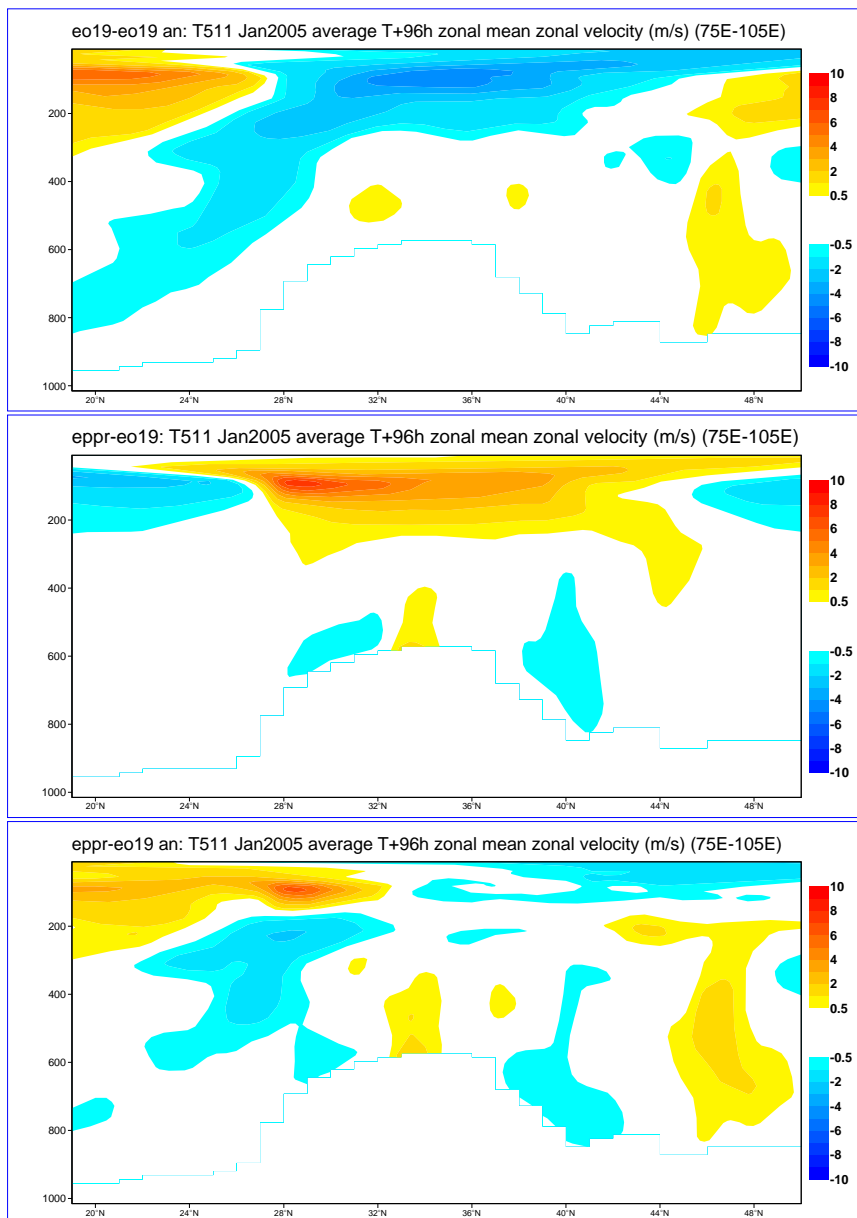
Figure 28: Experiment eppr zonal wind speed difference fields ($m\,s^{-1}$) zonally averaged between 75°E and 105°E for 96 hour T511 CY29R1 forecasts from 12Z on each day of January 2005 using the cutoff mountain technique in combination with the TOFD scheme. Top panel: control error; middle panel: impact of experiment; bottom panel: experiment error.
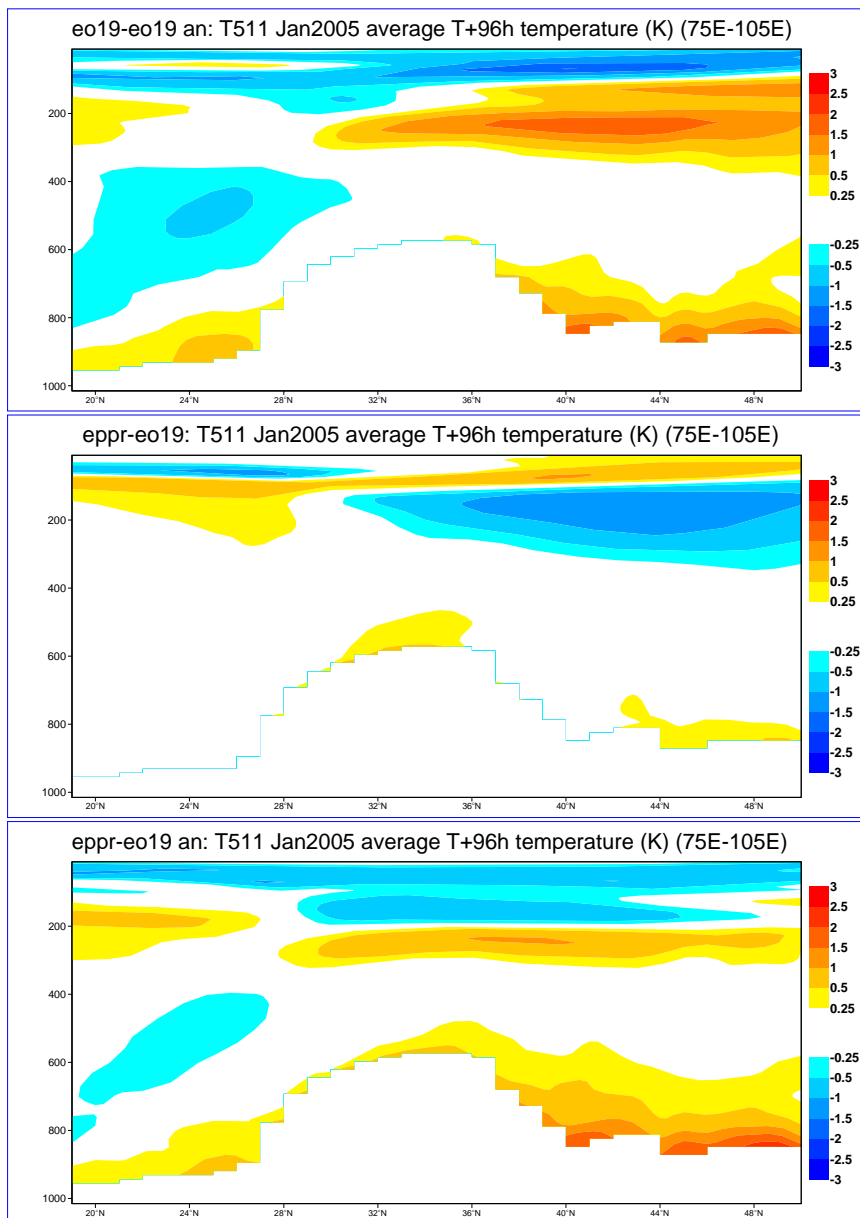
Figure 29: Experiment eppr mean temperature difference field (K) zonally averaged between 75°E *and* 105°E *for 96 hour T511 CY29R1 forecasts from 12Z on each day of January 2005 using the cutoff mountain technique in combination with the TOFD scheme. Top panel: control error; middle panel: impact of experiment; bottom panel: experiment error.*
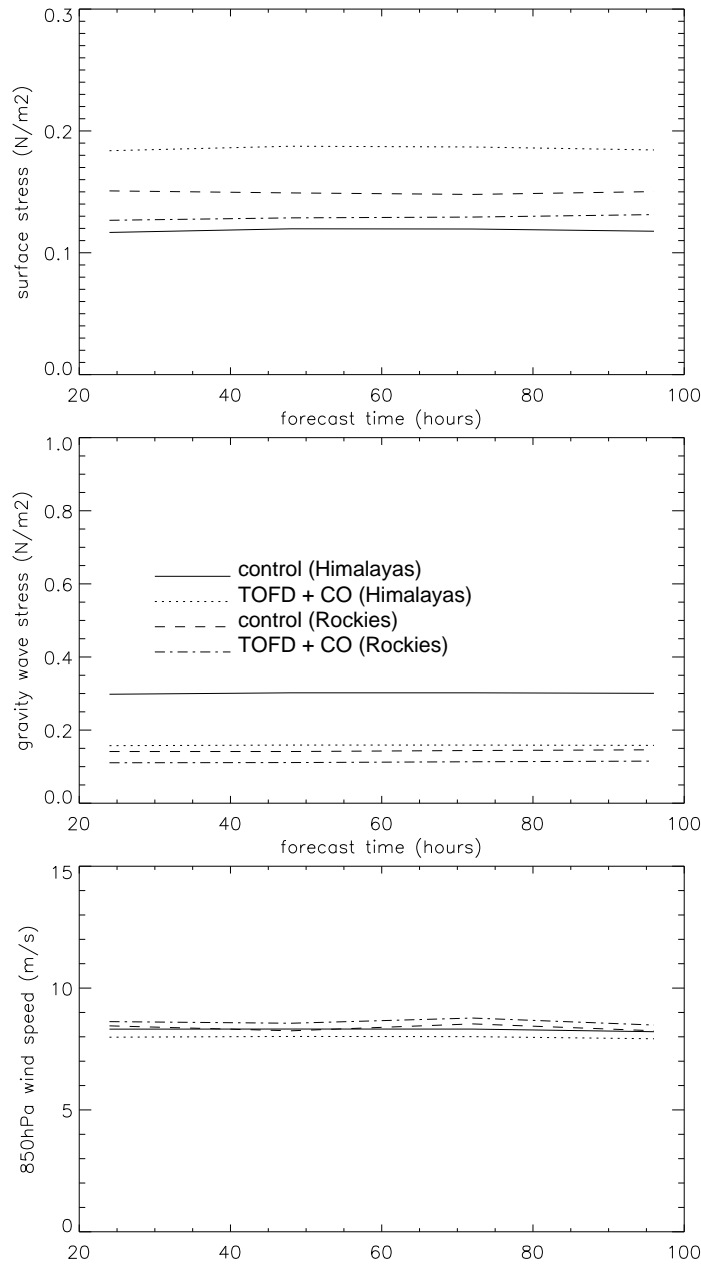
Figure 30: Sensitivity to forecast time of experiment eppr (and control eo19) surface stress (N m^{-2}; top panel), SSO stress (N m^{-2}; middle panel, labelled 'gravity wave stress'), and 850 hPa wind speed (m s^{-1}; bottom panel) averaged over the Himalayas (26ºN to 40ºN and 75ºE to 105ºE) and the Rockies (34ºN to 45ºN and 112ºW to 104ºW) from T511 CY29R1 forecasts from 12Z on each day of January 2005 using the cutoff mountain technique in combination with the TOFD scheme.

eo19-eo19 an: T511 Jan2005 average T+96h vertically integrated zonal wind error (Pa s) (level 1 to 60)

eppr-eo19: T511 Jan2005 average T+96h vertically integrated zonal wind error (Pa s) (level 1 to 60)

eppr-eo19 an: T511 Jan2005 average T+96h vertically integrated zonal wind error (Pa s) (level 1 to 60)
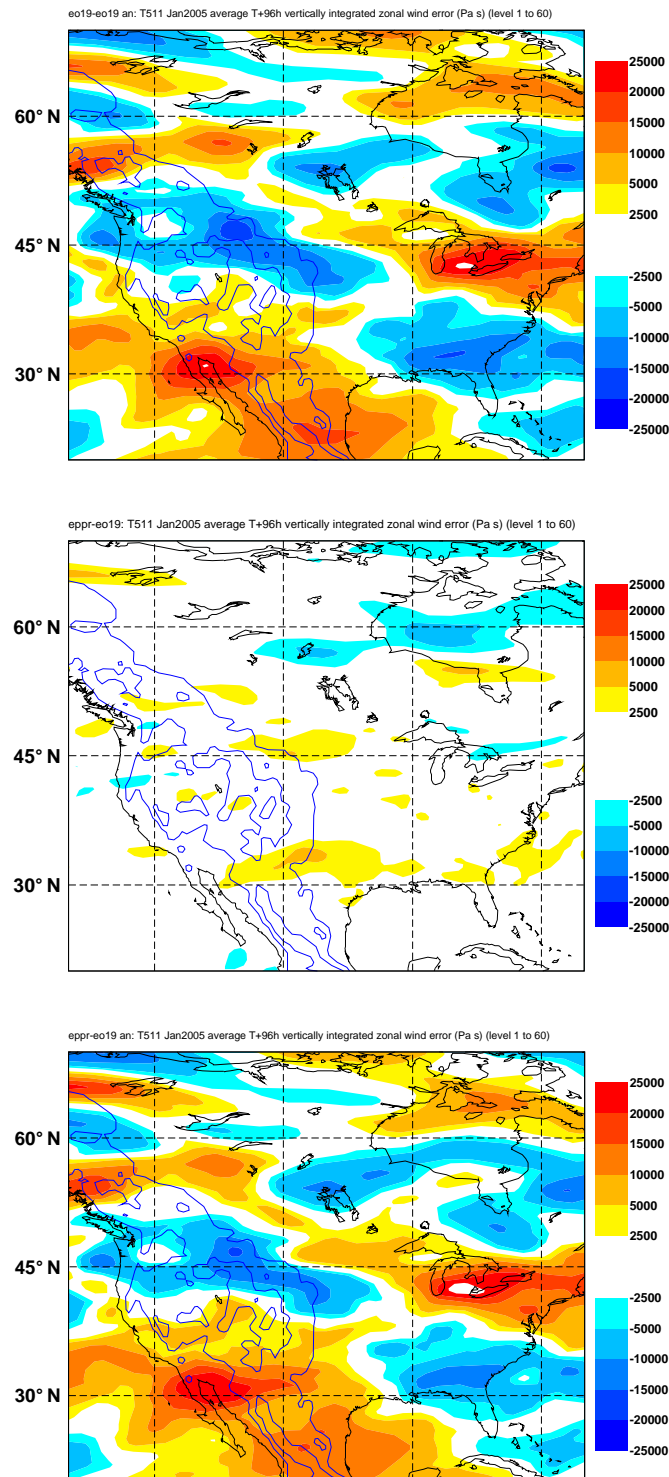
Figure 31: Experiment eppr average vertically integrated zonal wind difference fields (Pa s) over North America for 96 hour T511 CY29R1 forecasts from 12Z on each day of January 2005 using the cutoff mountain technique in combination with the TOFD scheme. Top panel: control error; middle panel: experiment impact; bottom panel: experiment impact. Also shown are contours of mean (T511) orography height from 1000 to 6000 m with a 1000 m interval.
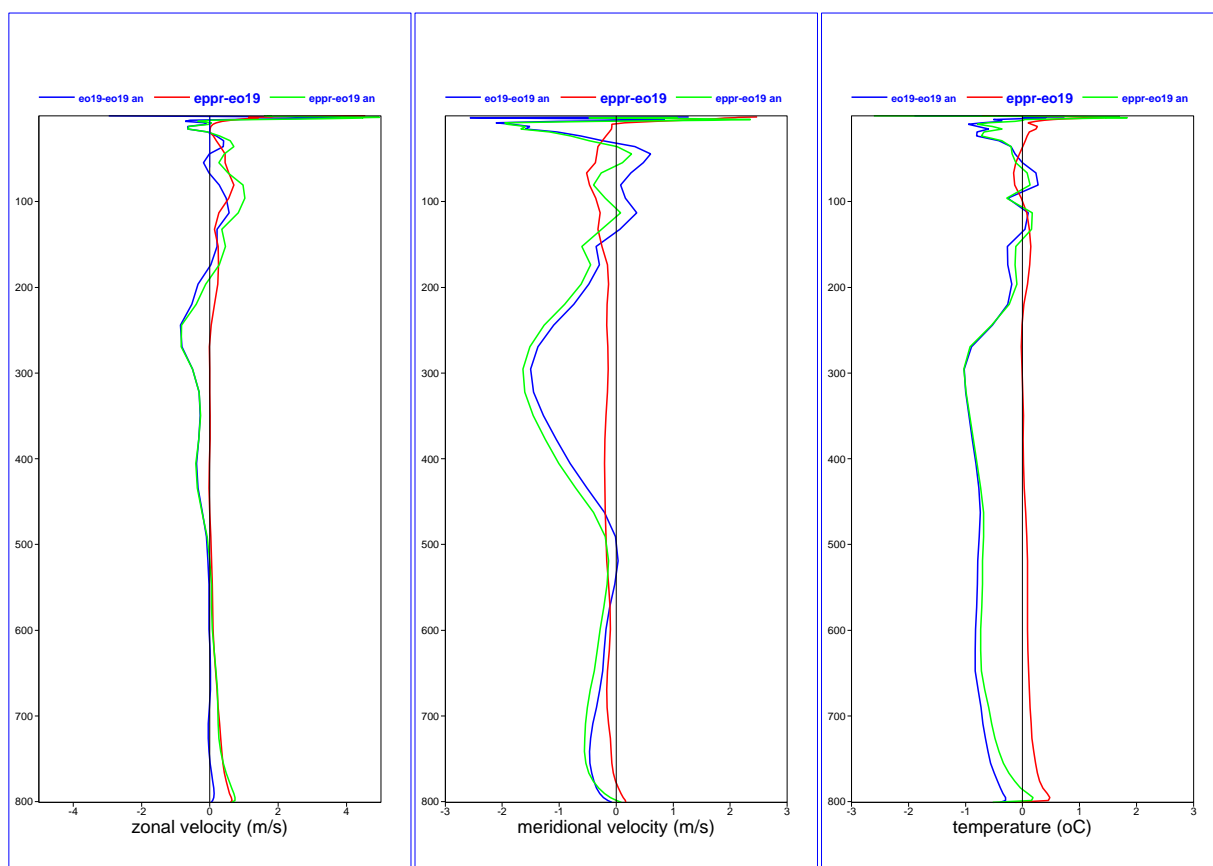
Figure 32: Experiment eppr vertical profiles of difference fields averaged over the Rockies (34ºN to 45ºN and 112ºW to 104ºW) for 96 hour T511 CY29R1 forecasts from 12Z on each day of January 2005 using the cutoff mountain technique in combination with the TOFD scheme. Left panel: zonal velocity (m s^{-1}); middle panel: meridional velocity (m s^{-1}); right panel: temperature (K). Blue lines: control error; red lines: impact of experiment; green lines: experiment error.
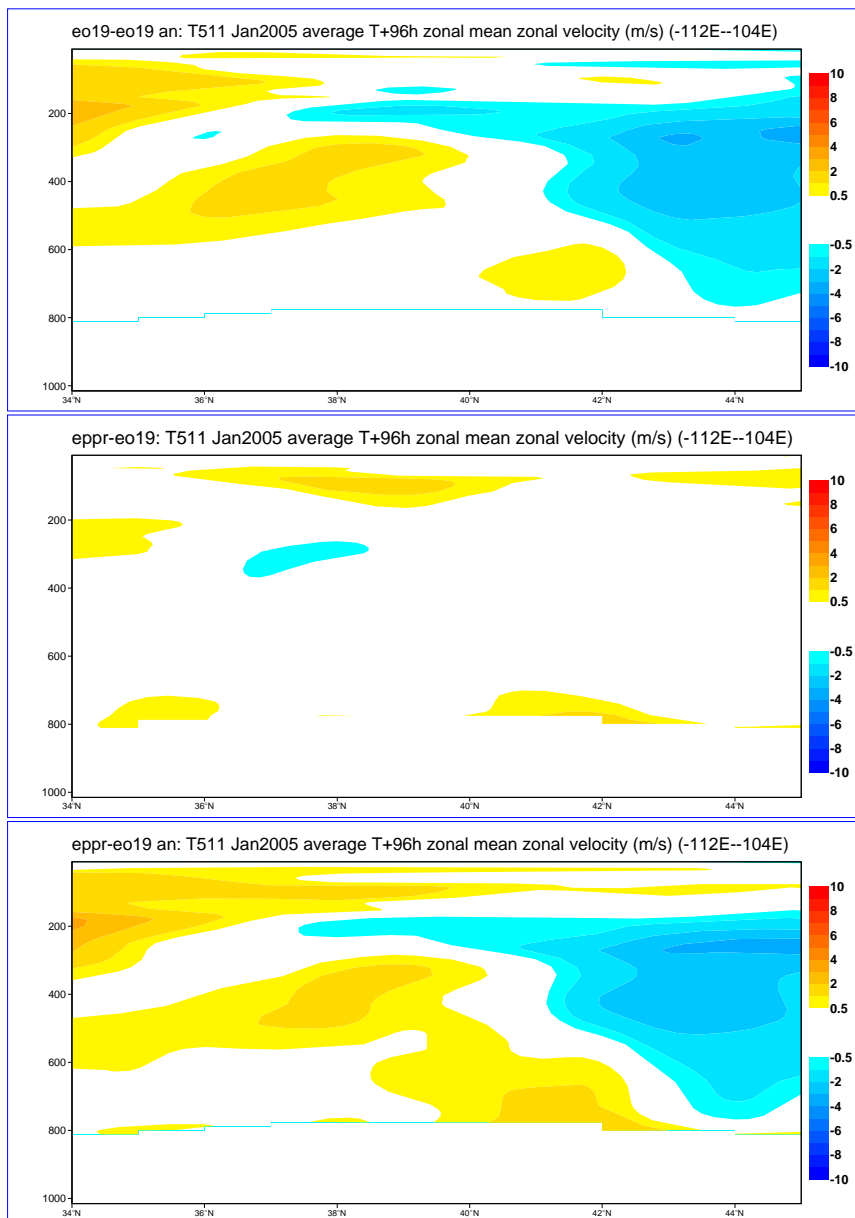
Figure 33: Experiment eppr zonal wind speed difference fields (m s^{-1}) zonally averaged between 112ºW and 104ºW from 96 hour T511 CY29R1 forecasts from 12Z on each day of January 2005 using the cutoff mountain technique in combination with the TOFD scheme. Top panel: control error; middle panel: impact of experiment; bottom panel: experiment error.

2.5 Evaluation of the cutoff mountain technique in combination with the turbulent orographic form drag scheme and revised values of G and Ric.

The experiment detailed in the previous section was repeated with G (see Eq. (2)) increased from its standard value of 0.33 to 1. This is experiment epi7. This change was suggested by Brown (2004a) to return (increase) the T511 parameterised wave torque to approximately their control values (as Brown (2004b) concluded that the main problem involved excessive T95 parameterised torques). This is perhaps not applicable as it has been shown that substantial velocity deficits are also apparent at T511 (see Fig. 3).

Additionally, the value of the critical Richardson number used in the gravity wave scheme to determine the stress profile was increased from 0.25 to 0.67. This was also suggested by Brown (2004a) as a way of depositing more of the gravity wave stress at lower levels of the atmosphere and therefore reduce excessive gravity wave stress above 100 hPa and limiting the systematic slowing relative to the analyses.

2.5.1 Himalayas

Fig. 34 shows the average vertically integrated zonal wind error in 96 hour forecasts from 12Z on each day of January 2005. Comparing with Fig. 26 shows that the larger tuning coefficient has significantly reduced the positive impact the cutoff mountain had on reducing the velocity deficit.

This is confirmed by Fig. 35, which also shows an additional slowing relative to the analyses at near-surface and mid-level (cf. Fig. 27), perhaps due to the increased critical Richardson number. Little further change is evident in meridional velocity and temperature on introduction of the different coefficients.

The reduction in magnitude and extent of the velocity speed-up is apparent from Fig. 36.

Fig. 37 shows surface stress values are insensitive to the tuning coefficient and critical Richardson number. However, as expected, the reduction in SSO stress over the Himalayas on implementation of the cutoff mountain (Fig. 30) has been lessened with the introduction of the larger tuning coefficient.

2.5.2 Rockies

Figs. 38 to 40 show that over the Rockies the cutoff mountain in combination with the TOFD scheme now has little impact on the upper level zonal flow. The impact of the TOFD scheme is still to increase near-surface zonal flow.

Fig. 37 shows that the increase in SSO stress due to increasing G and the reduction due to the cutoff mountain cancel each other out, explaining the negligible impact on upper level winds. Comparing Fig. 39 with Fig. 32 shows little change in meridional velocity and temperature in response to the coefficient changes.
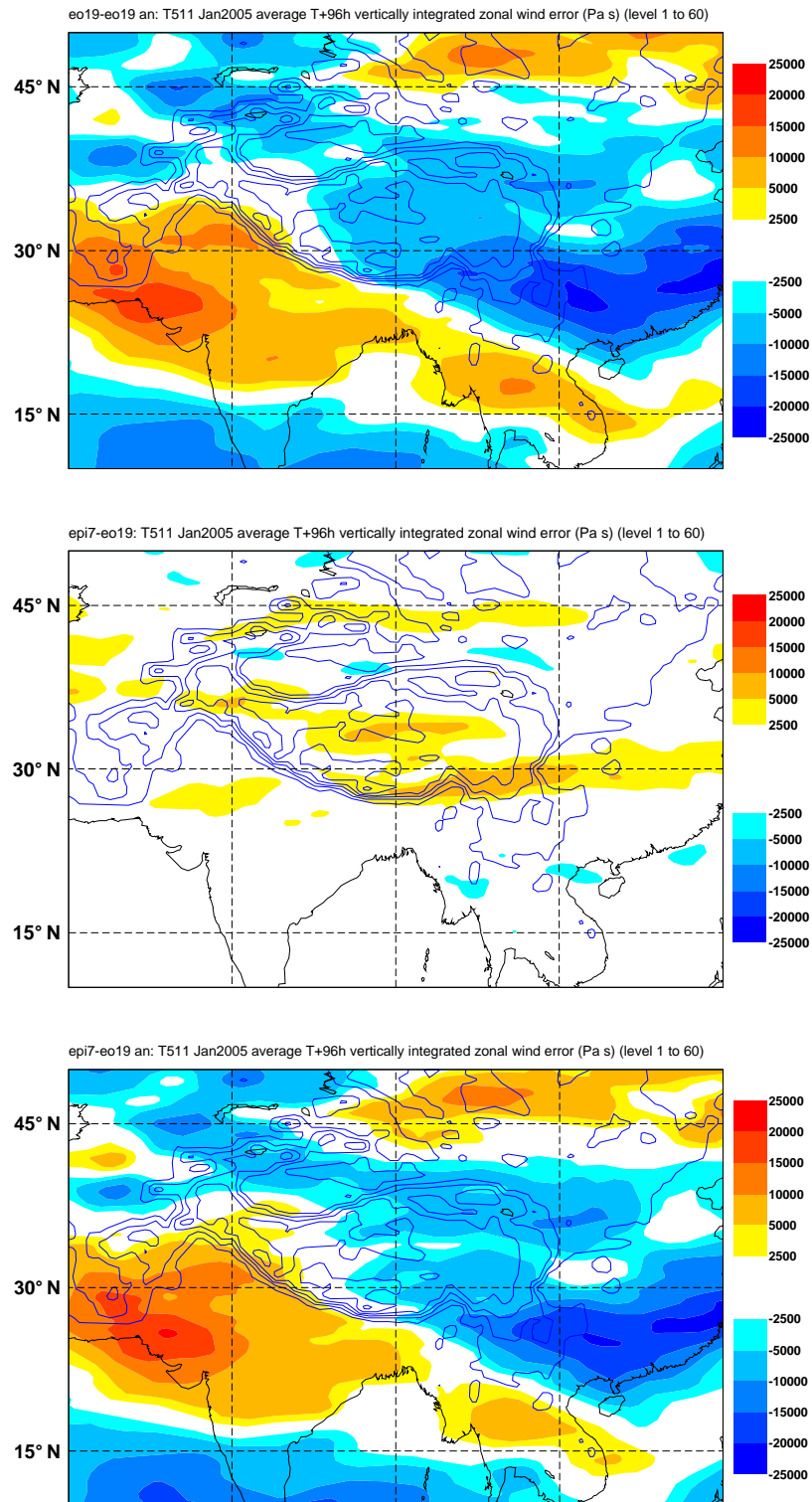
Figure 34: Experiment epi7 average vertically integrated zonal wind difference fields (Pa s) over the Himalayan region of south-east Asia for 96 hour T511 CY29R1 forecasts from 12Z on each day of January 2005 using the cutoff mountain technique in combination with the TOFD scheme and revised values of G and Ric. Top panel: control error; middle panel: impact of experiment; bottom panel: experiment error. Also shown are contours of mean (T511) orography height from 1000 to 6000 m with a 1000 m interval.
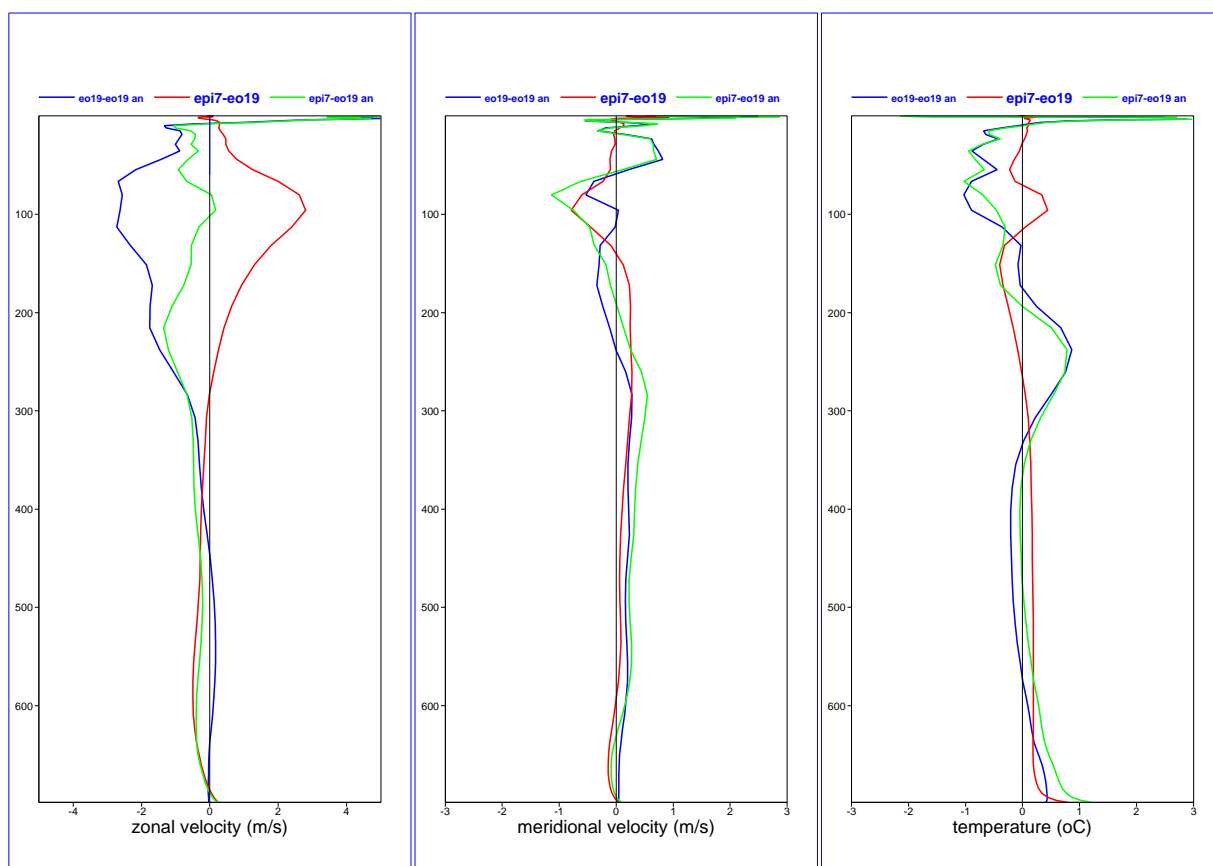
Figure 35: Experiment epi7 vertical profiles of difference fields averaged over the Himalayas (26ºN to 40ºN and 75ºE to 105ºE) for 96 hour T511 CY29R1 forecasts from 12Z on each day of January 2005 using the cutoff mountain technique in combination with the TOFD scheme and revised values of G and Ric. Left panel: zonal velocity ($m\,s^{-1}$); middle panel: meridional velocity ($m\,s^{-1}$); right panel: temperature (K). Blue lines: control error; red lines: impact of experiment; green lines: experiment error.
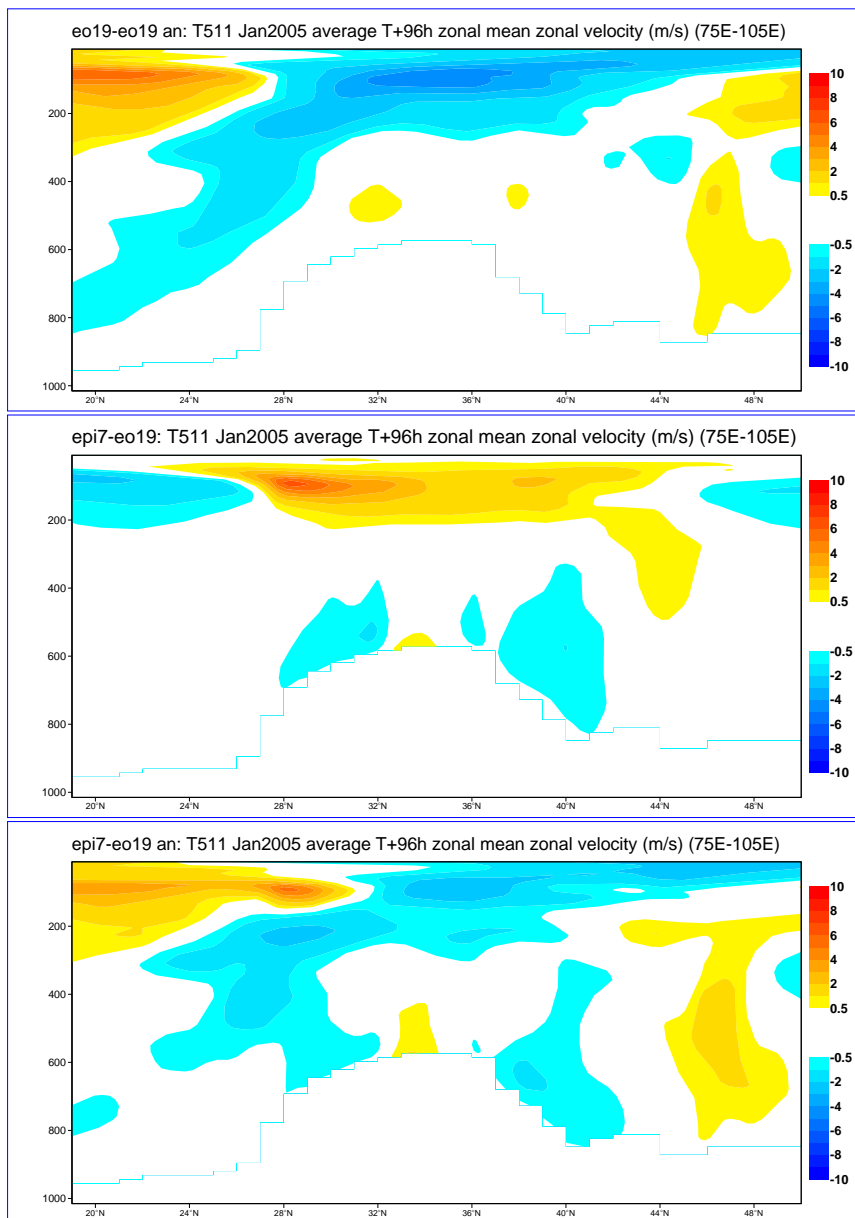
Figure 36: Experiment epi7 zonal wind speed difference fields (m s^{-1}) zonally averaged between 75°E and 105°E for 96 hour CY29R1 forecasts from 12Z on each day of January 2005 using the cutoff mountain technique in combination with the TOFD scheme and revised values of G and Ric. Top panel: impact of experiment; bottom panel: experiment error.
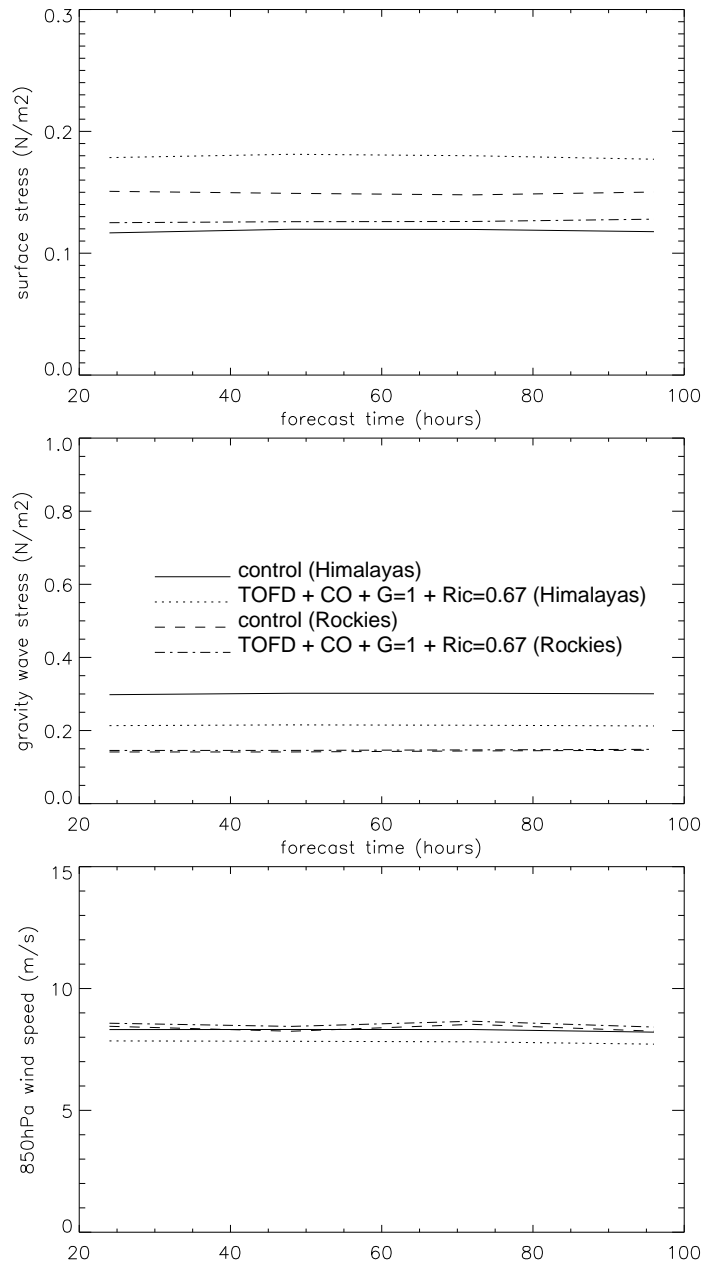
Figure 37: Sensitivity to forecast time of experiment epi7 (and control eo19) surface stress (N m^{-2}; top panel), SSO stress (N m^{-2}; middle panel, labelled 'gravity wave stress'), and 850 hPa wind speed (m s^{-1}; bottom panel) averaged over the Himalayas (26ºN to 40ºN and 75ºE to 105ºE) and the Rockies (34ºN to 45ºN and 112ºW to 104ºW) from T511 CY29R1 forecasts from 12Z on each day of January 2005 using the cutoff mountain technique in combination with the TOFD scheme and revised values of G and Ric.
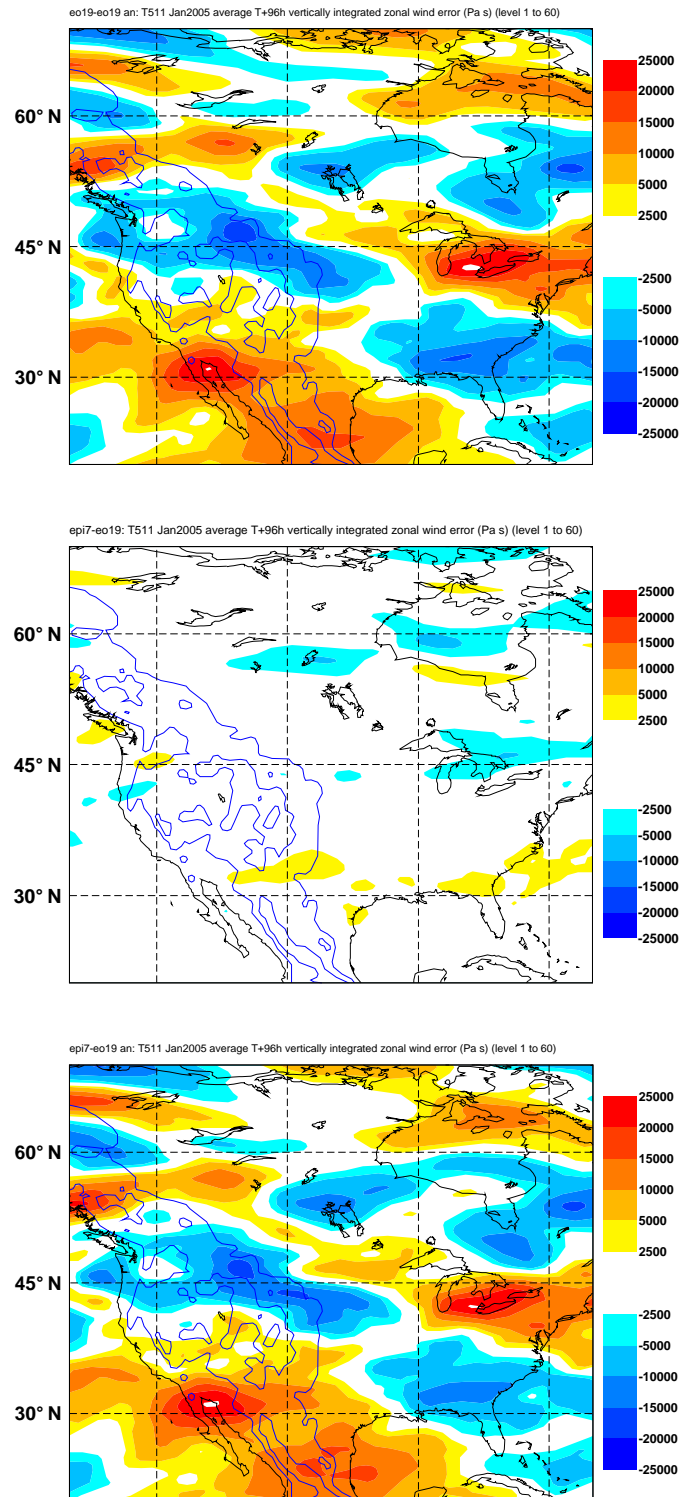
Figure 38: Experiment epi7 average vertically integrated zonal wind difference fields (Pa s) over North America for 96 hour T511 CY29R1 forecasts from 12Z on each day of January 2005 using the cutoff mountain technique in combination with the TOFD scheme and revised values of G and Ric. Top panel: control error; middle panel: experiment impact; bottom panel: experiment impact. Also shown are contours of mean (T511) orography height from 1000 to 6000 m with a 1000 m interval.
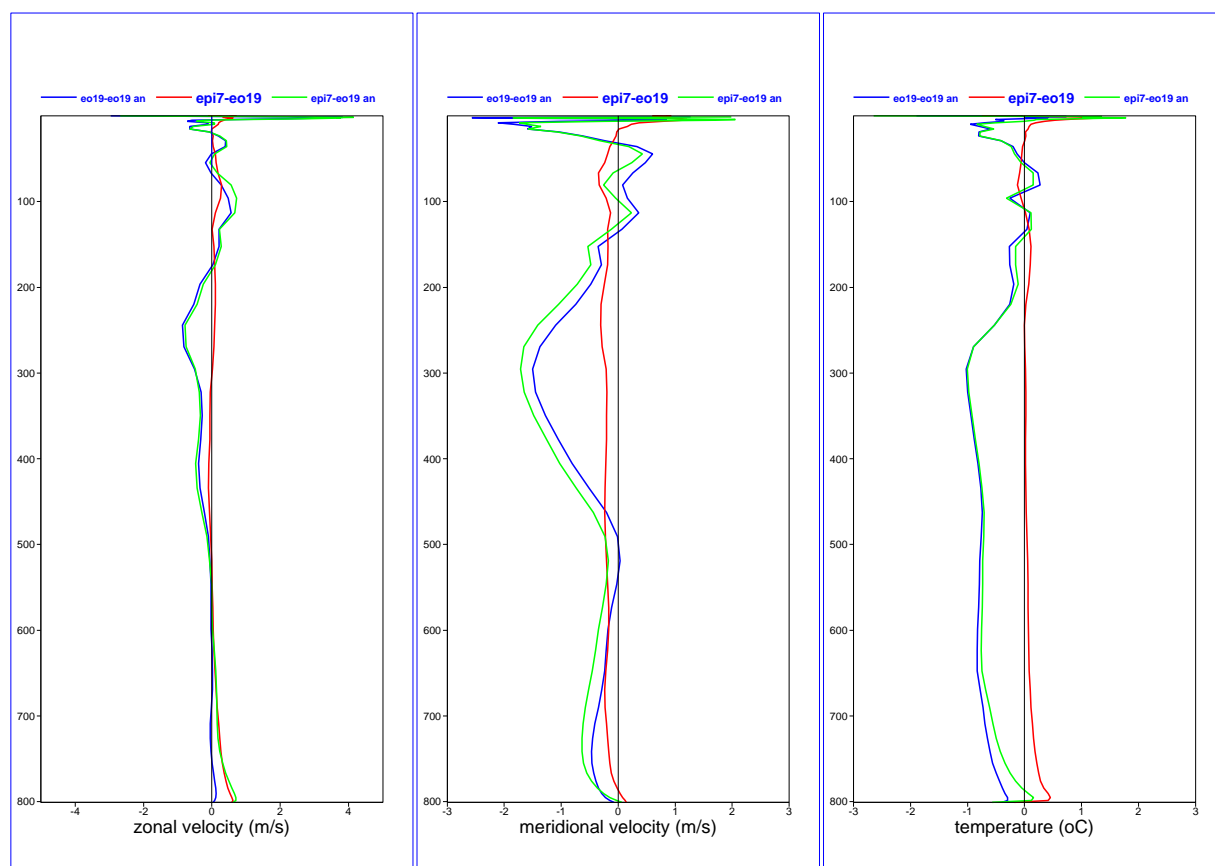
Figure 39: Experiment epi7 vertical profiles of difference fields averaged over the Rockies (34ºN to 45ºN and 112ºW to 104ºW) for 96 hour T511 CY29R1 forecasts from 12Z on each day of January 2005 using the cutoff mountain technique in combination with the TOFD scheme and revised values of G and Ric. Left panel: zonal velocity (m s^{-1}); middle panel: meridional velocity (m s^{-1}); right panel: temperature (K). Blue lines: control error; red lines: impact of experiment; green lines: experiment error.
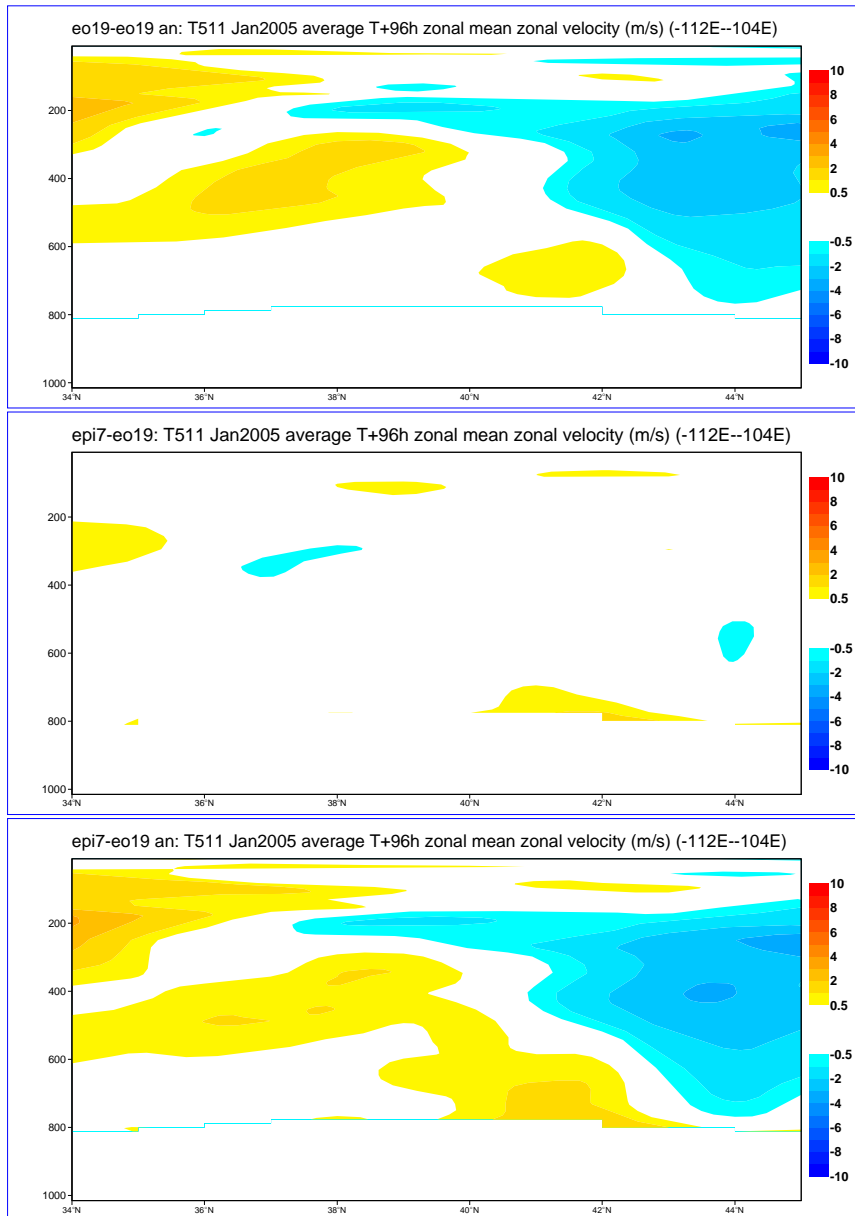
Figure 40: Experiment epi7 zonal wind speed difference fields ($m\,s^{-1}$) zonally averaged between $112^{o}W$ and $104^{o}W$ for 96 hour T511 CY29R1 forecasts from 12Z on each day of January 2005 using the cutoff mountain technique in combination with the TOFD scheme and revised values of G and Ric. Top panel: control error; middle panel: impact of experiment; bottom panel: experiment error.

2.6 Scores

2.6.1 East Asia

Fig. 41 and 42 show the root mean square (rms) error in 500 and 100 hPa geopotential height over East Asia. The TOFD and TOFD in combination with the cutoff mountain 500 hPa scores both show a positive impact after around day 4, indicating that the introduction of the TOFD scheme improves the forecast at mid level. At 100 hPa the addition of the cutoff mountain improves the scores considerably from day 1.

Figs. 43 to 44 show 850 and 200 hPa vector wind rms errors over East Asia. Again, the lower level score is improved using the TOFD scheme. At upper level, the TOFD scheme shows a positive impact (as discussed previously through the increased surface drag reducing near surface winds, resulting in reduced gravity wave drag). However, the cutoff mountain experiment has a much stronger impact on the score at this level.

Figs. 45 to 48 show mean temperature errors over East Asia, showing that the TOFD scheme and cutoff mountain produce warming at 850, 500, and 100 hPa, with cooling at 200 hPa. This is consistent with Fig. 27 and Fig. 29. Note that a cooling at 200 hPa over the Northern Hemisphere is also observed (not shown).

2.6.2 North America

Fig. 49 shows the experiments have a mostly neutral impact on North America 500 hPa geopotential scores. However, Fig. 50 shows that at 100 hPa the cutoff mountain in combination with the TOFD scheme shows a strong improvement from day 1 at 100 hPa.

Figs. 51 and 52 shows neutral impact on 850 and 200 hPa vector wind scores over North America.

Figs. 53 to 56 show mean temperature error at 850, 500, 200, and 100 hPa. These indicate a warming at 850, 200 and 100 hPa, and a decrease in error at 200 and 100 hPa.
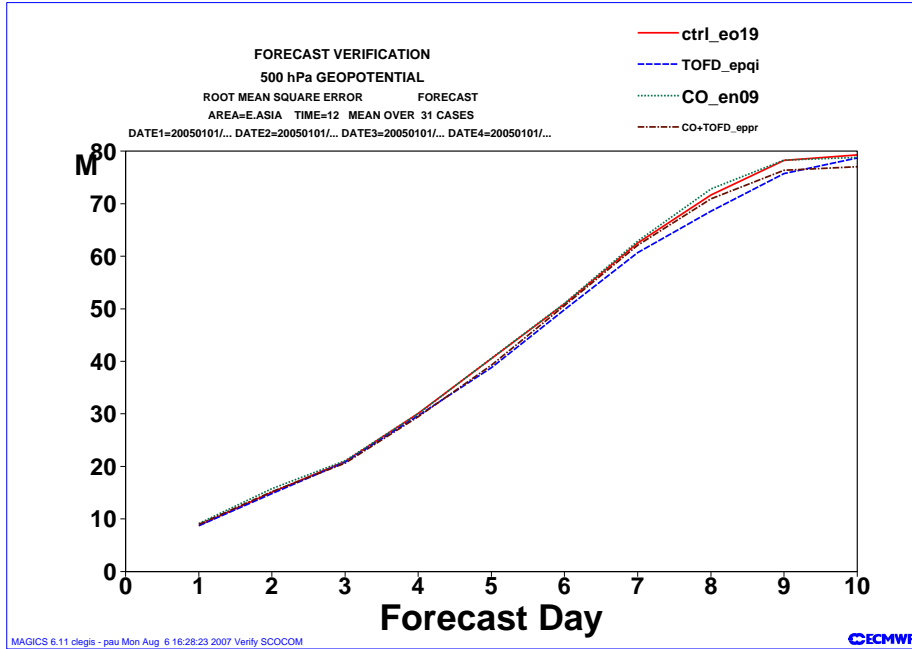
Figure 41: Mean 29R1 T511 500hPa geopotential root mean square error over E. Asia from 12Z on each day of January 2005. Red line labelled 'ctrl_eo19': control; blue line labelled 'tofd_epqi': TOFD only; green line labelled CO_en09: cutoff mountain technique only; brown line labelled 'CO+TOFD_epi7': cutoff mountain technique in combination with the TOFD scheme.
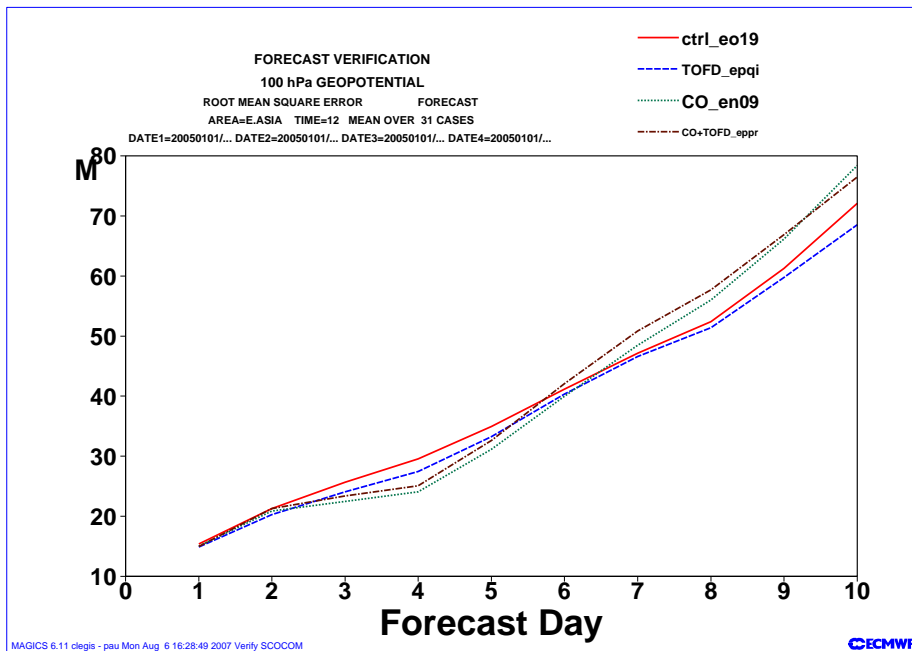
Figure 42: Mean 29R1 T511 100 hPa geopotential root mean square error over E. Asia from 12Z on each day of January 2005.
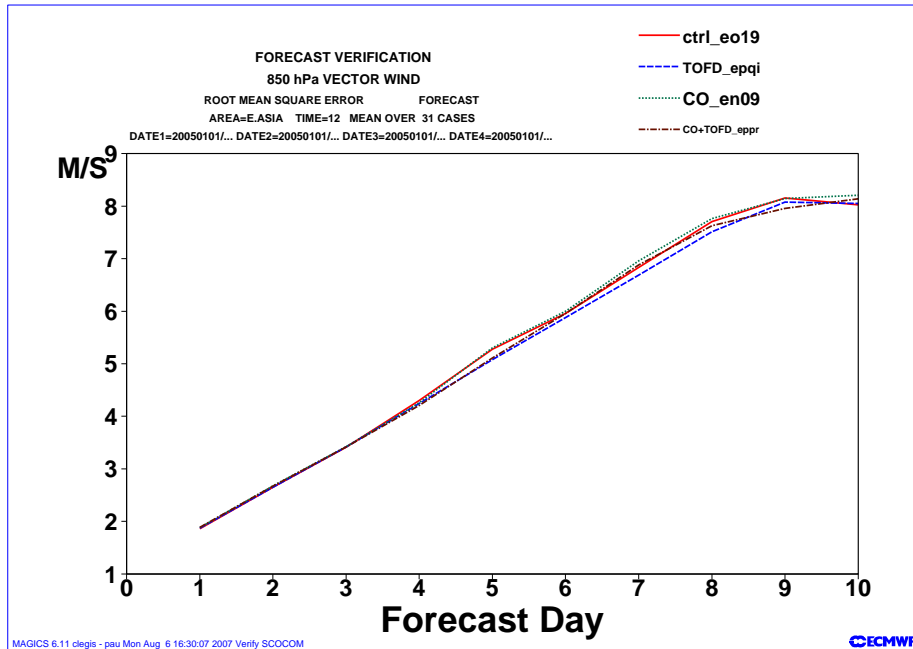
Figure 43: Mean 29R1 T511 850hPa vector wind root mean square error over E. Asia from 12Z on each day of January 2005. See Fig. 41 for details of legend.
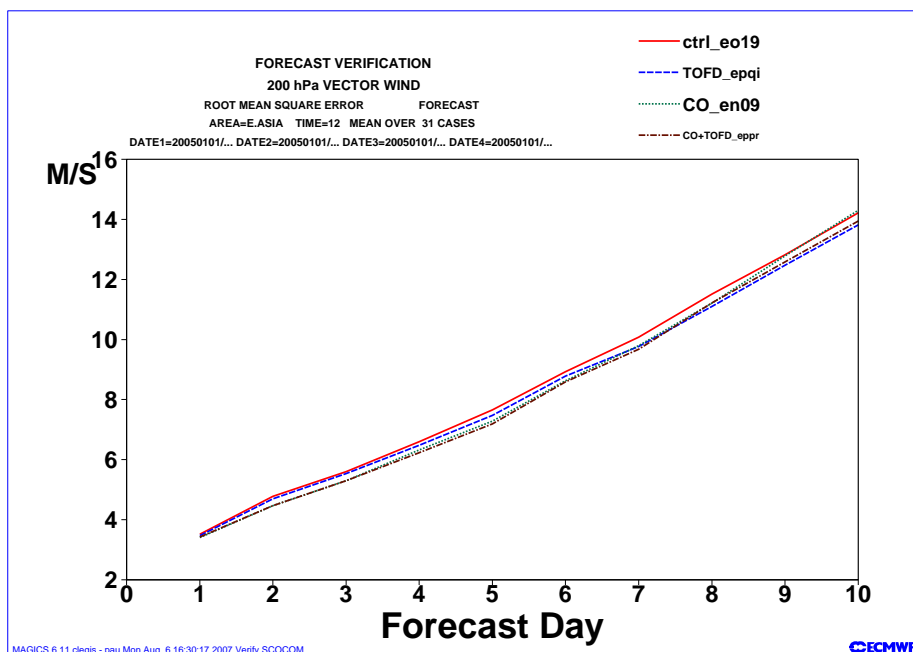
Figure 44: Mean 29R1 T511 200 hPa vector wind root mean square error over E. Asia from 12Z on each day of January 2005. See Fig. 41 for details of legend.
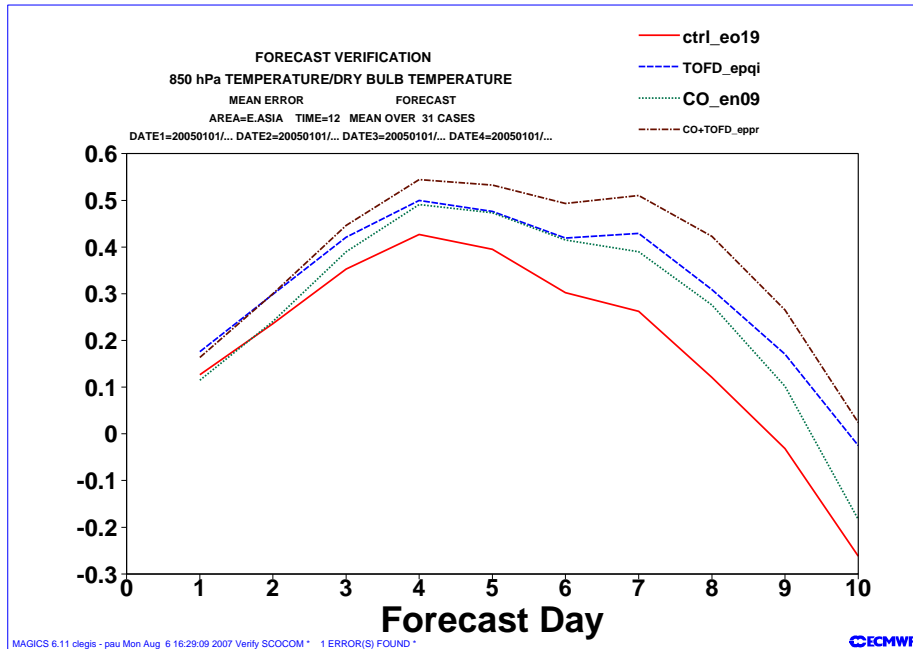
Figure 45: Mean 29R1 T511 850 hPa mean temperature error over E. Asia from 12Z on each day of January 2005. See Fig. 41 for details of legend.
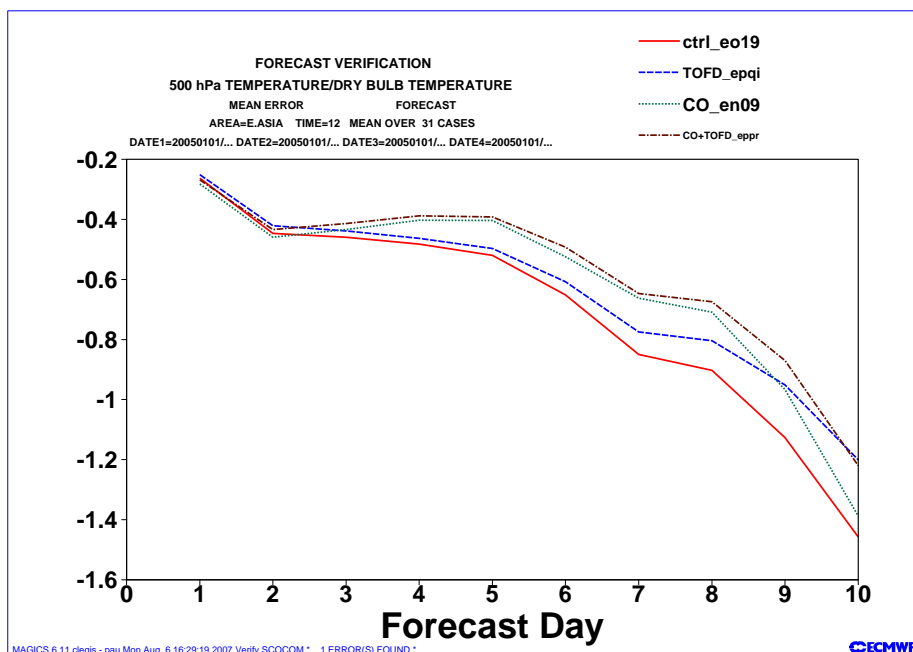
Figure 46: Mean 29R1 T511 500 hPa mean temperature error over E. Asia from 12Z on each day of January 2005. See Fig. 41 for details of legend.
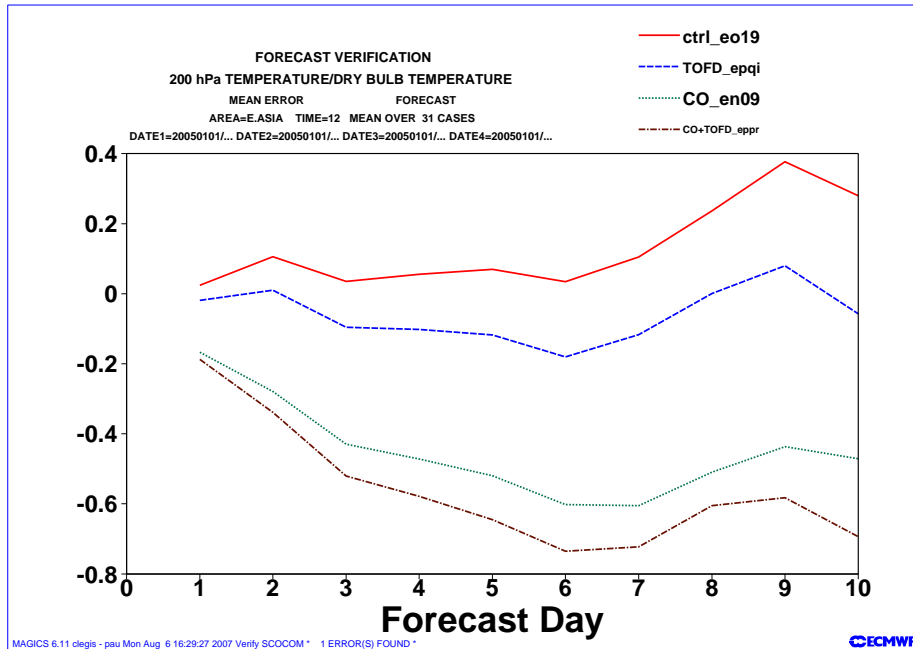
Figure 47: Mean 29R1 T511 200 hPa mean temperature error over E. Asia from 12Z on each day of January 2005. See Fig. 41 for details of legend.
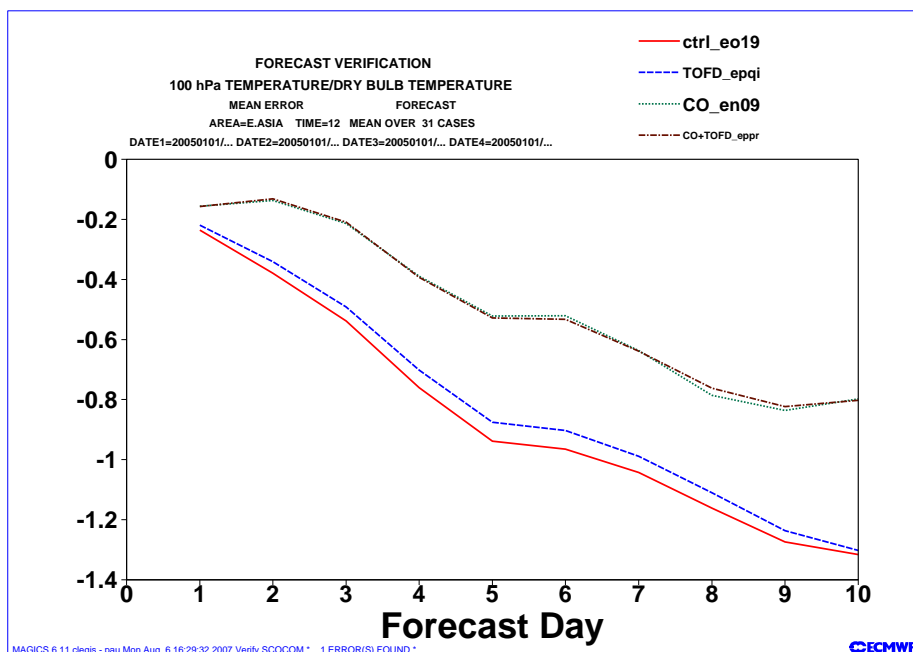
Figure 48: Mean 29R1 T511 100 hPa mean temperature error over E. Asia from 12Z on each day of January 2005. See Fig. 41 for details of legend.
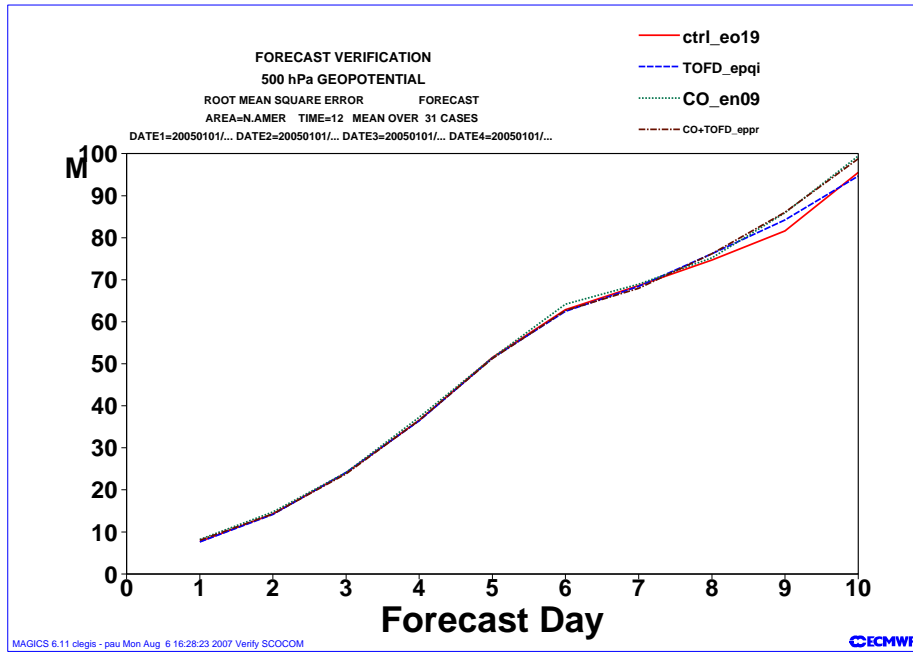
Figure 49: Mean 29R1 T511 500hPa geopotential root mean square error over N. Amer. from 12Z on each day of January 2005. See Fig. 41 for details of legend.
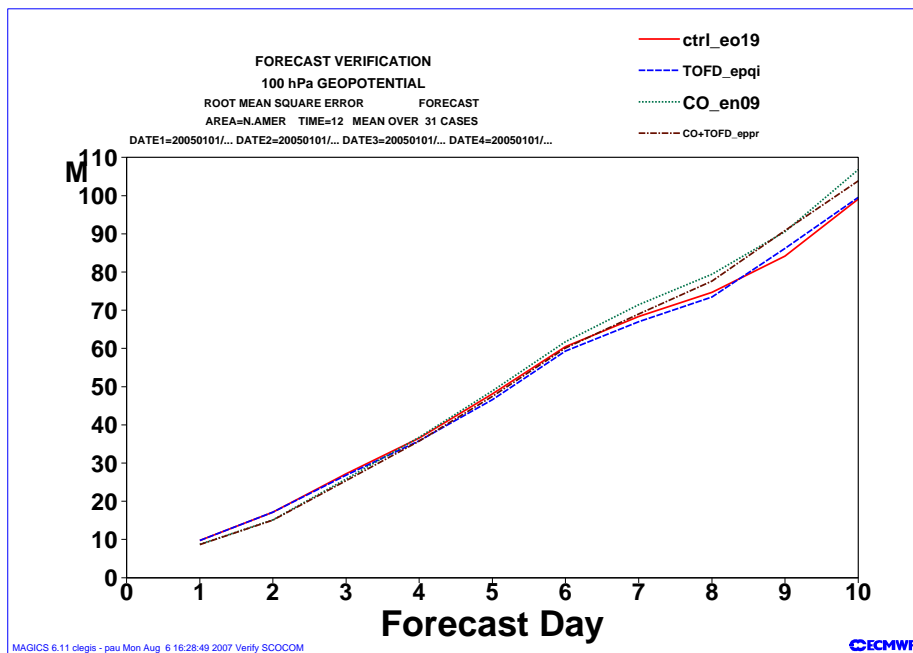
Figure 50: Mean 29R1 T511 100 hPa geopotential root mean square error over N. Amer. from 12Z on each day of January 2005. See Fig. 41 for details of legend.
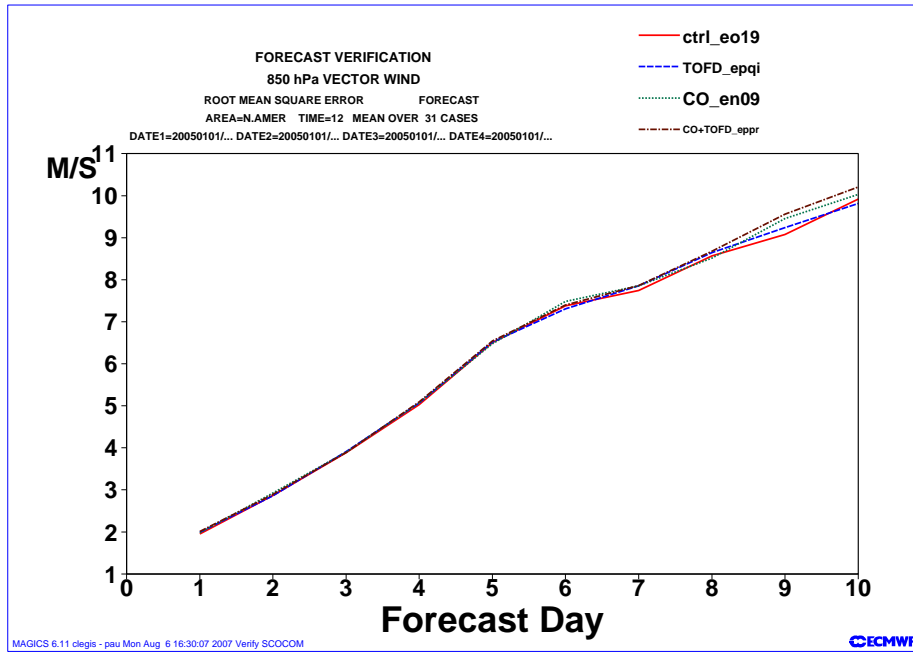
Figure 51: Mean 29R1 T511 850hPa vector wind root mean square error over N. Amer. from 12Z on each day of January 2005. See Fig. 41 for details of legend.
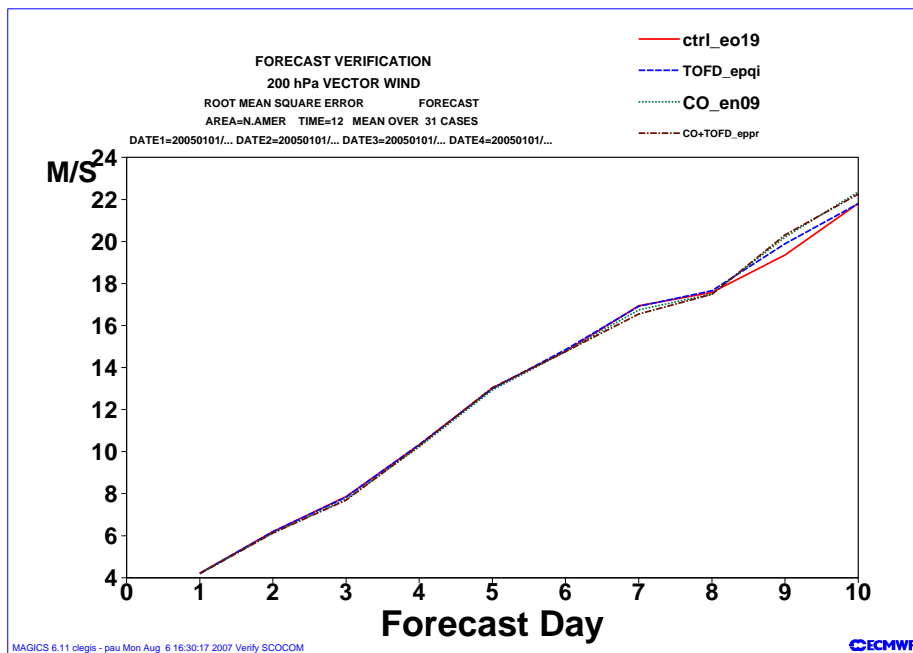
Figure 52: Mean 29R1 T511 200 hPa vector wind root mean square error over N. Amer. from 12Z on each day of January 2005. See Fig. 41 for details of legend.
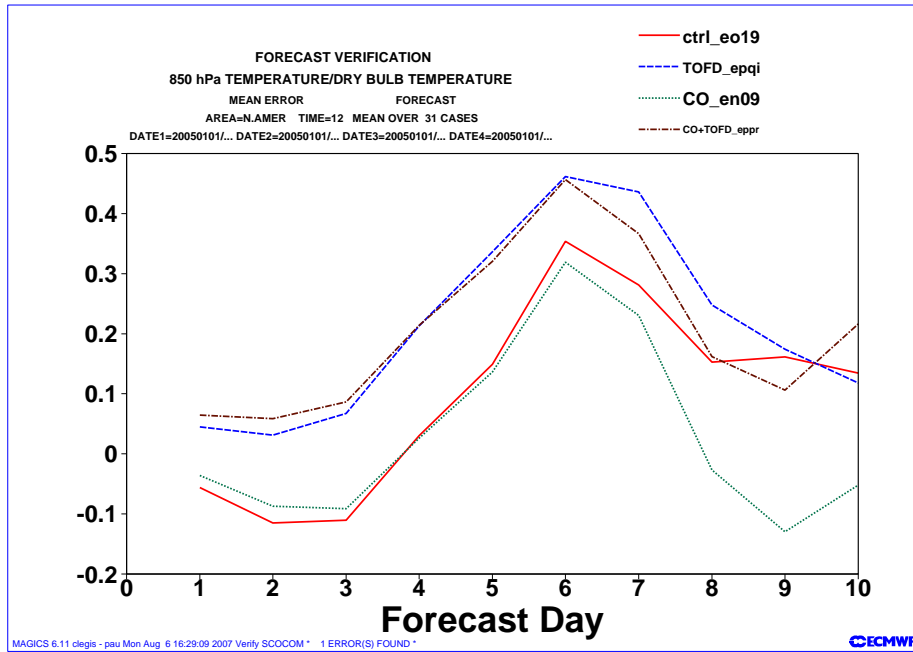
Figure 53: Mean 29R1 T511 850 hPa mean temperature error over N. Amer. from 12Z on each day of January 2005. See Fig. 41 for details of legend.
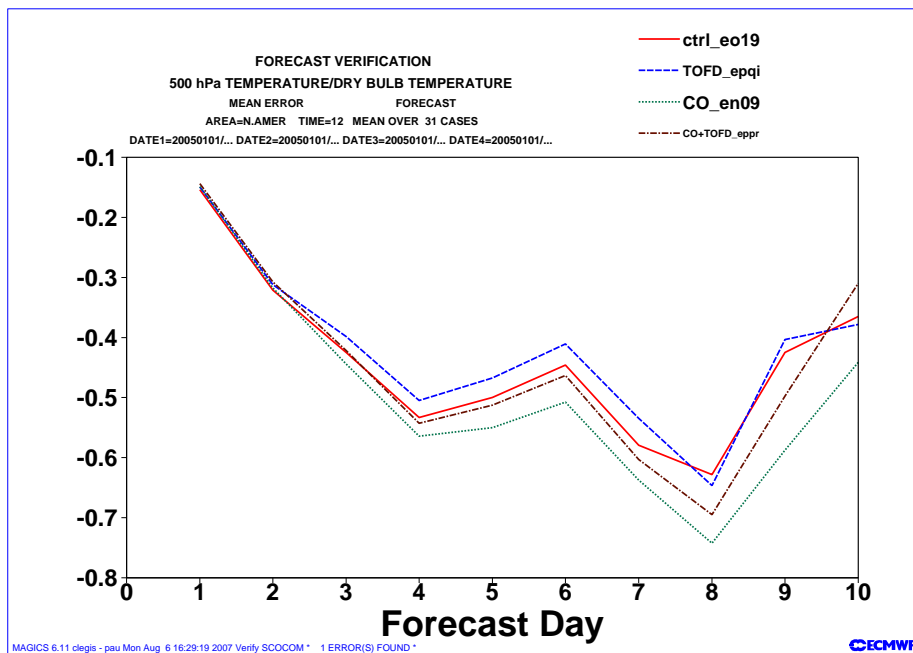
Figure 54: Mean 29R1 T511 500 hPa mean temperature error over N. Amer. from 12Z on each day of January 2005. See Fig. 41 for details of legend.
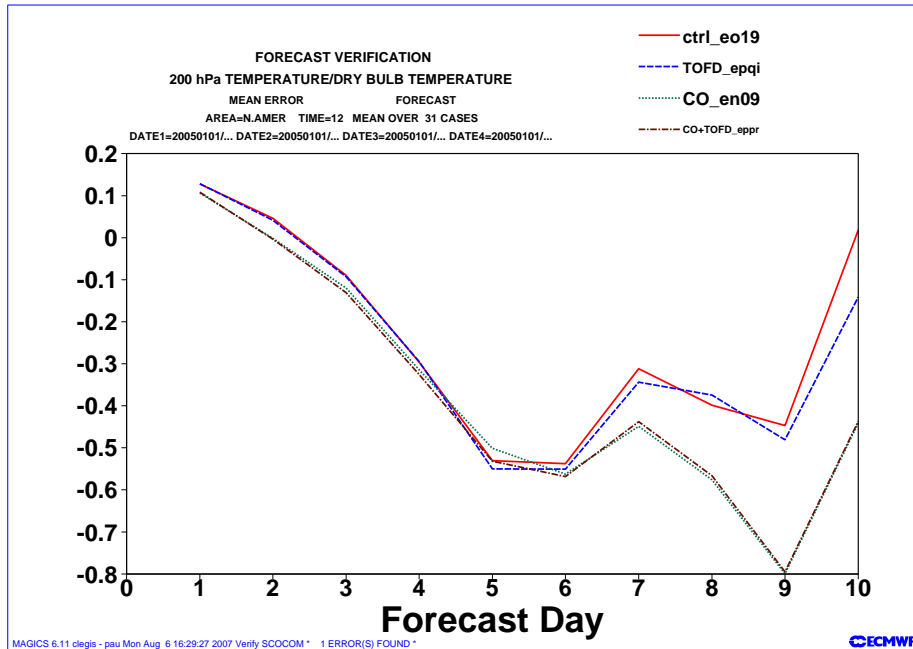
Figure 55: Mean 29R1 T511 200 hPa mean temperature error over N. Amer. from 12Z on each day of January 2005. See Fig. 41 for details of legend.
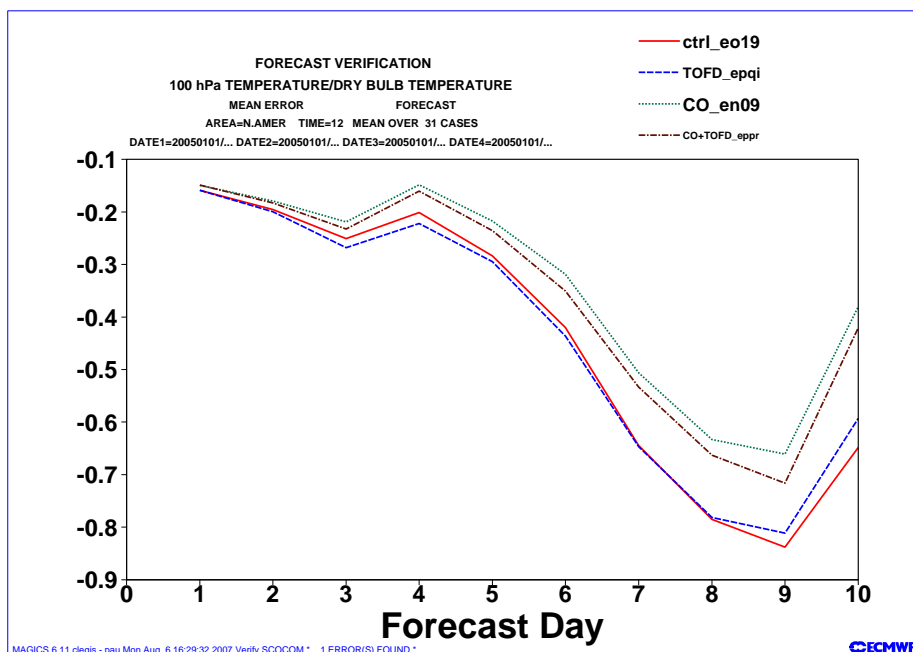
Figure 56: Mean 29R1 T511 100 hPa mean temperature error over N. Amer. from 12Z on each day of January 2005. See Fig. 41 for details of legend.

3   Evaluation of T511 springtime forecasts

3.1   Control results

Experiment en0a was run at T511 for each day of 10 March to 10 April 2004 at 12Z to produce a CY29R1 spring forecast.

Fig. 57 shows the en0a average vertically integrated zonal wind error (Pa s), indicating that the velocity deficit is smaller than the equivalent winter results (Fig. 1), particularly after 24 hours.

3.1.1   Himalayas

Fig. 58 presents a closer examination of the T511 control results for the Himalayan region, confirming that the spring vertically integrated zonal wind error is smaller than that of winter (Fig. 2). This is confirmed by comparing Fig. 59 with Fig. 4.

3.1.2   Rockies

Figs. 60 and 61 present a closer examination of the T511 control results for the Rockies. Comparing with Figs. 58 and 59 indicates that the wind error is smaller over the Rockies than the Himalayas. Comparing with Figs. 6 and 8 shows that the spring velocity error is slightly reduced compared to that at winter.
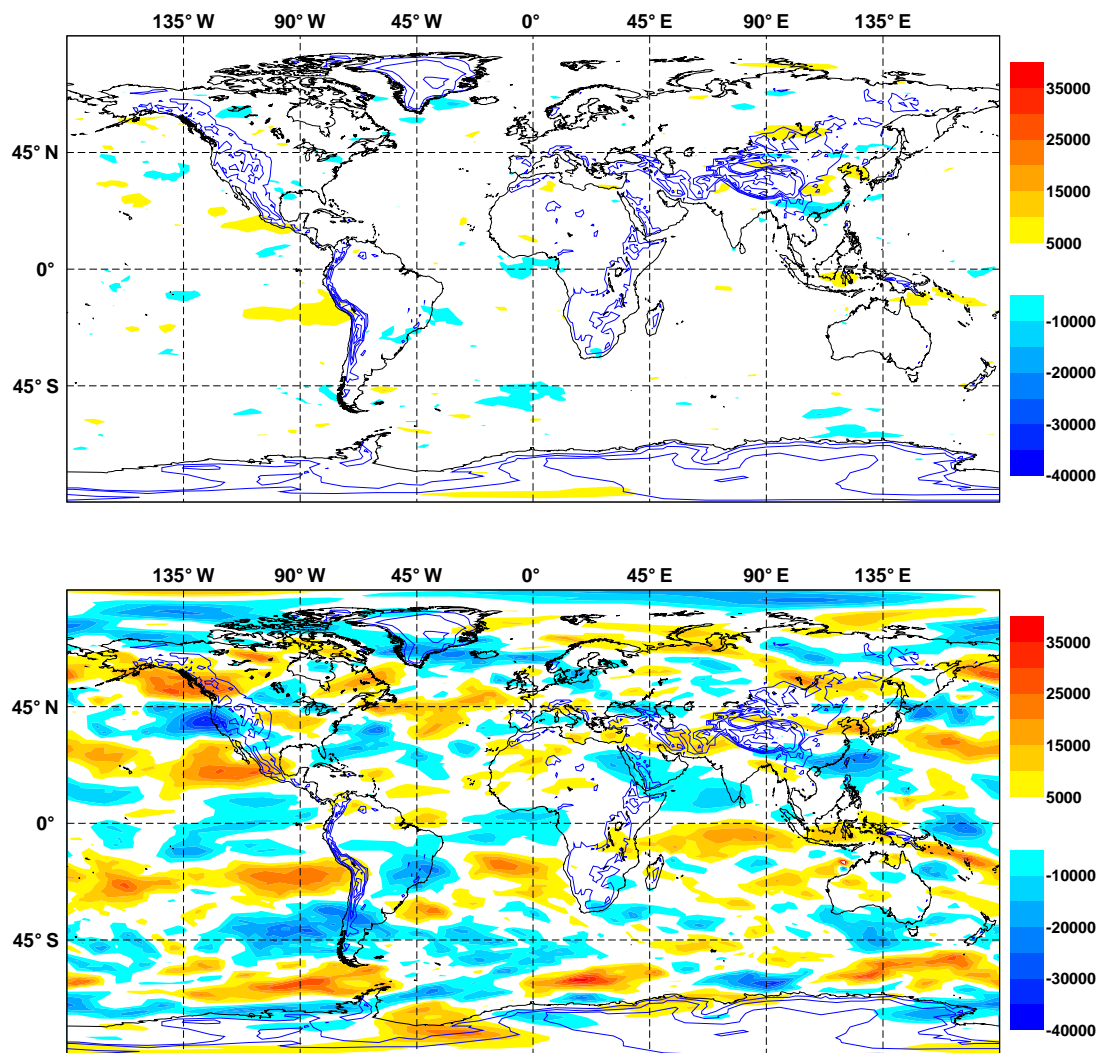
Figure 57: Experiment en0a average vertically integrated zonal wind error (Pa s) for 24 hour (top) and 96 hour (bottom) control T511 CY29R1 forecasts from 12Z on each day of 10 March to 10 April 2004. Also shown are contours of mean (T511) orography height from 1000 to 6000 m with a 1000 m interval.
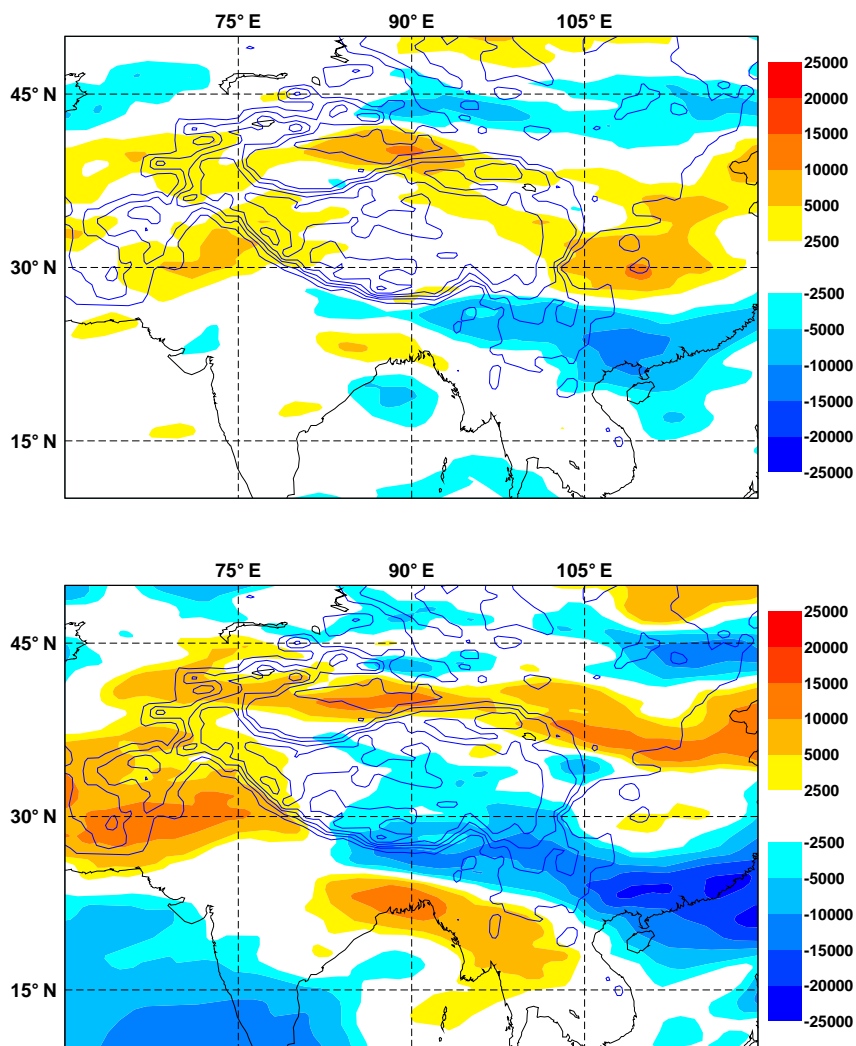
Figure 58: Experiment en0a average vertically integrated zonal wind error (Pa s) over the Himalayan region of south-east Asia for 24 hour (top) and 96 hour (bottom) control T511 CY29R1 forecasts from 12Z on each day of 10 March to 10 April 2004. Also shown are contours of mean (T511) orography height from 1000 to 6000 m with a 1000 m interval.
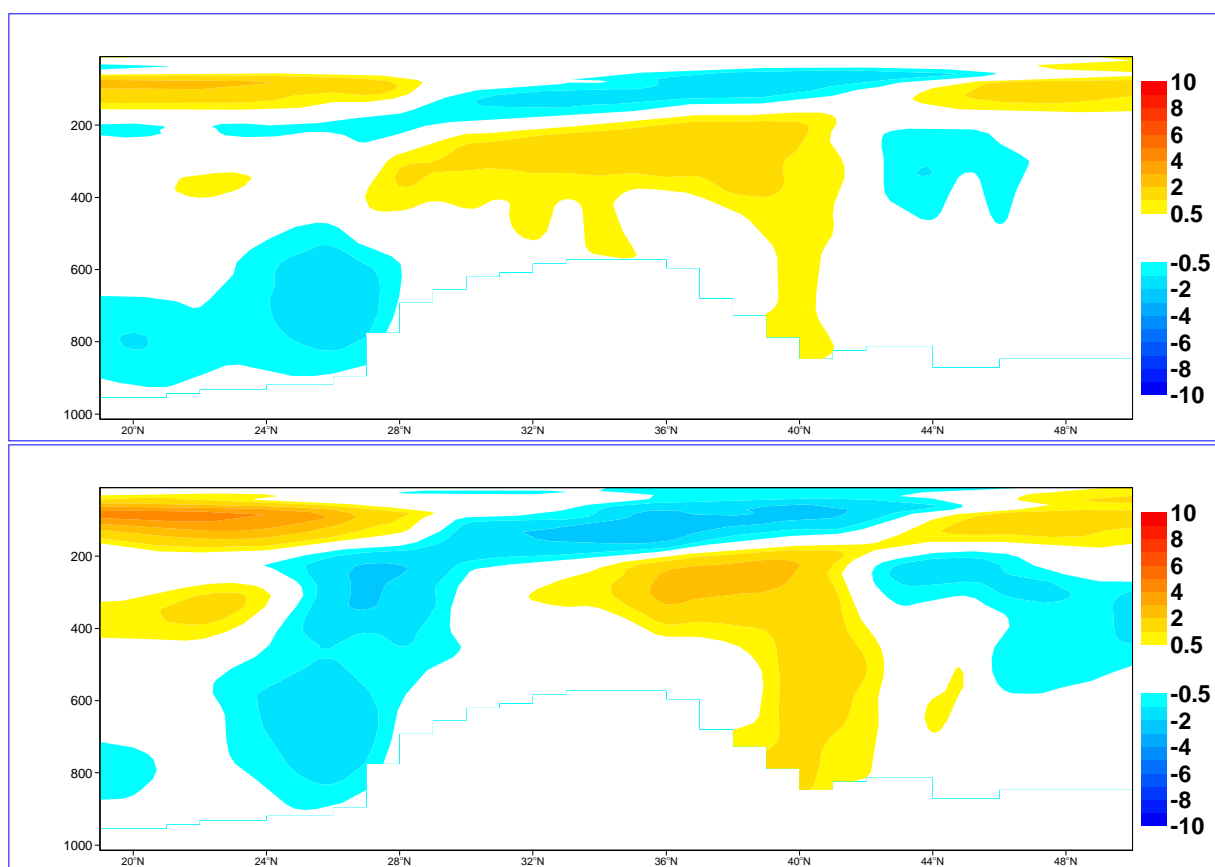
Figure 59: Experiment en0a mean zonal wind speed error (m s^{-1}) zonally averaged over the Himalayas between 75ºE and 105ºE for 24 hour (top) and 96 hour (bottom) control T511 CY29R1 forecasts from 12Z on each day of 10 March to 10 April 2004.
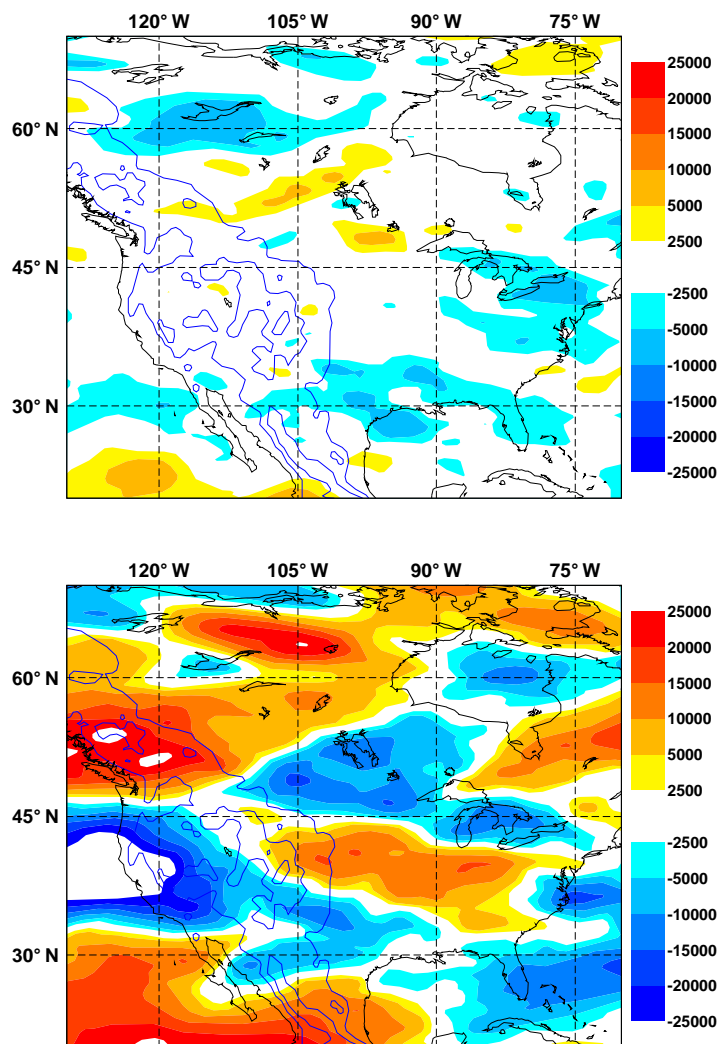
Figure 60: Experiment en0a average vertically integrated zonal wind error (Pa s) over North America for 24 hour (top) and 96 hour (bottom) control T511 CY29R1 forecasts from 12Z on each day of 10 March to 10 April 2004. Also shown are contours of mean (T511) orography height from 1000 to 6000 m with a 1000 m interval.
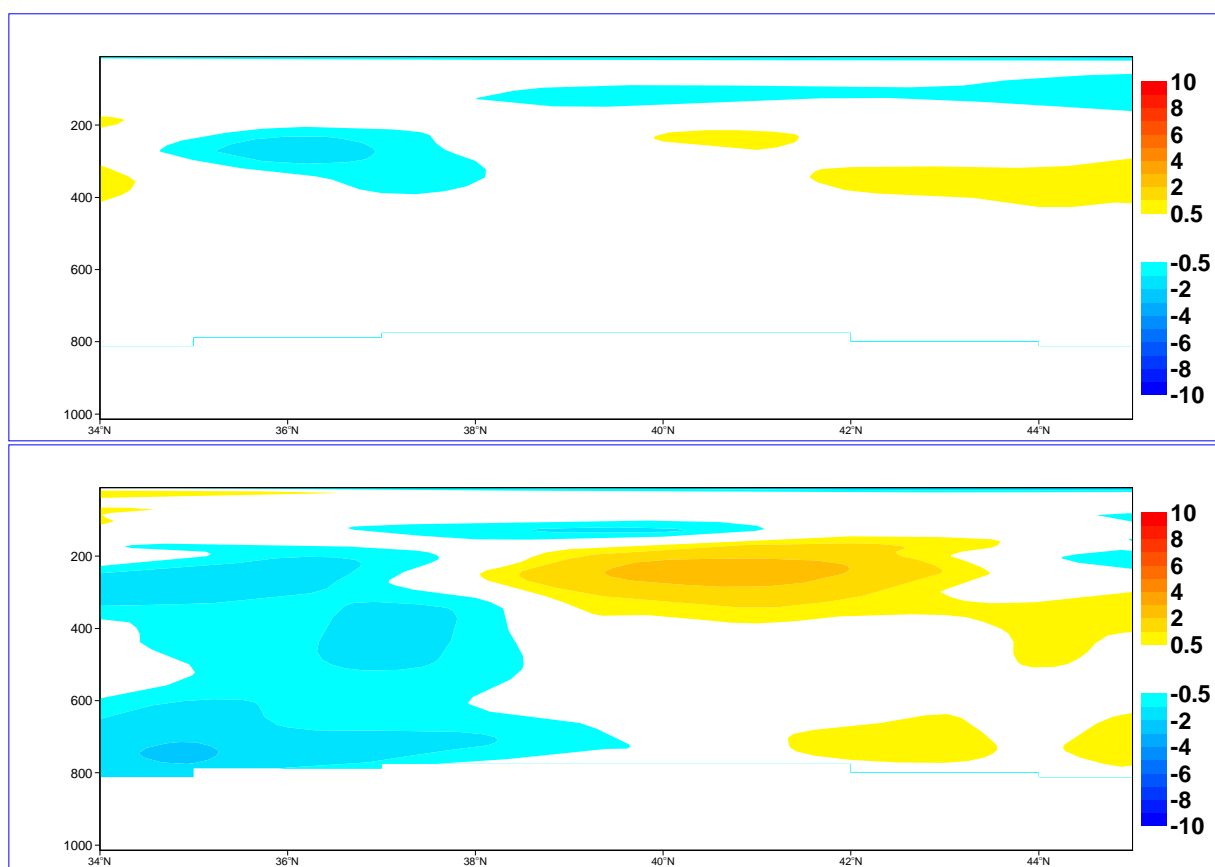
Figure 61: Experiment en0a mean zonal wind speed error (m s^{-1}) zonally averaged over the Rockies between 112°W and 104°W for 24 hour (top) and 96 hour (bottom) control T511 CY29R1 forecasts from 12Z on each day of 10 March to 10 April 2004.

3.2 Evaluation of the turbulent orographic form drag scheme in combination with the cutoff mountain

Experiment eq7e was ran at T511 for each day of 10 March to 10 April 2004 at 12Z to produce CY29R1 spring forecasts with the TOFD scheme in combination with the cutoff mountain technique.

3.2.1 *Himalayas*

Fig. 62 shows the average vertically integrated zonal wind error for 96 hour forecasts. The middle panel shows the impact of the experiment is to speed up the flow over the Himalayas, resulting in a quite large positive bias over most of the region. This impact is confirmed by Fig. 63, which shows that the negative velocity bias is replaced by a positive velocity bias. Fig. 64 confirms that in terms of zonal velocity the impact of the experiment is overly excessive.

3.2.2 *Rockies*

Figs. 65 to 67 indicate that the impact of the experiment is minimal over the Rockies.
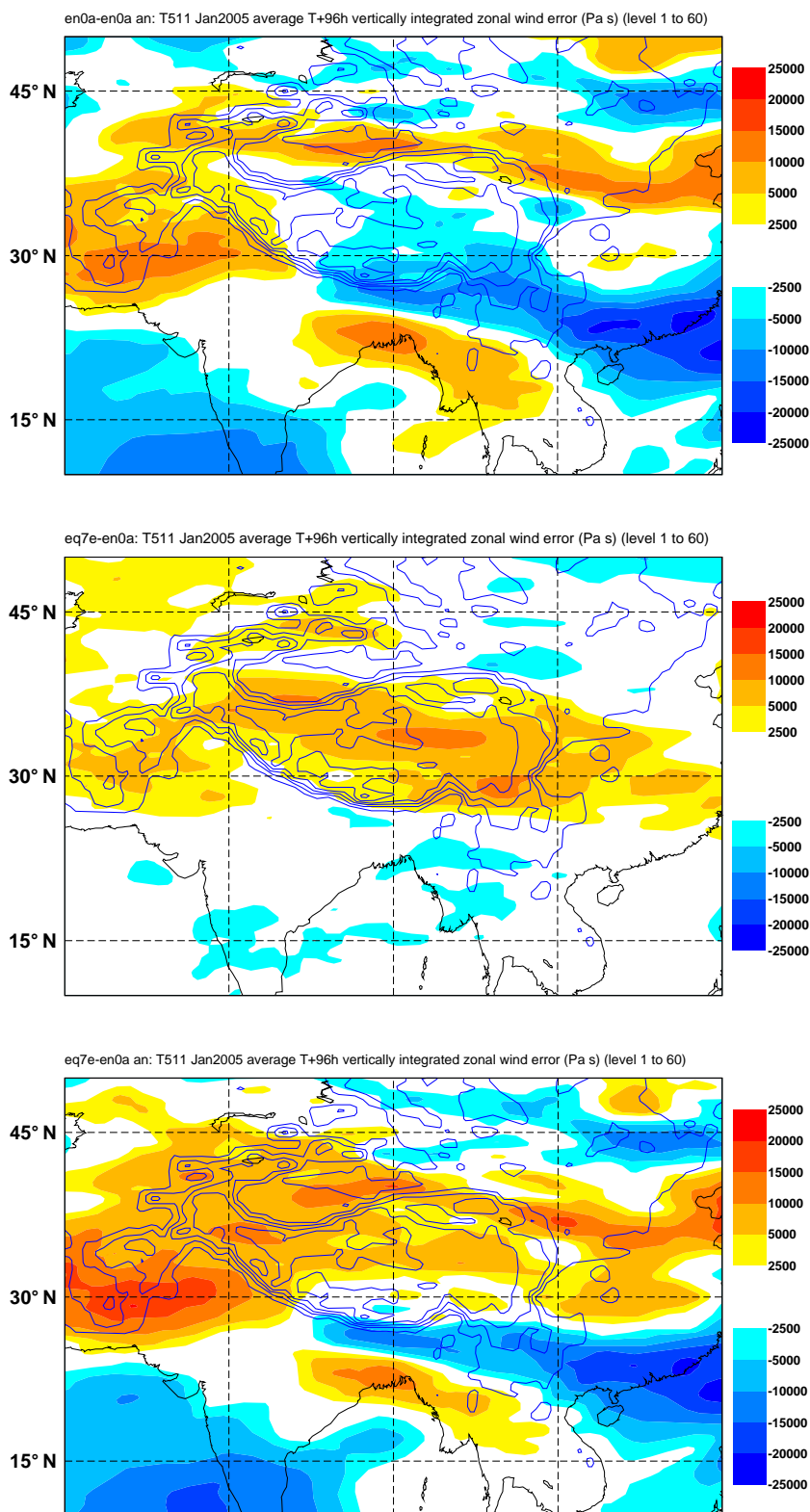
Figure 62: Experiment eq7e average vertically integrated zonal wind difference fields (Pa s) over the Himalayan region of south-east Asia for 96 hour T511 CY29R1 forecasts from 12Z on each day of 10 March to 10 April 2004 using the cutoff mountain technique in combination with the TOFD scheme. Top panel: control error; middle panel: impact of experiment; bottom panel: experiment error. Also shown are contours of mean (T511) orography height from 1000 to 6000 m with a 1000 m interval.
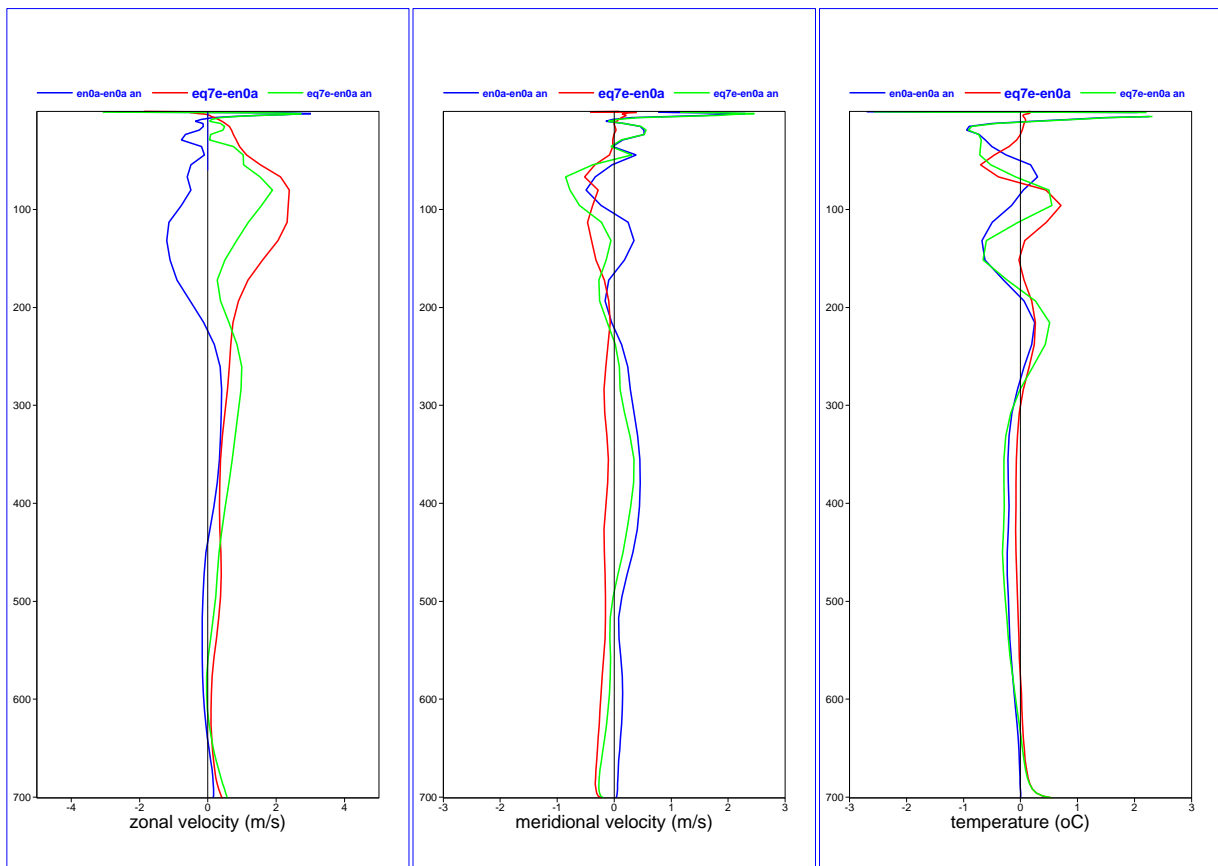
Figure 63: Experiment eq7e vertical profiles of difference fields averaged over the Himalayas (26°N to 40°N and 75°E to 105°E) for 96 hour T511 CY29R1 forecasts from 12Z on each day of 10 March to 10 April 2004 using the cutoff mountain technique in combination with the TOFD scheme. Left panel: zonal velocity (m s⁻¹); middle panel: meridional velocity (m s⁻¹); right panel: temperature (K). Blue lines: control error; red lines: impact of experiment; green lines: experiment error.
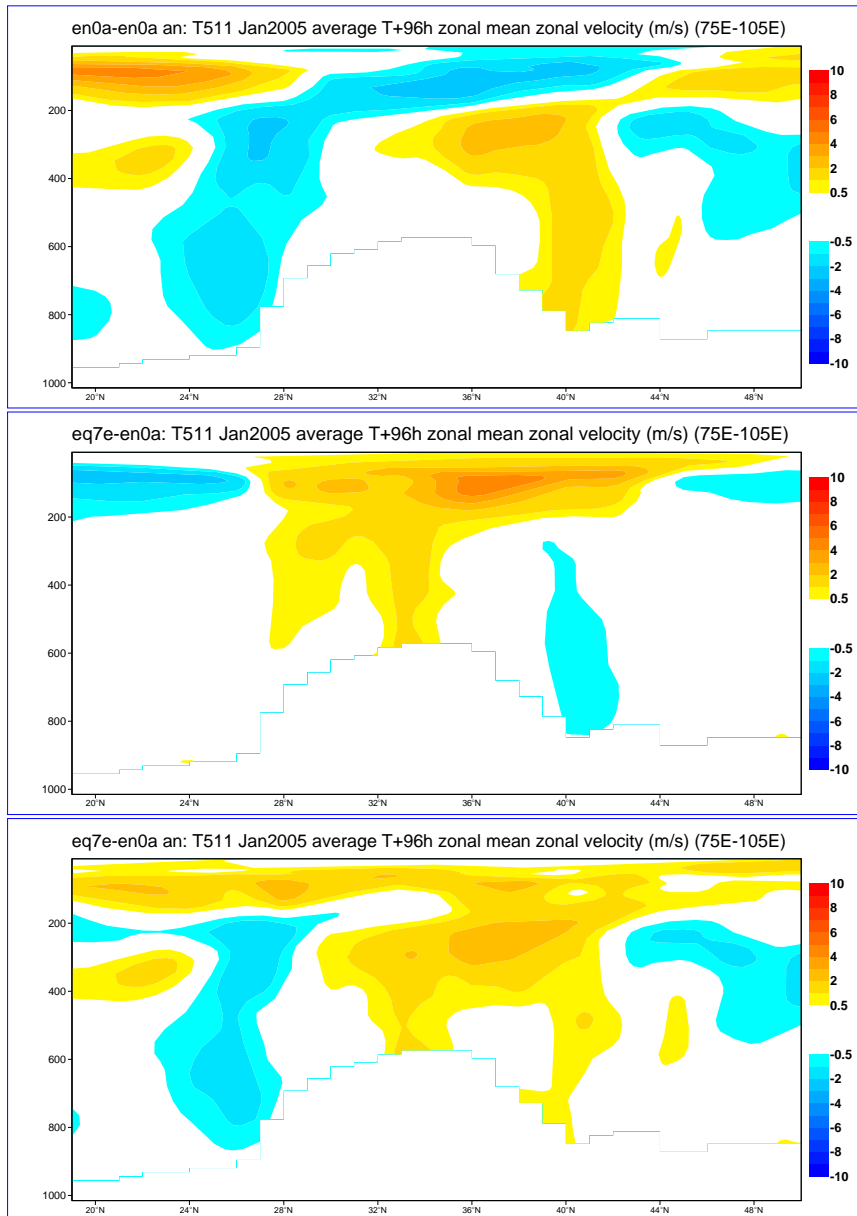
Figure 64: Experiment eq7e mean zonal wind difference fields (m s^{-1}) zonally averaged over the Himalayas between 75°E and 105°E for 96 hour CY29R1 forecasts from 12Z on each day of 10 March to 10 April 2004 using the cutoff mountain technique in combination with the TOFD scheme. Top panel: control error; middle panel: impact of experiment; bottom panel: experiment error.
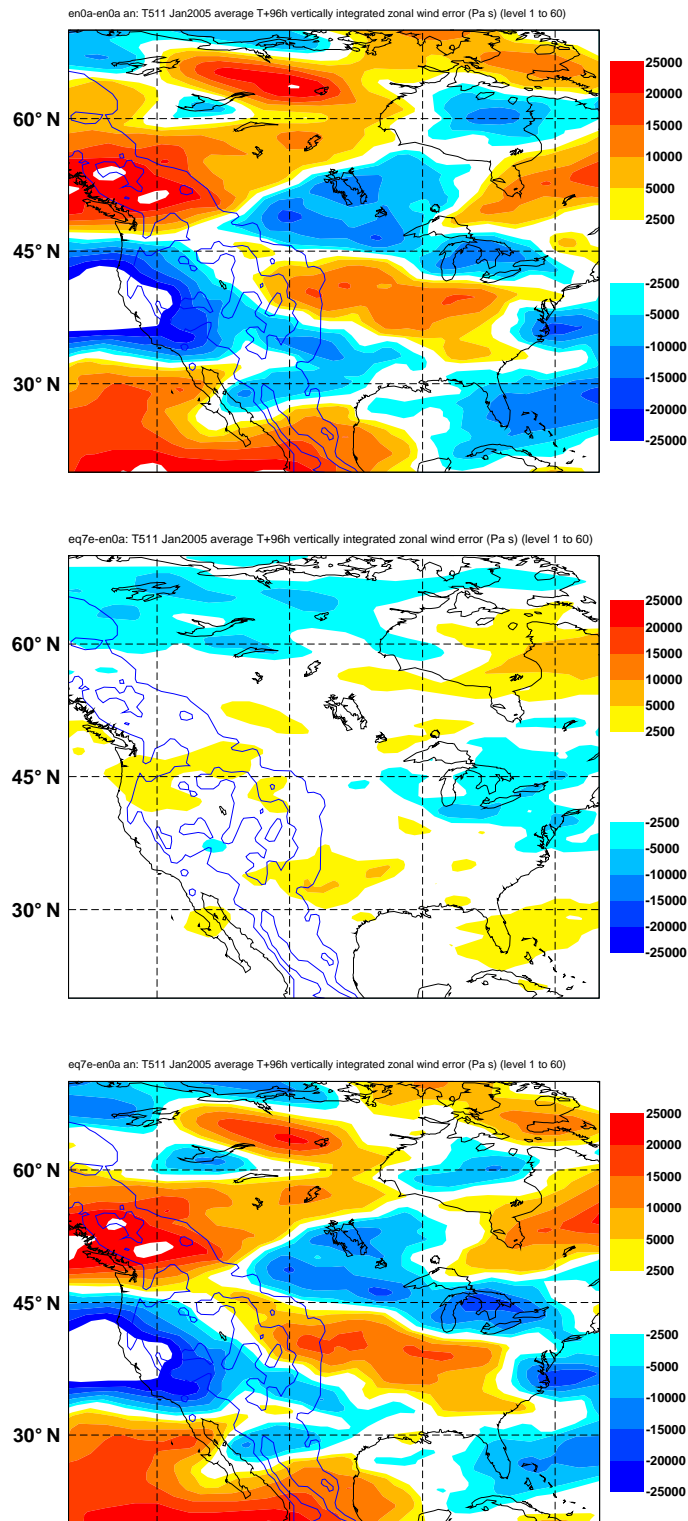
Figure 65: Experiment eq7e average vertically integrated zonal wind difference fields (Pa s) over North America for 96 hour T511 CY29R1 forecasts from 12Z on each day of 10 March to 10 April 2004 using the cutoff mountain technique in combination with the TOFD scheme. Top panel: control error; middle panel: experiment impact; bottom panel: experiment impact. Also shown are contours of mean (T511) orography height from 1000 to 6000 m with a 1000 m interval.
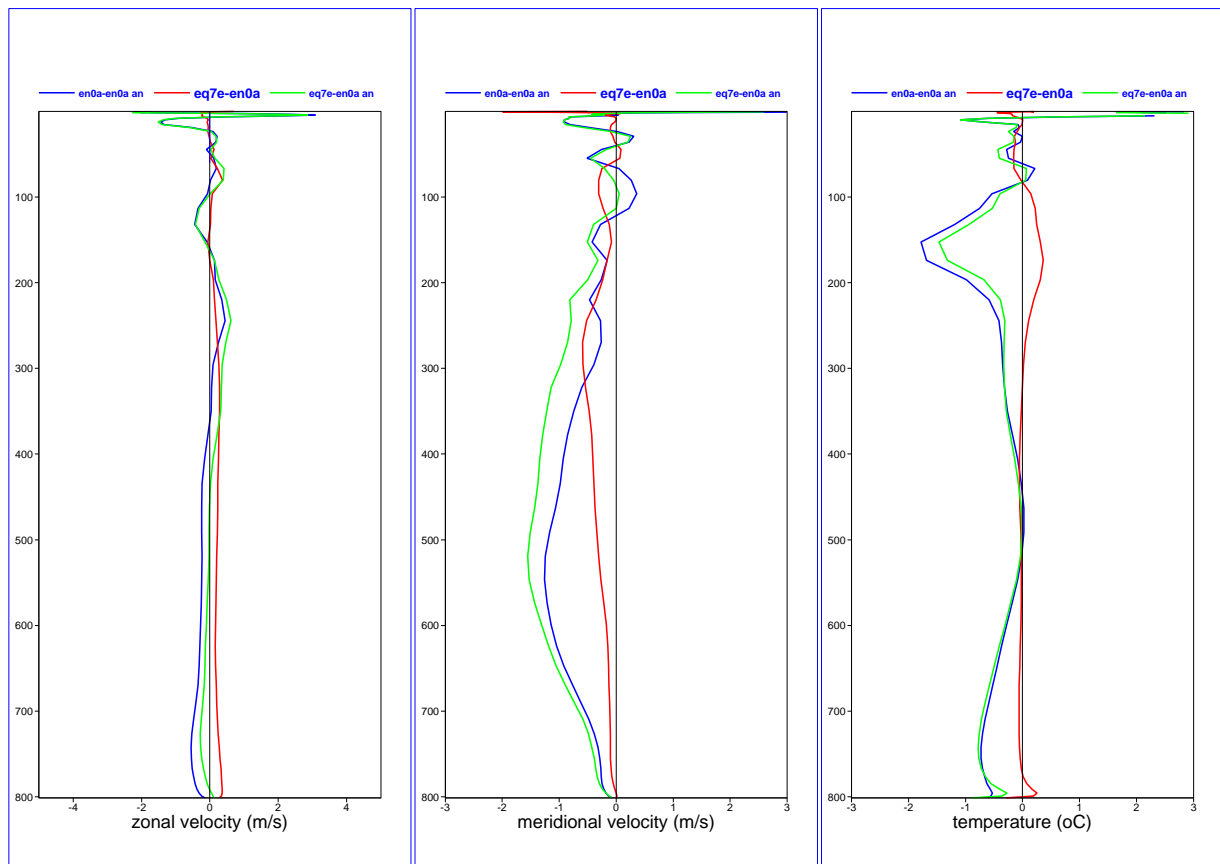
Figure 66: Experiment eq7e vertical profiles of difference fields averaged over the Rockies (34°N to 45°N and 112°W to 104°W) for 96 hour T511 CY29R1 forecasts from 12Z on each day of 10 March to 10 April 2004 using the cutoff mountain technique in combination with the TOFD scheme. Left panel: zonal velocity (m s^{-1}); middle panel: meridional velocity (m s^{-1}); right panel: temperature (K). Blue lines: control error; red lines: impact of experiment; green lines: experiment error.
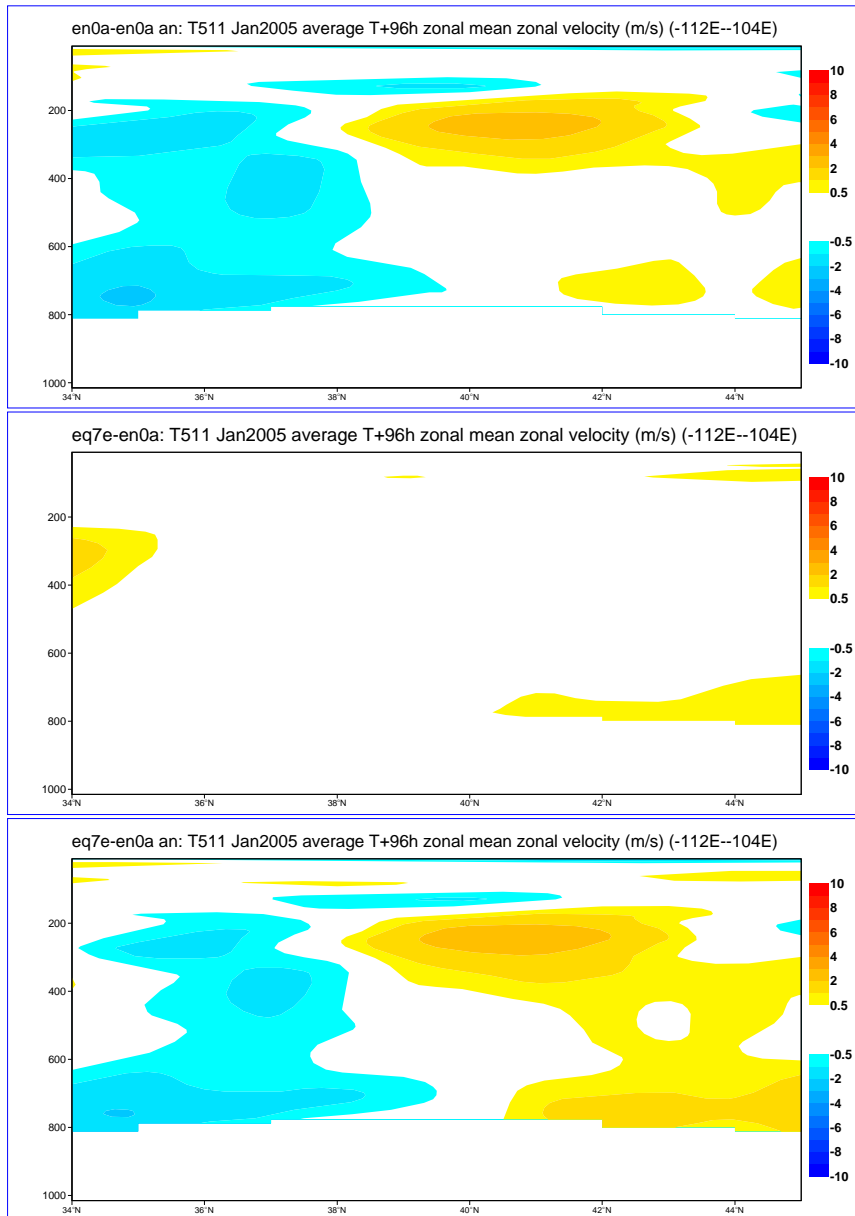
Figure 67: Experiment eq7e zonal wind speed difference fields (m s^{-1}) zonally averaged over the Rockies between 112°W and 104°W for 96 hour T511 CY29R1 forecasts from 12Z on each day of 10 March to 10 April 2004 using the cutoff mountain technique in combination with the TOFD scheme. Top panel: control error; middle panel: impact of experiment; bottom panel: experiment error.

4 Evaluation of T95 wintertime forecasts

4.1 Control results

Experiment epql was run at T95 for each day of January 2005 at 12Z to produce control CY29R1 winter forecasts.

Fig. 68 shows the epql average vertically integrated zonal wind error (Pa s) for 24 hour (top) and 96 hour (bottom) forecasts. Areas of significant velocity deficit are evident downstream of much of the Earth's orography. Comparing with the equivalent plot at T511 (Fig. 1) shows that the velocity deficit is stronger at T95 (Brown 2004a).

4.1.1 Himalayas

Fig. 69 presents a closer examination of the T95 control results for the Himalayan region, confirming the marked velocity deficit. After 96 hours this has reached around -40000 Pa s over and downstream of the Himalayas. Fig. 70 shows that the velocity deficit is considerable throughout much of the atmosphere, reaching around 10 m s^{-1} at upper levels.

Fig. 3 shows 96 hour T95 mean vertical profiles of zonal velocity (left), meridional velocity (middle), and temperature (right) errors averaged over the Himalayan region. The zonal wind error is around -2 m s^{-1} below 400 hPa, increasing to around -4 m s^{-1} by 200 hPa. The meridional velocity error is approximately 1 m s^{-1} at lower ($\sim$ 500 hPa) and upper levels ($\sim$ 100 hPa). At near-surface the temperature error is positive, though this quickly changes to a negative bias of around -0.75 K which persists to a height of around 300 hPa. Above this height the bias varies between 1 and -1 K. The errors at T95 are noticeably larger than those at T511.

4.1.2 Rockies

Fig. 71 presents a closer examination of the T95 control results for the Rockies. As with the Himalayas, the decrease in resolution (compared to T511 (Fig. 6)) results in an increase in wind error. This is confirmed by Fig. 72, which also emphasises the large regions of velocity surplus.

Fig. 7 shows the equivalent of Fig. 3, but averaged over the Rockies. Although the zonal velocity bias is small throughout the depth of the atmosphere, it has reversed from being predominately negative at T511 to positive at T95. This is consistent with the results discussed above. The meridional velocity error is around 2 m s^{-1} for most of the depth of the atmosphere. The temperature error is between -1 and -2 K up to 300 hPa. Above this height it is around 1 K. Both the meridional velocity and temperature errors are larger at T95 than T511.
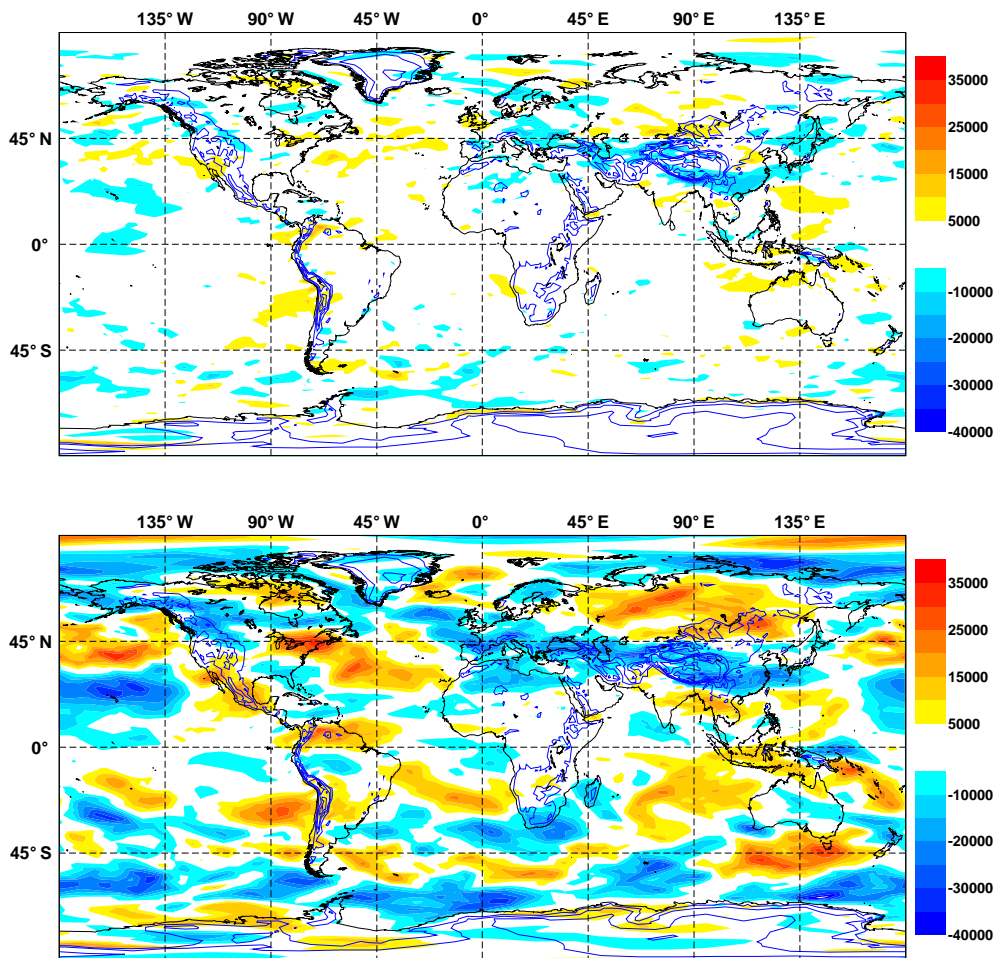
Figure 68: Experiment epql average vertically integrated zonal wind error for 24 hour (top) and 96 hour (bottom) control T95 CY29R1 forecasts from 12Z on each day of January 2005. Also shown are contours of mean (T511) orography height from 1000 to 6000 m with a 1000 m interval.
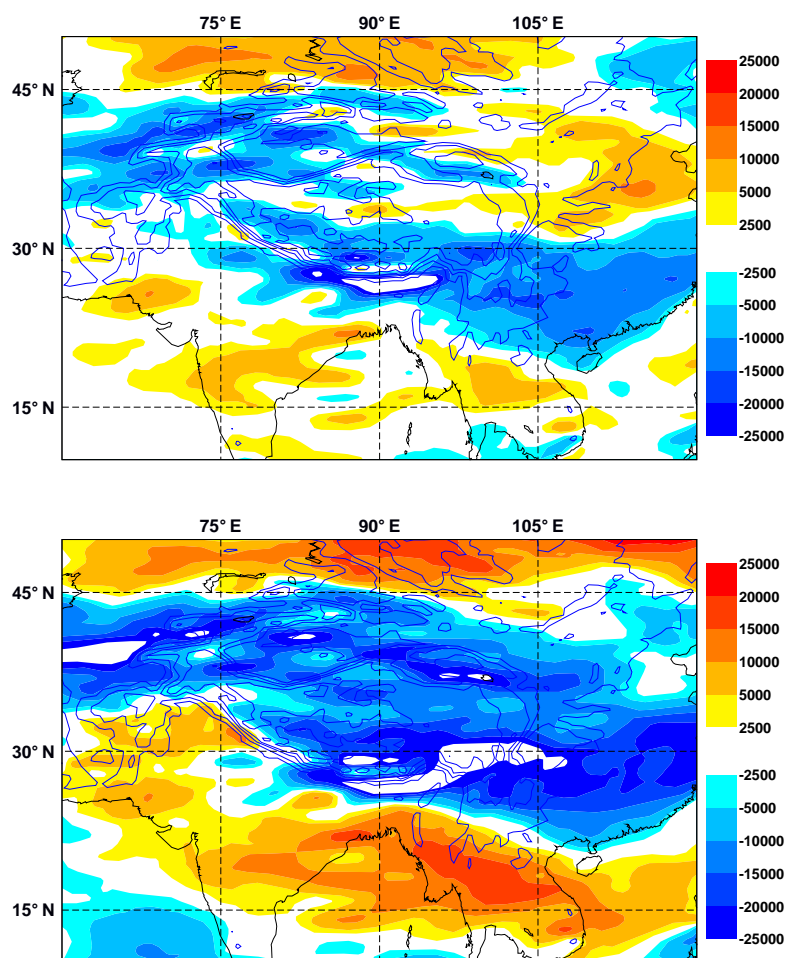
Figure 69: Experiment epql average vertically integrated zonal wind error over the Himalayan region of south-east Asia for 24 hour (top) and 96 hour (bottom) control T95 CY29R1 forecasts from 12Z on each day of January 2005. Also shown are contours of mean (T511) orography height from 1000 to 6000 m with a 1000 m interval.
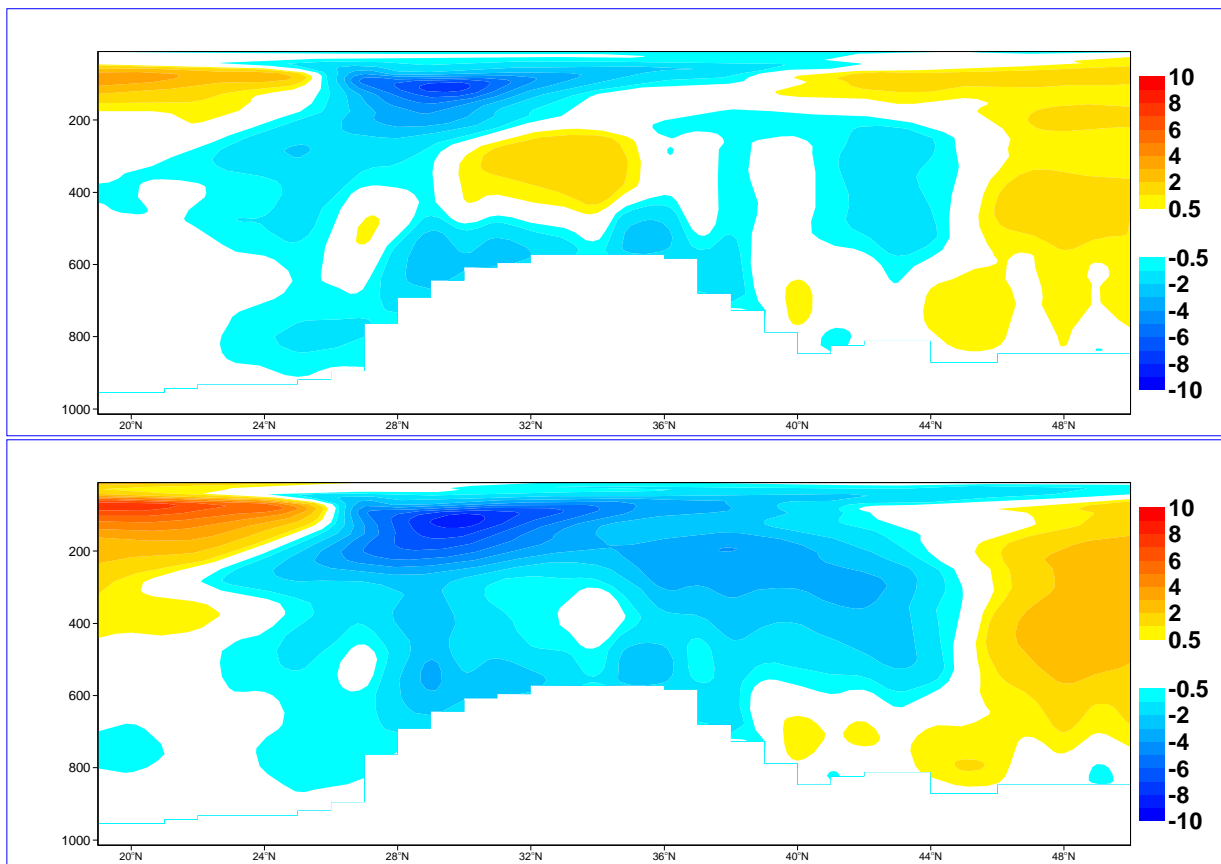
Figure 70: Experiment epql mean zonal wind speed error zonally averaged over the Himalayas between 75ºE and 105ºE from 24 hour (top) and 96 hour (bottom) control T95 CY29R1 forecasts from 12Z on each day of January 2005.
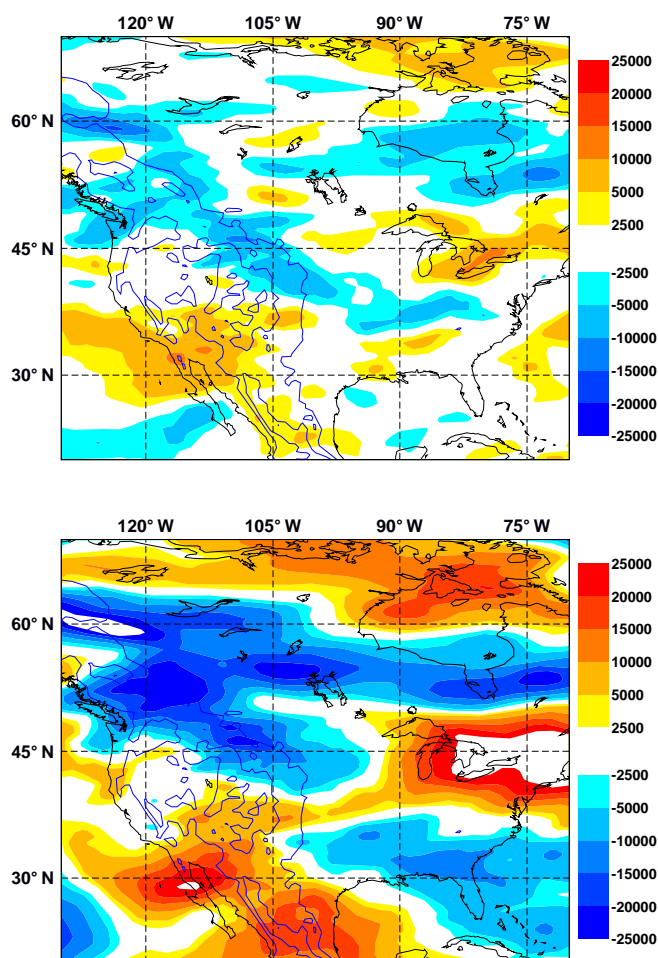
Figure 71: Experiment epql average vertically integrated zonal wind error over North America in 24 hour (top) and 96 hour (bottom) control T95 CY29R1 forecasts from 12Z on each day of January 2005. Also shown are contours of mean (T511) orography height from 1000 to 6000 m with a 1000 m interval.
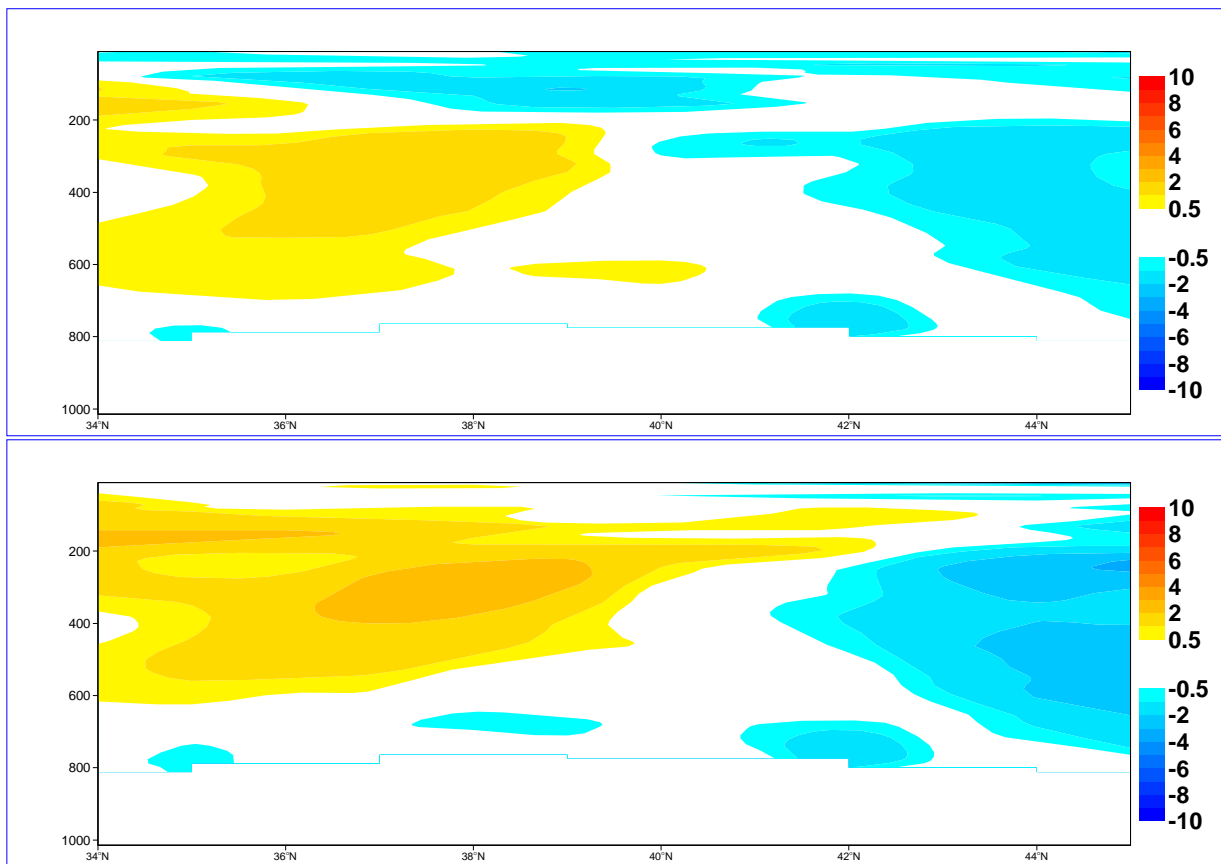
Figure 72: Experiment epql mean zonal wind speed error zonally averaged over the Rockies between 112ºW *and* 104ºW *in 24 hour (top) and 96 hour (bottom) control T95 CY29R1 forecasts from 12Z on each day of January 2005.*

4.2 Evaluation of the cutoff mountain technique in combination with the turbulent orographic form drag scheme

Experiment eprb was ran at T95 for each day of January 2005 at 12Z to produce CY29R1 winter forecasts with the TOFD scheme in combination with the cutoff mountain technique.

4.2.1 *Himalayas*

Fig. 73 shows average vertically integrated zonal wind difference fields for 96 hour forecasts. The impact of the experiment (middle panel) is much stronger than the equivalent T511 results (Fig. 26). Accordingly, the bottom panel shows a large reduction in the velocity deficit over and downwind of the Himalayas.

Fig. 74 shows that the speed up in zonal velocity occurs throughout much of the troposphere, with the maximum impact at around 100 hPa, which broadly reduces the bias. Meridional velocity and temperature biases are also largely reduced.

Fig. 75 confirms that the impact of the experiment is to increase the zonal flow through much of the atmosphere, and in particular above 200 hPa.

4.2.2 *Rockies*

Fig. 76 shows that at T95 the impact of the experiment is smaller over the Rockies than the Himalayas. However, comparing to the equivalent T511 results (Fig. 31) shows, over the Rockies, considerably greater impact at T95.

Fig. 77 shows that the experiment causes a modest increase in zonal velocity throughout the depth of the atmosphere, resulting in an increase in the already positive zonal velocity bias. Biases in meridional velocity and temperature are reduced.

The almost uniform speed up of zonal flow throughout the atmosphere is confirmed by Fig. 78.
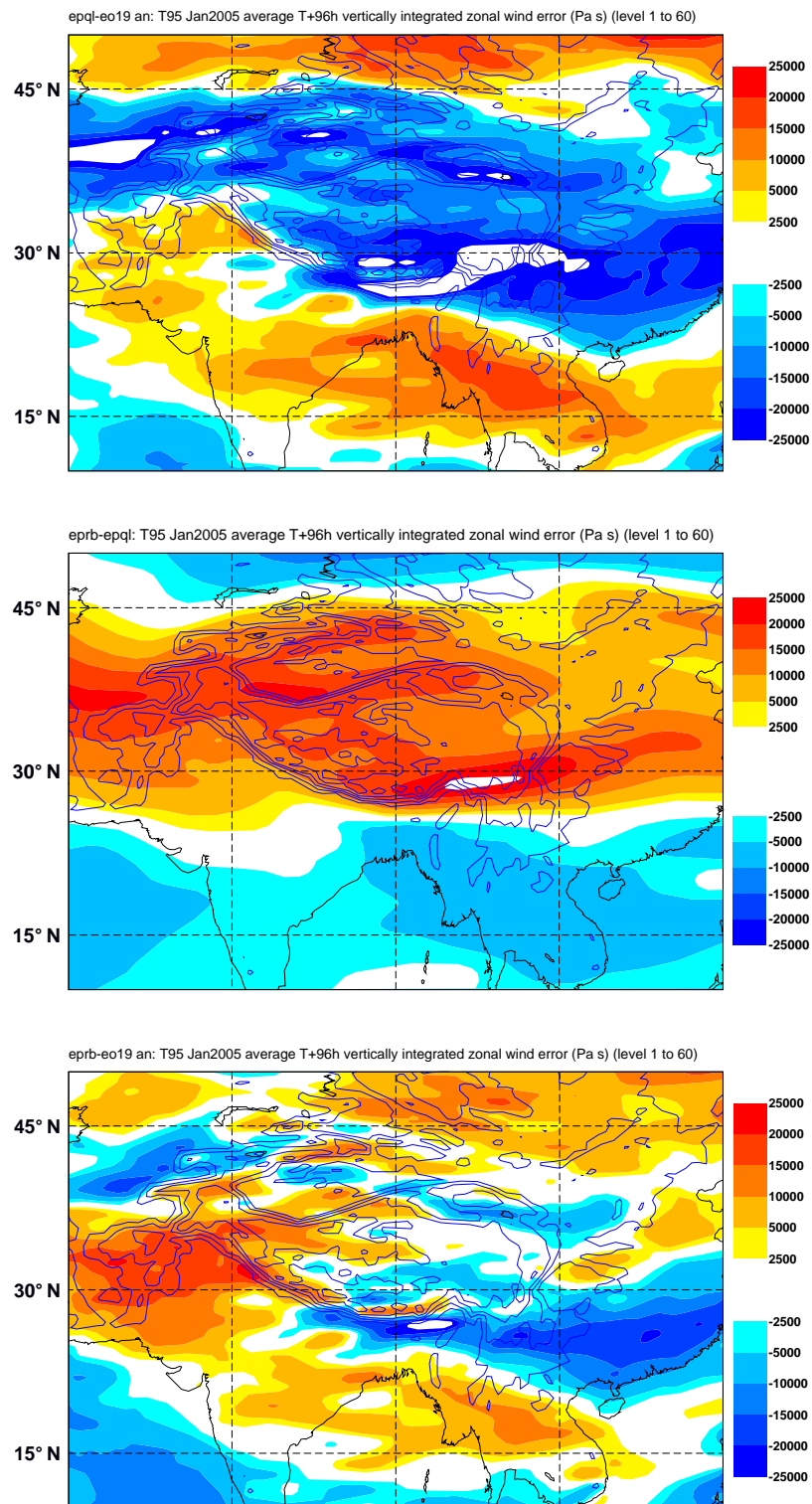
Figure 73: Experiment eprb average vertically integrated zonal wind difference field over the Himalayan region of south-east Asia for 96 hour T95 CY29R1 forecasts from 12Z on each day of January 2005 using the cutoff mountain technique in combination with the TOFD scheme. Top panel: control error; middle panel: impact of experiment; bottom panel: experiment error. Also shown are contours of mean (T511) orography height from 1000 to 6000 m with a 1000 m interval.
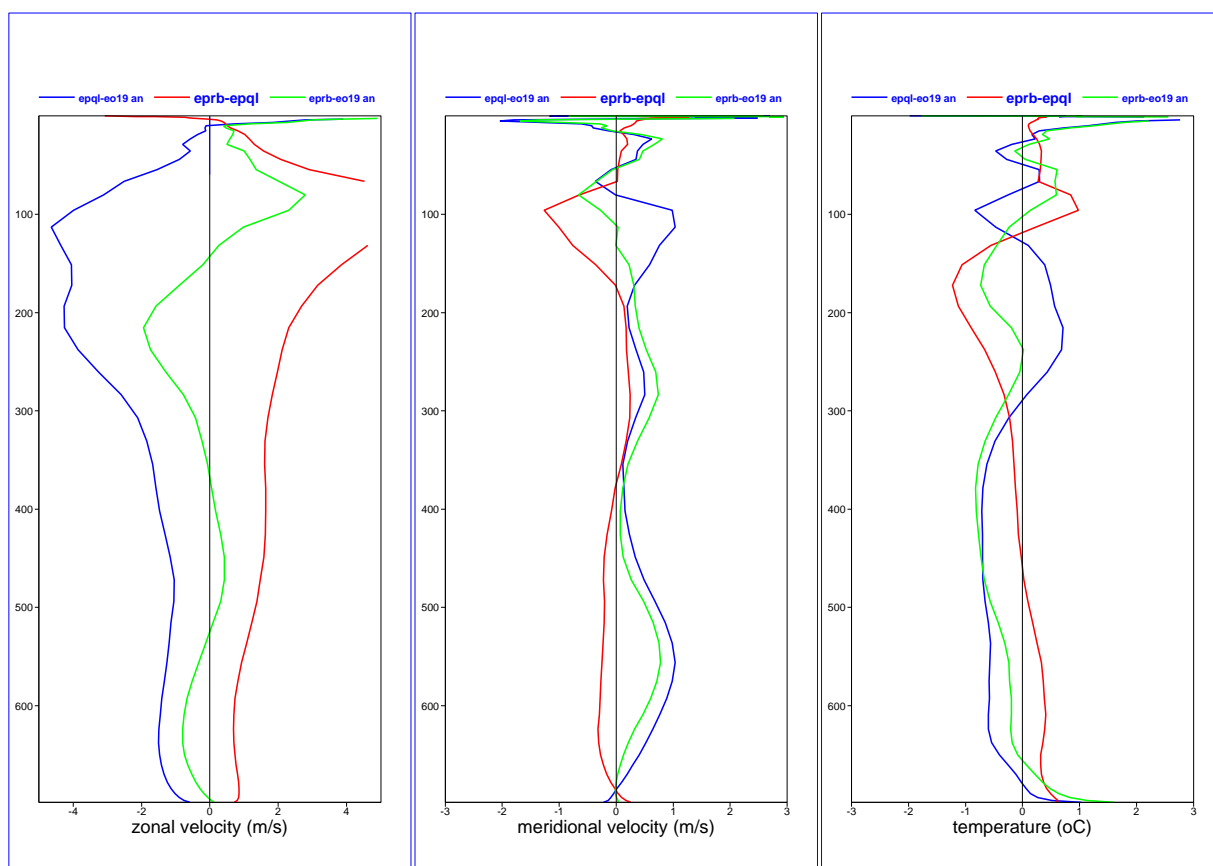
Figure 74: Experiment eprb vertical profiles of difference fields averaged over the Himalayas (26ºN to 40ºN and 75ºE to 105ºE) for 96 hour T95 CY29R1 forecasts from 12Z on each day of January 2005 using the cutoff mountain technique in combination with the TOFD scheme. Left panel: zonal velocity; middle panel: meridional velocity; right panel: temperature. Blue lines: control error; red lines: impact of experiment; green lines: experiment error.
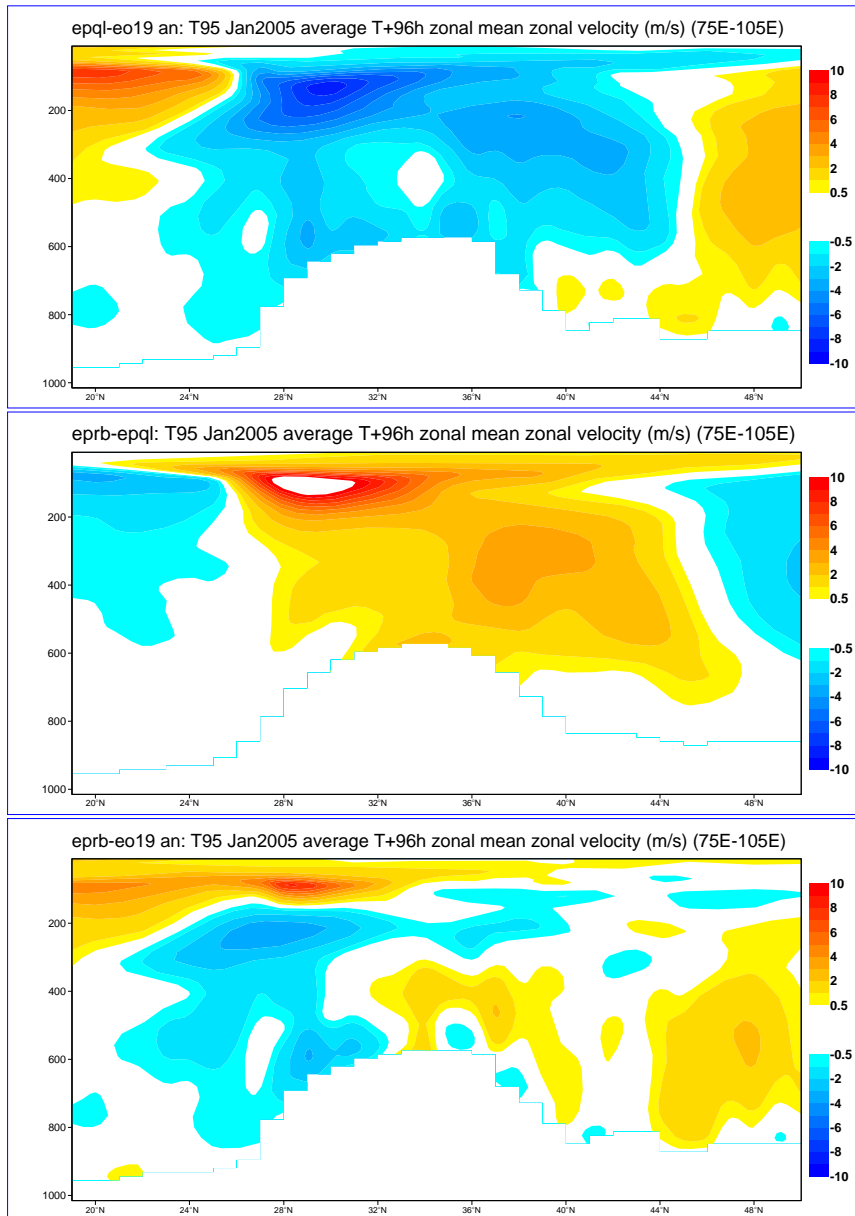
Figure 75: Experiment eprb mean zonal wind speed difference fields, zonally averaged over the Himalayas between 75^oE and 105^oE for 96 hour T95 CY29R1 forecasts from 12Z on each day of January 2005 using the cutoff mountain technique in combination with the TOFD scheme. Top panel: control error; middle panel: impact of experiment; bottom panel: experiment error.

epql-eo19 an: T95 Jan2005 average T+96h vertically integrated zonal wind error (Pa s) (level 1 to 60)

eprb-epql: T95 Jan2005 average T+96h vertically integrated zonal wind error (Pa s) (level 1 to 60)

eprb-eo19 an: T95 Jan2005 average T+96h vertically integrated zonal wind error (Pa s) (level 1 to 60)
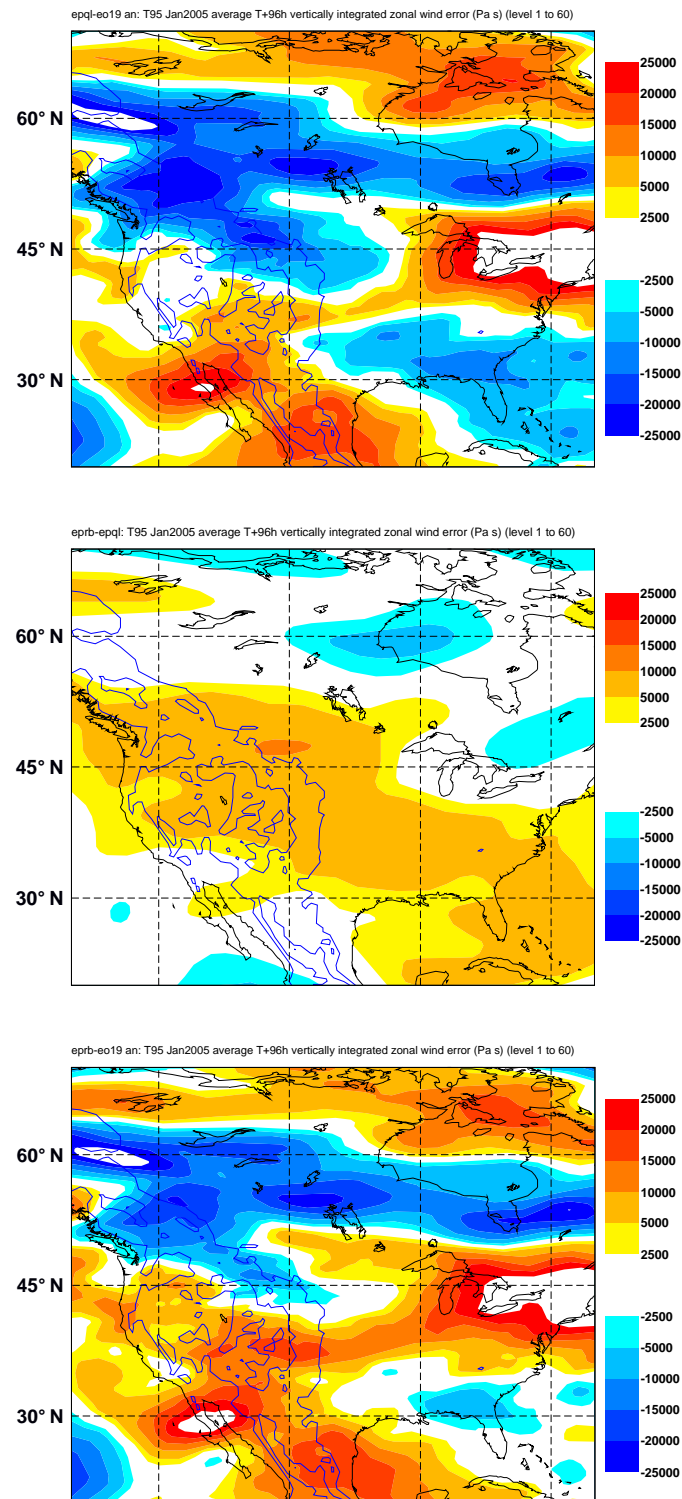
Figure 76: Experiment eprb average vertically integrated zonal wind difference field over North America for 96 hour T95 CY29R1 forecasts from 12Z on each day of January 2005 using the cutoff mountain technique in combination with the TOFD scheme. Top panel: control error; middle panel: experiment impact; bottom panel: experiment impact. Also shown are contours of mean (T511) orography height from 1000 to 6000 m with a 1000 m interval.
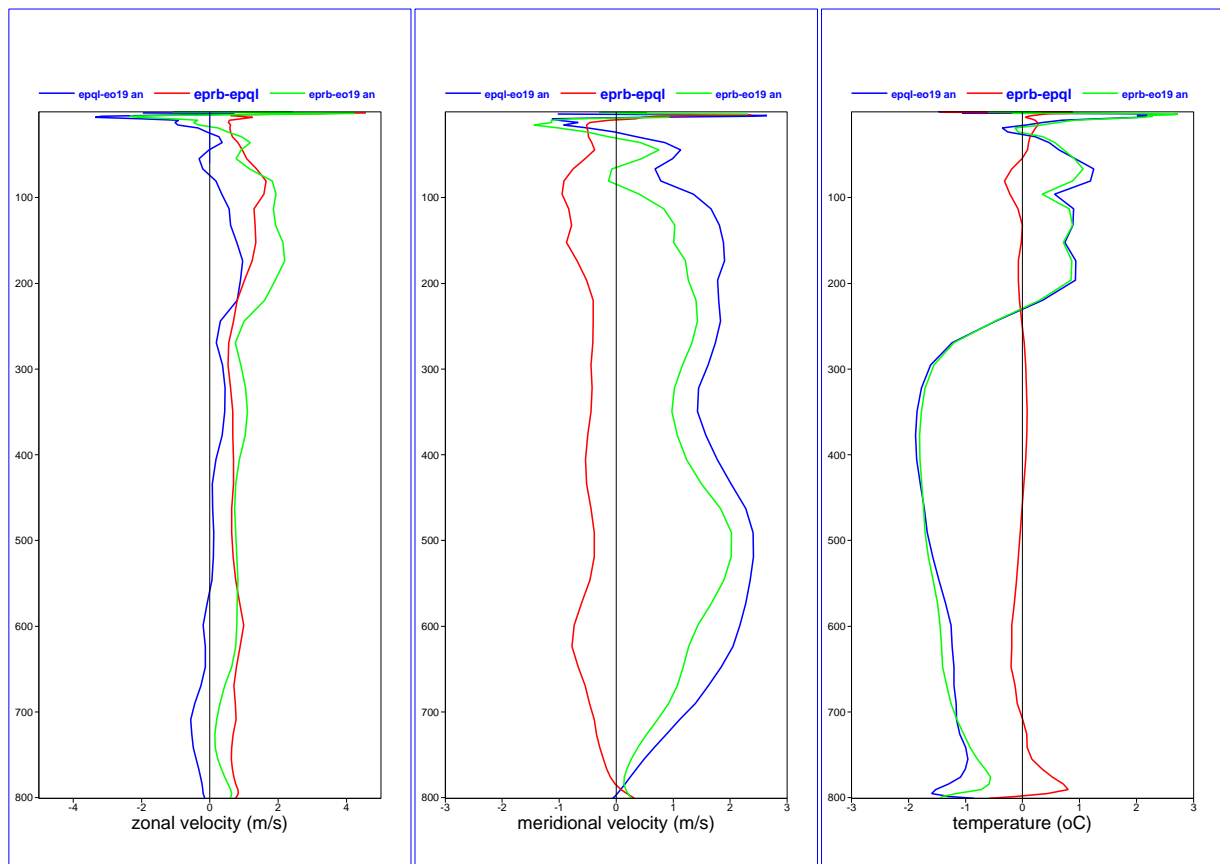
Figure 77: Experiment eprb vertical profiles of difference fields averaged over the Rockies (34°N to 45°N and 112°W to 104°W) for 96 hour T95 CY29R1 forecasts from 12Z on each day of January 2005 using the cutoff mountain technique in combination with the TOFD scheme. Left panel: zonal velocity; middle panel: meridional velocity; right panel: temperature. Blue lines: control error; red lines: impact of experiment; green lines: experiment error.
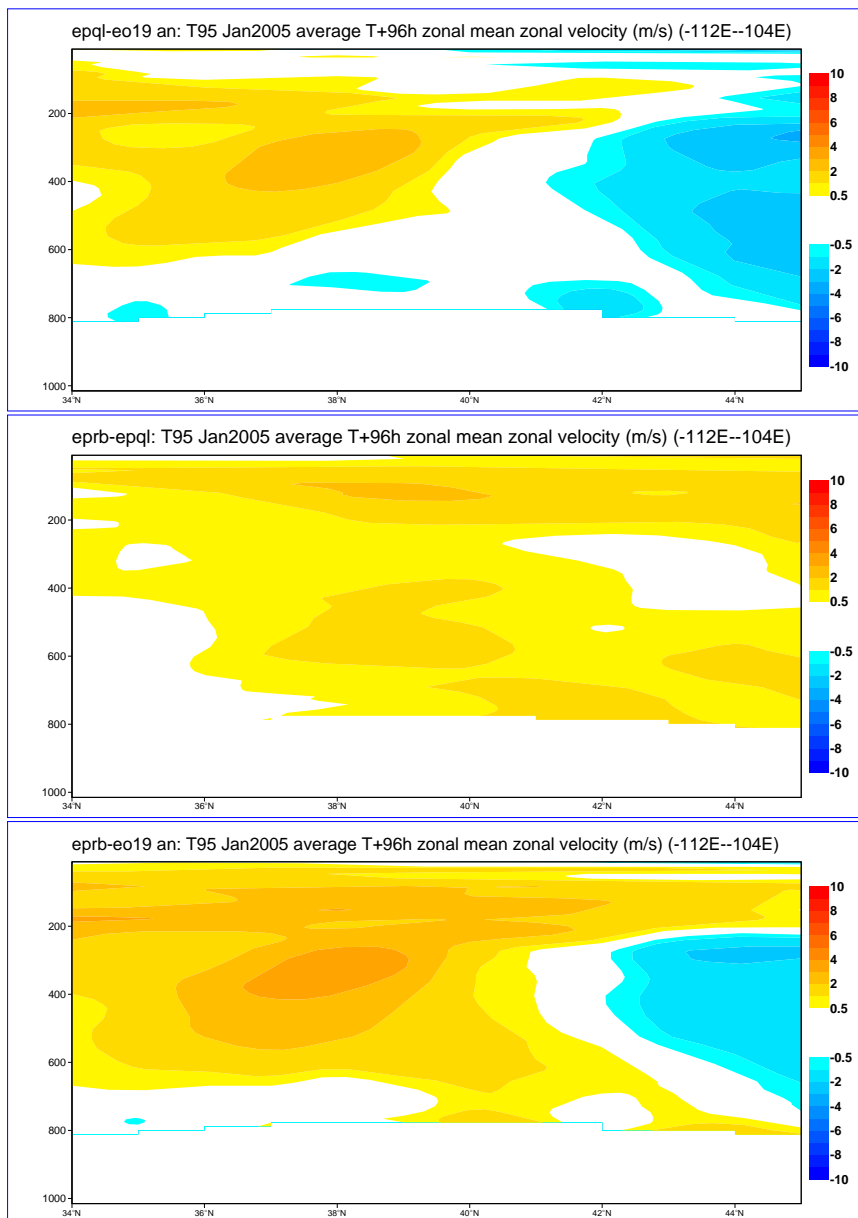
Figure 78: Experiment eprb zonal wind speed difference fields zonally averaged over the Rockies between 112°W and 104°W for 96 hour T95 CY29R1 forecasts from 12Z on each day of January 2005 using the cutoff mountain technique in combination with the TOFD scheme. Top panel: impact of experiment; bottom panel: experiment error.

5 Joint implicit calculation of momentum tendency coefficients

Experiments eq3d and eq3c were run at T95 on 1, 6, 12, 18, 24, 30 of January 2001, 2002, 2003, 2004 at 12Z with the TOFD scheme in combination with the cutoff mountain (TOFD + CO) and time steps of 300 and 3600 s respectively. Experiments eq3b and eq39 are identical experiments, with the exception that they included the joint implicit calculation of momentum tendency coefficients (TOFD + CO + IMPVDF) (see section 1.3).

Fig. 79 compares the mean relative difference (%) between long (3600 s) and short (300 s) runs of the TOFD + CO and TOFD + CO + IMPVDF experiments, averaged over the Himalayan region and as a function of forecast time. Relative differences of the east-west component of surface stress and SSO stress, and 850 hPa zonal velocity are displayed. Fig. 80 shows a similar result, but averaged over the Rockies. The results show a significant reduction in surface stress and SSO stress (and to a lesser extent zonal velocity at 850 hPa) time step sensitivity when using the joint implicit calculation.
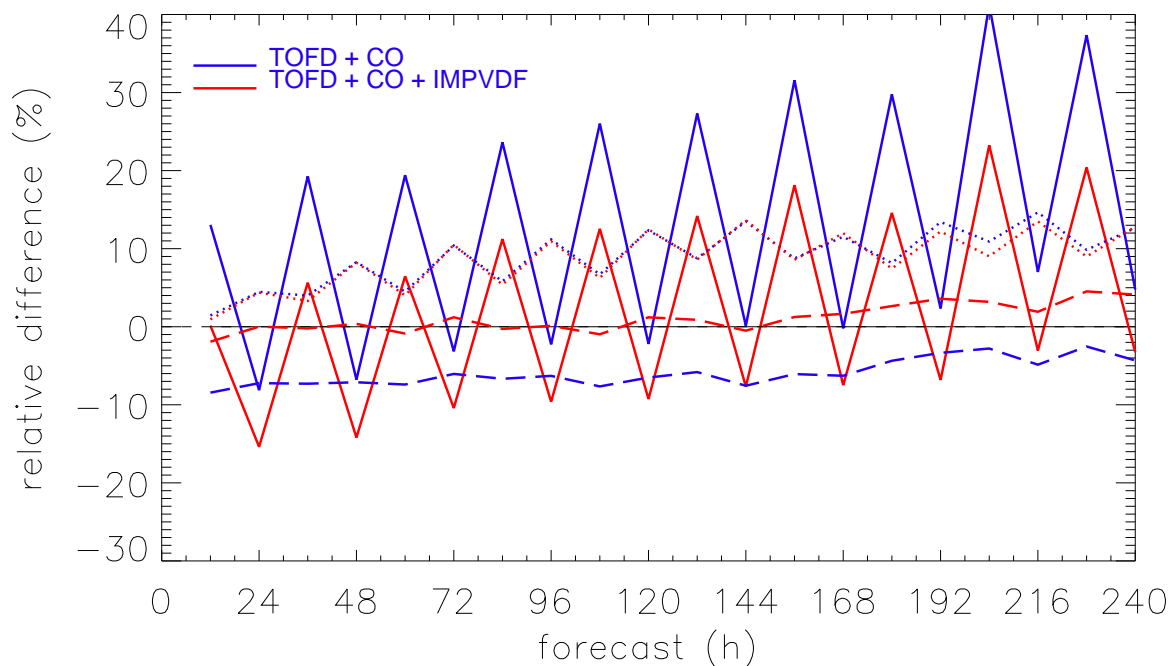
Figure 79: Sensitivity to forecast time of mean relative differences (%) averaged over the Himalayas in east-west component of surface stress (solid lines) and SSO stress (dashed lines), and zonal velocity at 850 hPa (dotted lines), between long (3600 s) and short (300 s) time step T95 forecasts from 12 UTC on 1, 6, 12, 18, 24, 30 of January 2001, 2002, 2003, 2004. Blue lines: TOFD + CO (i.e. eq3c - eq3d); red lines: TOFD + CO + IMPVDF (i.e. eq39 - eq3b). (Domain size 68°E to 110°E and 23°N to 47°N.)
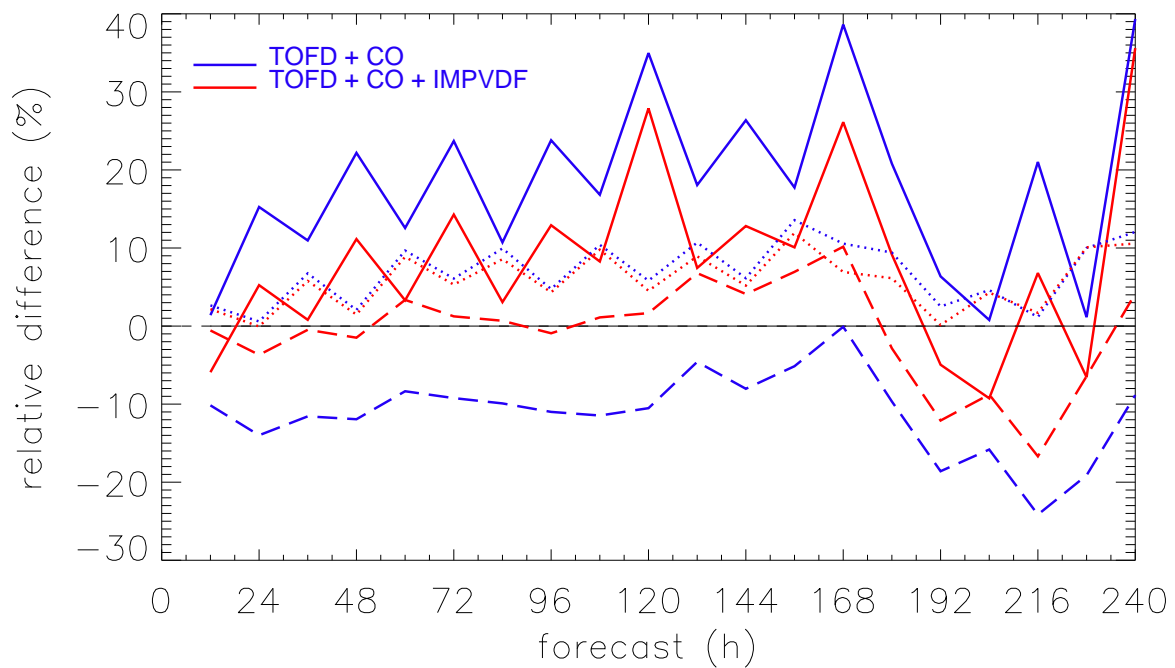
Figure 80: Sensitivity to forecast time of mean relative differences (%) averaged over the Rockies in east-west component of surface stress (solid lines) and SSO stress (dashed lines), and zonal velocity at 850 hPa (dotted lines), between long (3600 s) and short (300 s) time step T95 forecasts from 12 UTC on 1, 6, 12, 18, 24, 30 of January 2001, 2002, 2003, 2004. Blue lines: TOFD + CO (i.e. eq3c - eq3d); red lines: TOFD + CO + IMPVDF (i.e. eq39 - eq3b). (Domain size 125°W to 100°W and 30°N to 59°N.)

6   Further retuning of the cutoff mountain height

Figs. 76 to 78 showed that over the Rockies there was a positive zonal wind bias in T95 CY29R1 control wintertime forecasts, and that the implementation of the cutoff mountain technique in combination with the TOFD scheme increased this bias (primarily due to the cutoff mountain) and spread it over much of the atmosphere. While Figs. 73 to 75 showed that over the Himalayas there was a predominately negative wind bias in T95 CY29R1 control wintertime forecasts, however, the modifications resulted in a positive bias at upper levels. Therefore, it is perhaps no surprise that when these two changes were implemented operationally in CY31R1, positive zonal wind biases were apparent in T159 wintertime climate runs for that cycle, along with a large cold bias over the winter pole (Holton, 1992). To reduce these biases a retuning of the cutoff mountain modification was required to increase the drag. This was achieved by doubling the effective mountain height H_{eff} (see Eq. (4)).

6.1   Evaluation of T159 wintertime forecasts

Experiment eues was run for each day of 10 to 15 November 2006 at 12Z to produce a control T159 CY31R1 (i.e. TOFD + CO) winter forecast. Experiment eueu was identical, with the exception that a value of $2H_{eff}$ was used (i.e. TOFD + CO($2H_{eff}$)). Output was compared with the CY31R1 operational analysis.

6.1.1   Himalayas

Fig. 81 shows eueu average vertically integrated difference fields for 96 hour forecasts. The control error (top panel) shows a large velocity surplus to the north of the Himalayas. (The equivalent T95 CY29R1 result is the bottom panel of Fig. 73, which shows a (smaller) velocity surplus upwind and either side of the Himalayas.) The middle panel of Fig. 81 shows that the impact of doubling the effective mountain height is to decelerate the flow, resulting in a reduction in the wind error (bottom panel).

A positive bias in the zonal wind control error is also evident in Fig. 82, which shows eueu vertical profiles of difference fields averaged over the Himalayas, which reach a maximum of around 2.5 m s^{-1}. (The equivalent T95 CY29R1 result is the experiment error in Fig. 74, which again is smaller, and has a maximum of around 2 m s^{-1} at a level of 100 hPa.) The atmospheric response to the experiment is confirmed, and shows a deceleration throughout the entire atmosphere, but a maximum deceleration of around 2 m s^{-1} at a height just above 100 hPa. This causes a decrease in the positive zonal wind error at this upper level, but also a small increase in the already negative zonal wind bias below. Related to this was a small increase in meridional wind error. Temperature was largely unaffected.

Fig. 83 shows eueu mean zonal wind speed difference fields, zonally averaged over the Himalayas. The positive bias is evident in the top panel, and as with Fig. 81 sits to the north. (The equivalent T95 CY29R1 result is the bottom panel of Fig. 75, which again shows a slightly smaller positive error.) The distinct upper level peak in deceleration from the experiment is confirmed.

Fig. 84 confirms that the experiment increases SSO stress over the Himalayas, but only slightly. This is accompanied by a negligible reduction in surface stress. The mean 850 hPa zonal wind speed is around 11 m s^{-1}, which is higher than the value of 8 m s^{-1} measured in the equivalent T95 CY29R1 experiment (cf. Fig. 30), and is perhaps the explanation as to why the zonal wind control error over the Himalayas at T159 is slightly larger than the equivalent error at T95 CY29R1. Note, the mean SSO stress is approximately 0.1 N m^{-2}, which is smaller than that the equivalent T95 CY29R1 value (around 0.15 N m^{-2}), and consistent with T159 having

a finer resolution (i.e. smaller value of μ) and corresponding smaller value of parameterised gravity wave drag (Smith et al., 2006).

6.1.2 Rockies

The top panel of Fig. 85 confirms that over the Rockies a strong positive zonal wind bias dominates. (The equivalent T95 CY29R1 result is the bottom panel of Fig. 76, which shows a much smaller positive zonal wind bias, as well as significant regions of velocity deficit.) The impact of the experiment causes a strong deceleration over the Rockies, which considerably reduces the positive wind bias, and which is much stronger than the deceleration achieved over the Himalayas (Fig. 81).

Fig. 86 shows that over the Rockies the maximum control zonal wind bias is around 4 m s^{-1}, and that the deceleration as a result of the experiment is between 1 and 2 m s^{-1} and is limited to levels above 400 hPa. (The equivalent T95 CY29R1 result is the experiment error in Fig. 77, which has a maximum of around 2 m s^{-1}.) The impact on meridional temperature is minimal, and the impact on temperature is to reduce the positive bias below 400 hPa.

The large positive zonal wind bias over the Rockies is again confirmed by Fig. 87, which also demonstrates the beneficial impact of the experiment in reducing it. (Again, this bias is around twice as large as the equivalent T95 CY29R1 result, which is the bottom panel of Fig. 78.)

Fig. 84 shows that the surface stress, SSO stress, and 850 hPa zonal wind speed are larger over the Rockies than the Himalayas. Moreover, as a result of the experiment, the SSO stress over the Rockies increases by over a quarter, significantly more than the corresponding increase over the Himalayas, and consistent with a much larger deceleration occurring over the Rockies. This is consistent with the much higher value of zonal wind speed over the Rockies. The mean 850 hPa zonal wind speed of around 17 m s^{-1} is much higher than the value of 8 m s^{-1} measured in the equivalent T95 CY29R1 experiment (cf. Fig. 30), which is perhaps the explanation as to why the control error in zonal velocity and SSO stress over the Rockies at T159 are considerably larger than the equivalent values at T95 CY29R1.
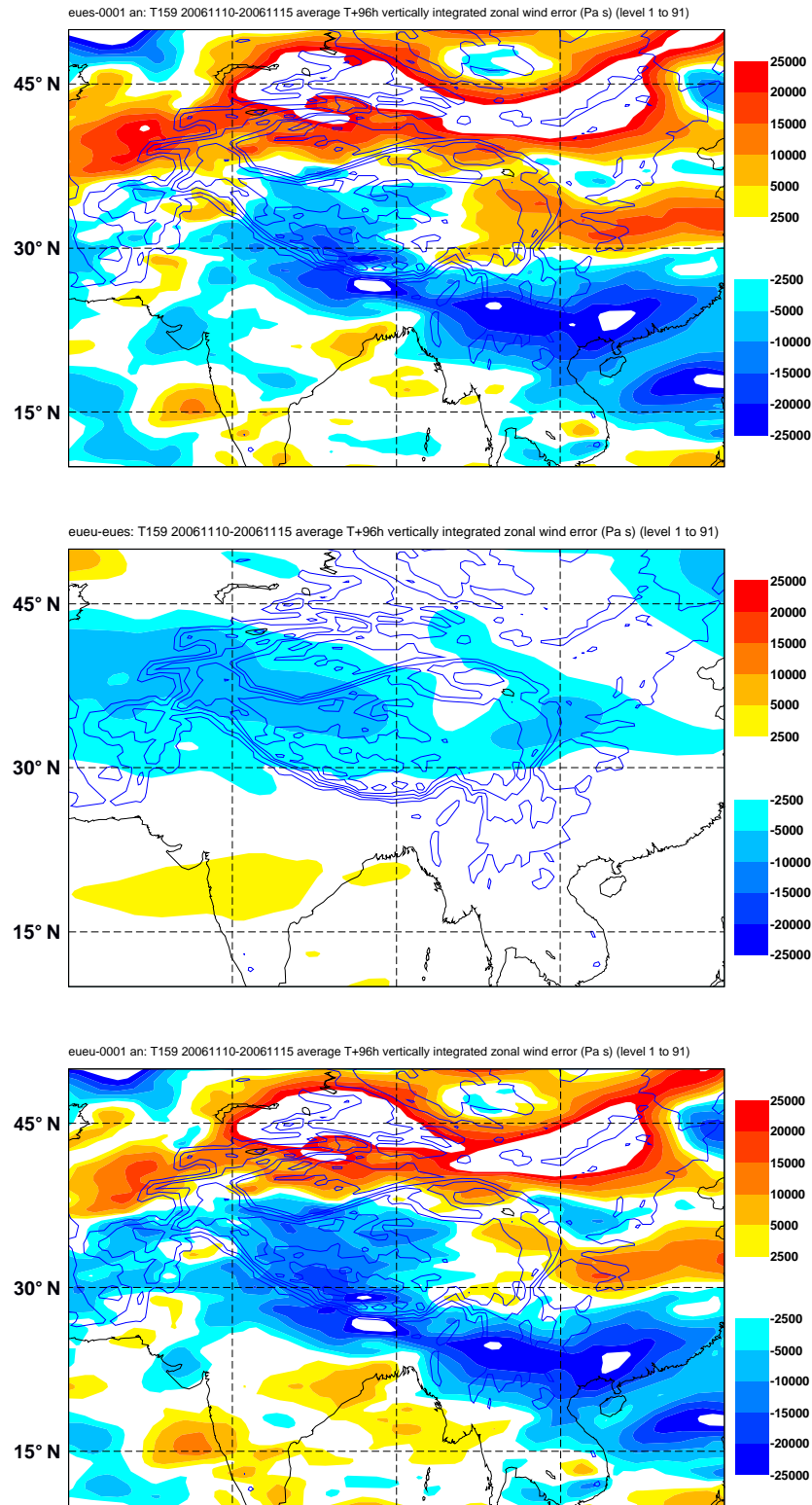
Figure 81: Experiment eueu average vertically integrated zonal wind difference fields (Pa s) over the Himalayan region of south-east Asia for 96 hour T159 CY31R1 forecasts from 12Z on each day of 10 to 15 November 2006 using a value $2H_{eff}$. Top panel: control error; middle panel: impact of experiment; bottom panel: experiment error. Also shown are contours of mean (T159) orography height from 1000 to 6000 m with a 1000 m interval.
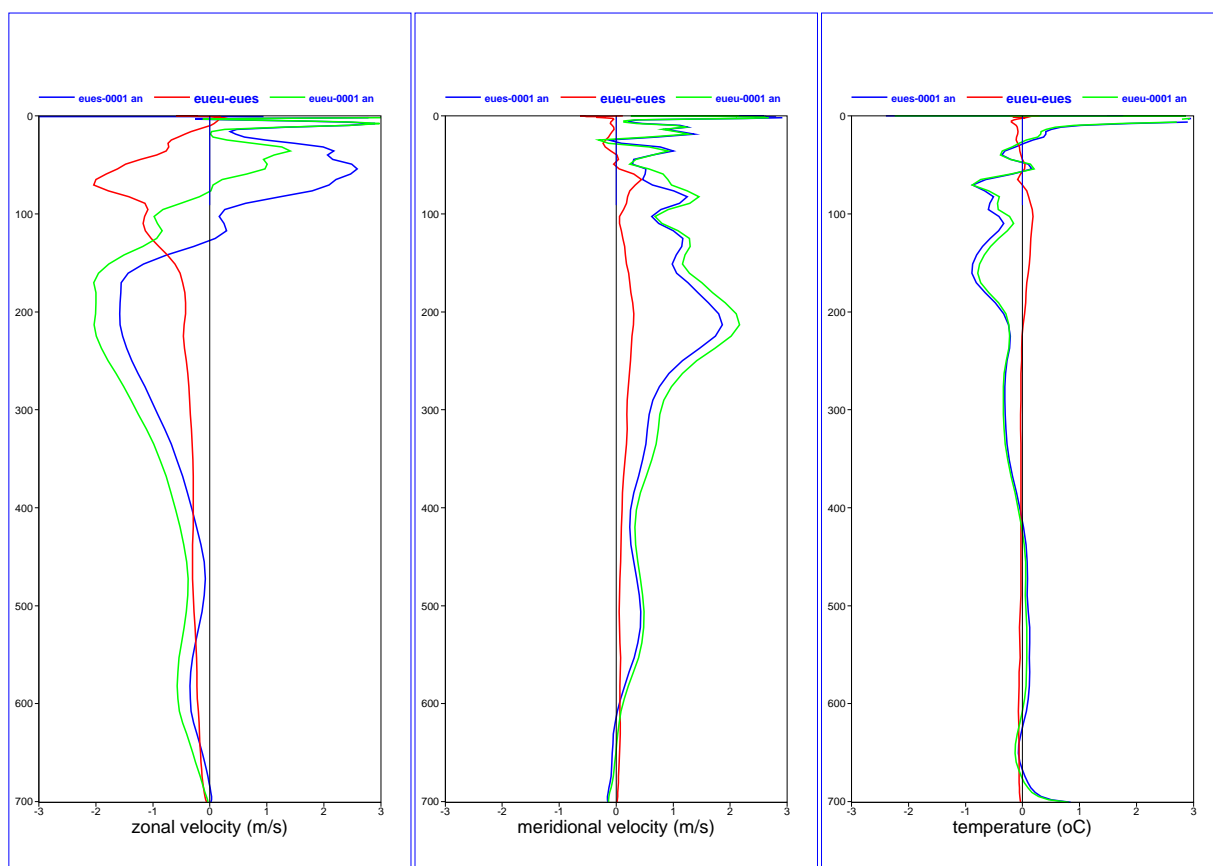
Figure 82: Experiment eueu vertical profiles of difference fields averaged over the Himalayas (26ºN to 40ºN and 75ºE to 105ºE) for 96 hour T159 CY31R1 forecasts from 12Z on each day of 10 to 15 November 2006 using a value $2H_{eff}$. Left panel: zonal velocity (m s^{-1}); middle panel: meridional velocity (m s^{-1}); right panel: temperature (K). Blue lines: control error; red lines: impact of experiment; green lines: experiment error.
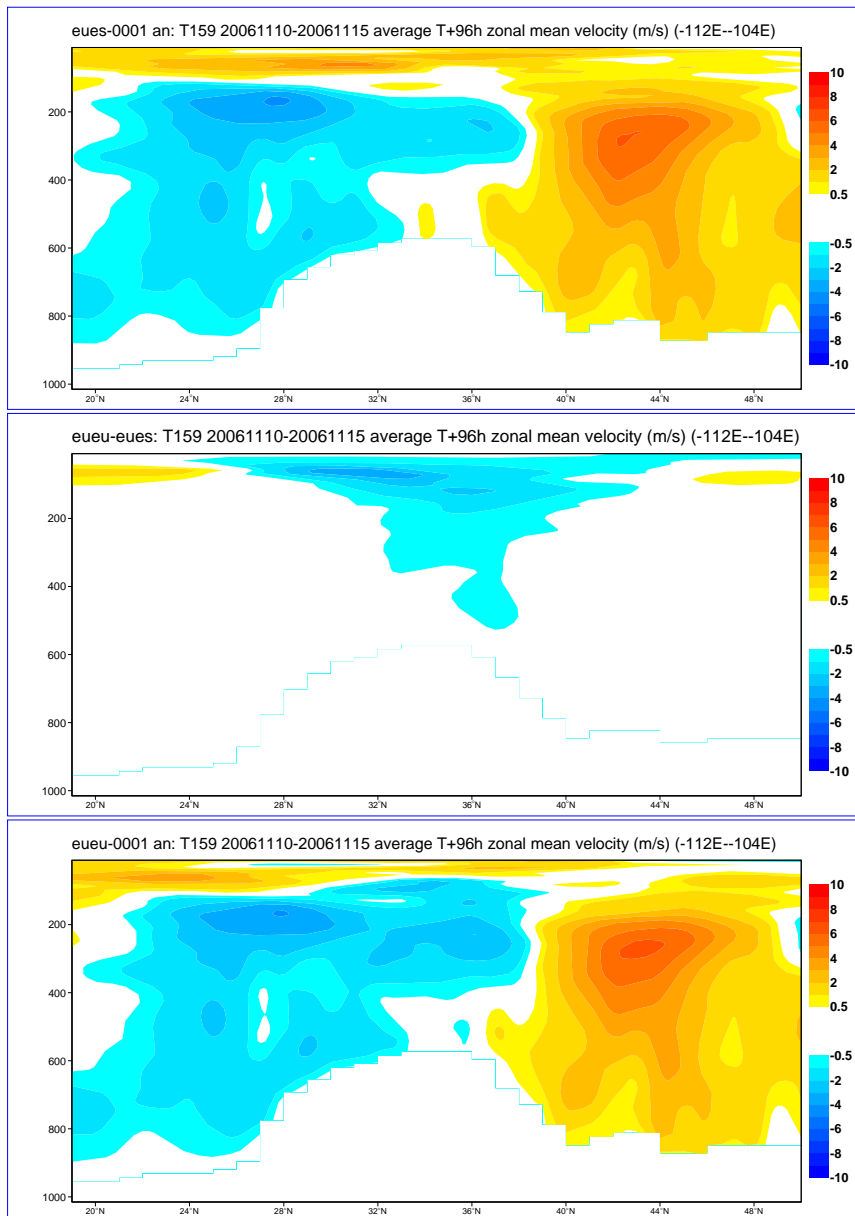
Figure 83: Experiment eueu mean zonal wind speed difference field (m s⁻¹) zonally averaged over the Himalayas between 75°E and 105°E for 96 hour T159 CY31R1 forecasts from 12Z on each day of 10 to 15 November 2006 using a value 2H_{eff}. Top panel: control error; middle panel: impact of experiment; bottom panel: experiment error.
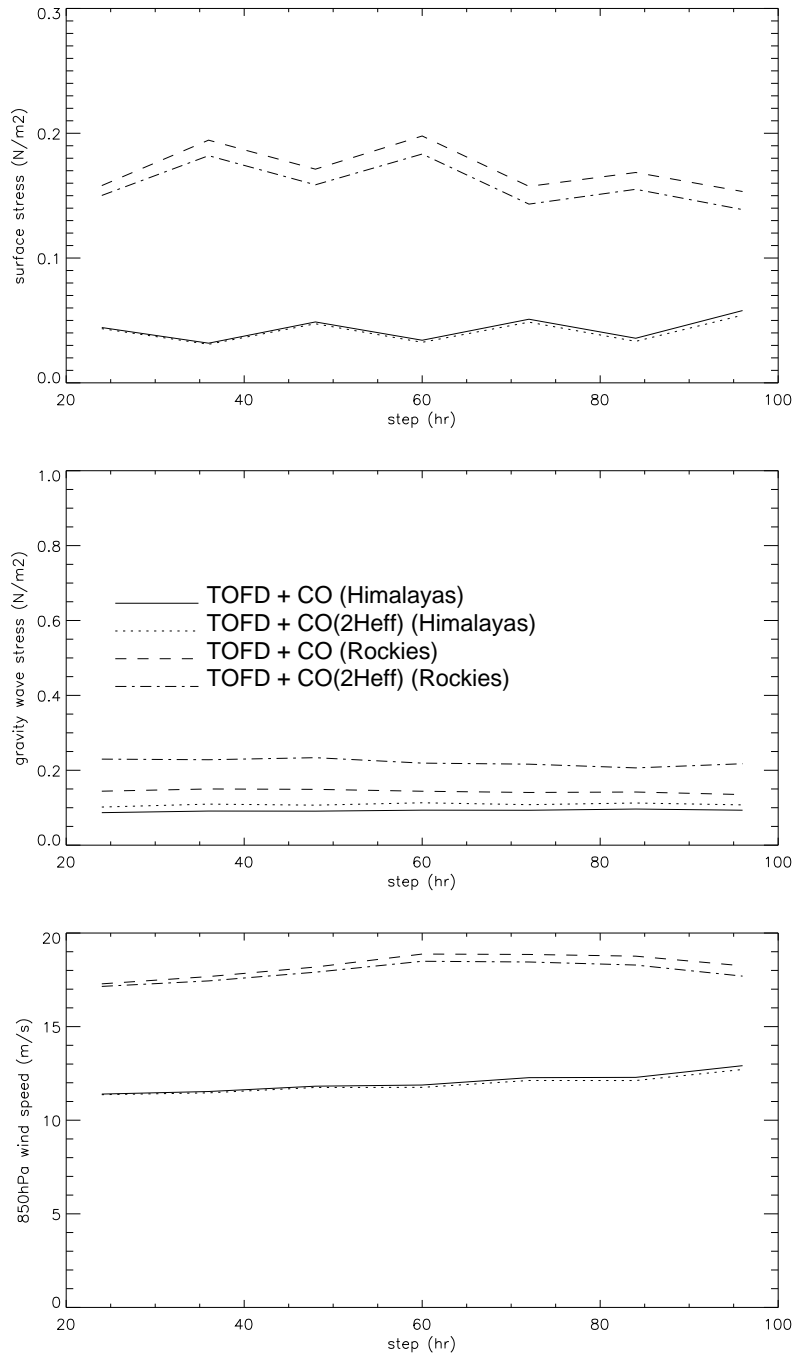
Figure 84: Sensitivity to forecast time of experiment eueu (and control eues) surface stress (N m^{-2}; top panel), SSO stress (N m^{-2}; middle panel, labelled 'gravity wave stress'), and 850 hPa wind speed (m s^{-1}; bottom panel) averaged over the Himalayas (26°N to 40°N and 75°E to 105°E) and the Rockies (34°N to 45°N and 112°W to 104°W) for T159 CY31R1 forecasts from 12Z on each day of 10 to 15 November 2006 using a value 2H$_{eff}$.
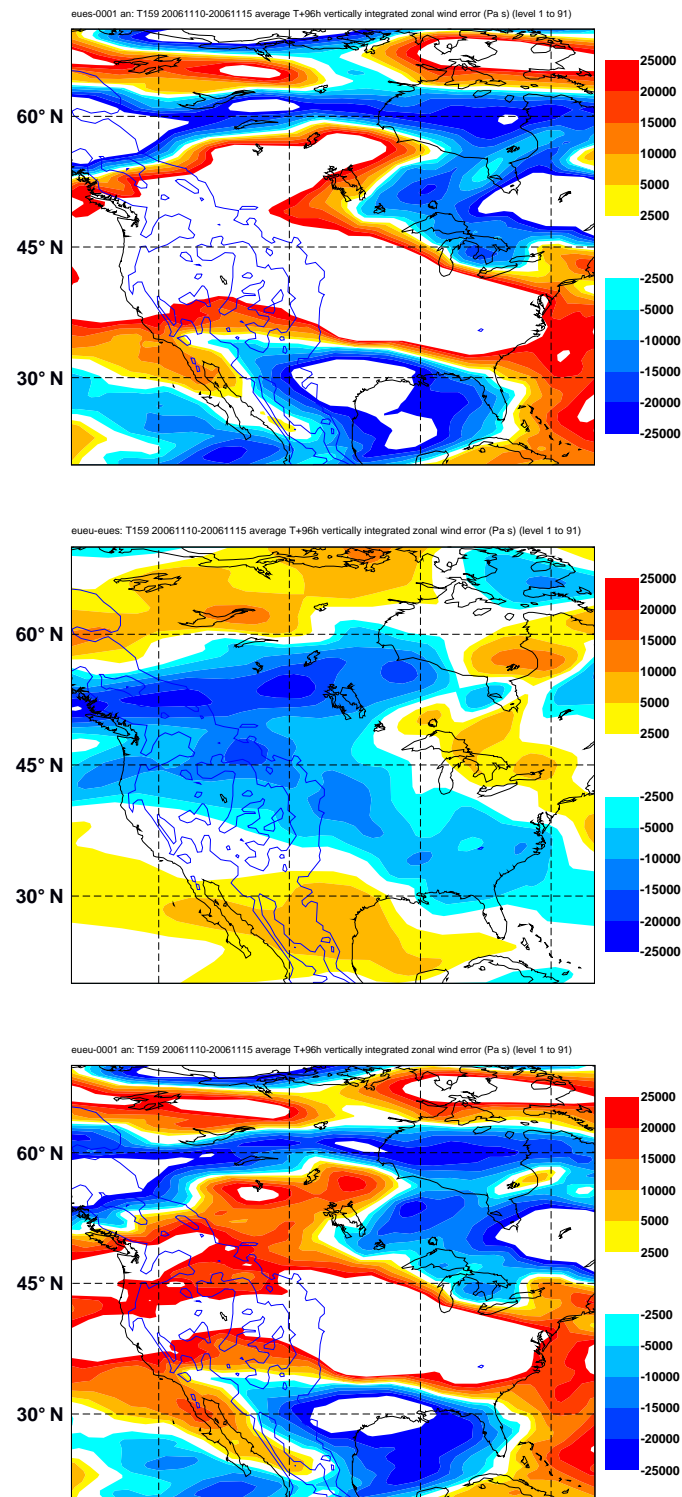
Figure 85: Experiment eueu average vertically integrated zonal wind difference fields (Pa s) over North America for 96 hour T159 CY31R1 forecasts from 12Z on each day of 10 to 15 November 2006 using a value $2H_{eff}$. Top panel: control error; middle panel: impact of experiment; bottom panel: experiment error. Also shown are contours of mean (T159) orography height from 1000 to 6000 m with a 1000 m interval.
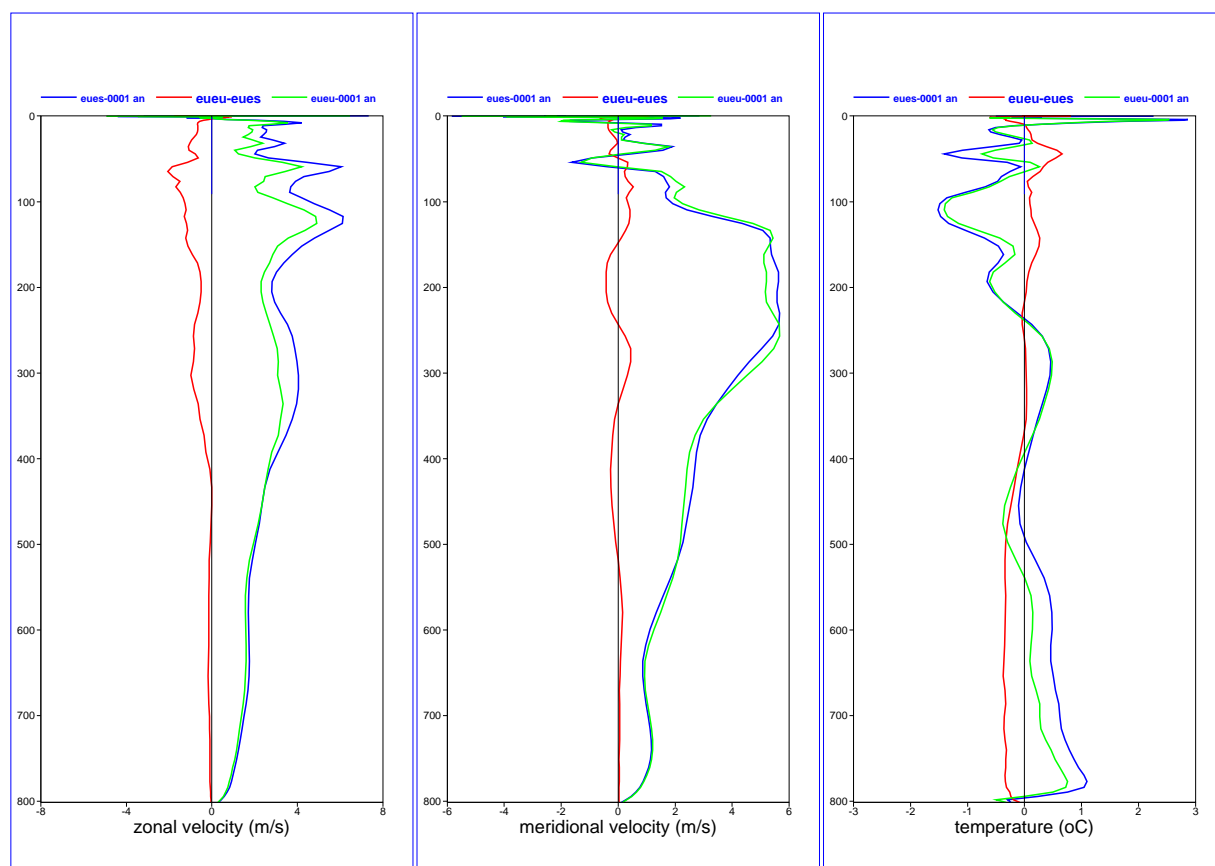
Figure 86: Experiment eueu vertical profiles of difference fields averaged over the Rockies (34ºN to 45ºN and 112ºW to 104ºW) for 96 hour T159 CY31R1 forecasts from 12Z on each day of 10 to 15 November 2006 using a value $2H_{eff}$. Left panel: zonal velocity ($m\ s^{-1}$); middle panel: meridional velocity ($m\ s^{-1}$); right panel: temperature (K). Blue lines: control error; red lines: impact of experiment; green lines: experiment error.
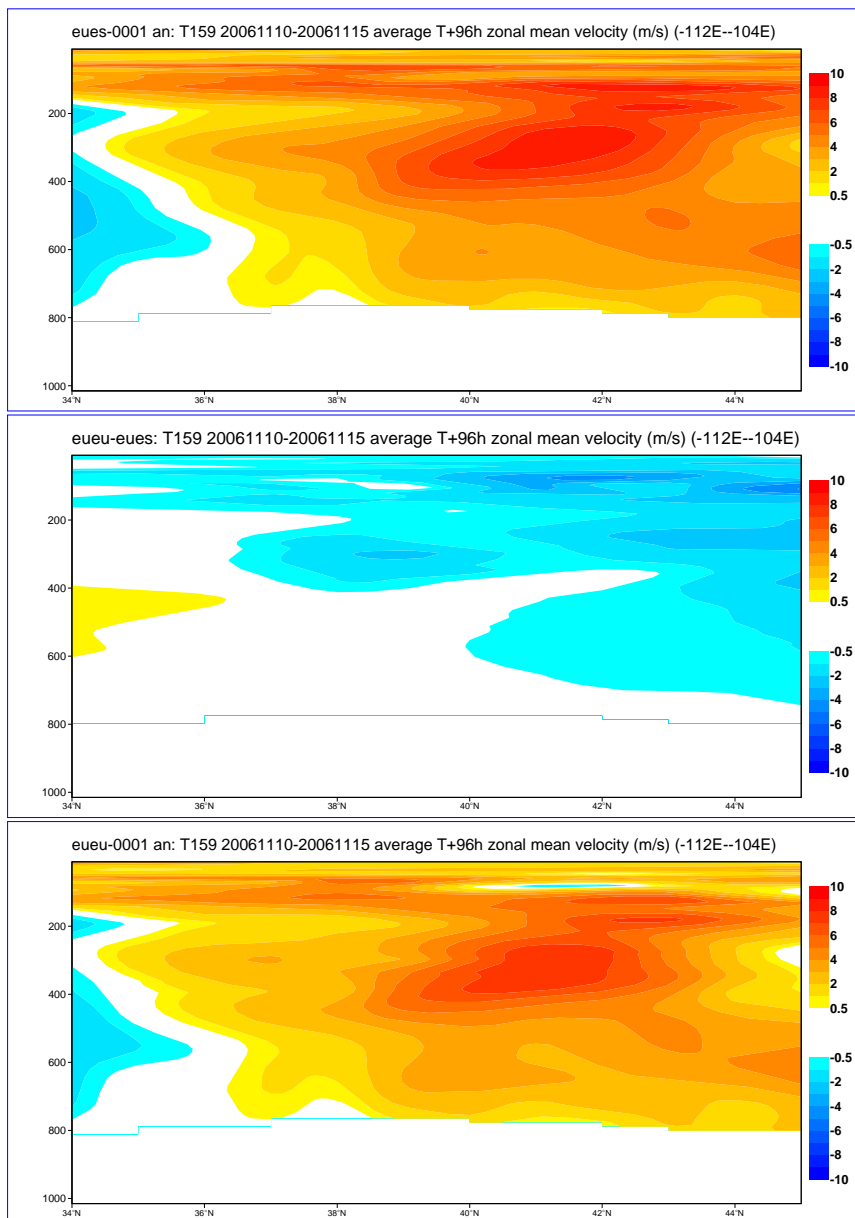
Figure 87: Experiment eueu zonal wind speed difference field (m s^{-1}) zonally averaged over the Rockies between 112ºW and 104ºW for 96 hour T159 CY31R1 forecasts from 12Z on each day of 10 to 15 November 2006 using a value 2H$_{eff}$. Top panel: control error; middle panel: impact of experiment; bottom panel: experiment error.

6.2 Evaluation of T511 wintertime forecasts

Experiment euen was run for each day of 10 to 15 November 2006 at 12Z to produce a control T511 CY31R1 winter forecast. Experiment euev was identical, with the exception that a value of $2H_{eff}$ was used (TOFD + CO($2H_{eff}$)). Output was compared with CY31R1 operational analysis.

6.2.1 Himalayas

Fig. 88 shows euev average vertically integrated difference fields for 96 hour forecasts. The control error (top panel) shows an area of velocity surplus to the north of the Himalayas. (The equivalent T511 CY29R1 result is the bottom panel of Fig. 26.) The control error is significantly reduced when compared to the previous T159 result (Fig. 81). The impact of the experiment decelerates the flow, although to a lesser extent to that at T159.

Fig. 89 shows a positive bias in zonal velocity control error at upper levels, reaching 2 m s^{-1}. (The equivalent T511 CY29R1 experiment error is the bottom panel in Fig. 27, which shows a similar profile shape but reduced values, for example reaching a maximum of 1 m s^{-1}.) The deceleration is broadly similar to that at T159 (cf. Fig. 82).

Fig. 90 shows euev mean zonal wind speed difference fields, showing a velocity surplus/deficit to the north/south of the Himalayas in control error. (The equivalent T511 CY29R1 result is the bottom panel of Fig. 28, which again shows a smaller bias.) Again, the deceleration at T511 is broadly similar to that at T159 (cf. Fig. 83).

Fig. 91 shows plots of surface stress, SSO stress, and 850 hPa wind averaged over the Himalayas. Values of SSO stress are smaller than the equivalent values at T159 (cf. Fig. 84), however, the experiment results in only a small increase in SSO stress over the Himalayas.

6.2.2 Rockies

Fig. 92 shows a strong positive bias in the control error at T511, but that this is less than that at T159 (cf. Fig. 85). (The equivalent T511 CY29R1 control error is the bottom panel of Fig. 31, and is considerably smaller than here.) The impact of the experiment at T511 is smaller than that at T159 (cf. Fig. 92).

Fig. 93 shows the bias in zonal wind is around 4 m s^{-1} above 400 hPa, and is comparable to the bias at T159 (cf. Fig. 86). (The equivalent T511 CY29R1 result is the experiment error in Fig. 32, which again is much smaller.) The impact of the experiment reduces the error, however it still remains positive.

Fig. 94 shows euev mean zonal wind speed difference fields, again showing a large velocity surplus in the control error. (The equivalent T511 CY29R1 result is the bottom panel of Fig. 33.) Again, the deceleration at T511 is similar to that at T159, as shown by Fig. 87.

Fig. 91 shows plots of surface stress, SSO stress, and 850 hPa wind averaged over the Rockies. Values of SSO stress are smaller than the equivalent values at T159 (cf. Fig. 84), however, as at T159 the modification increases the SSO stress by over a third. Surface stress values decrease in compensation.
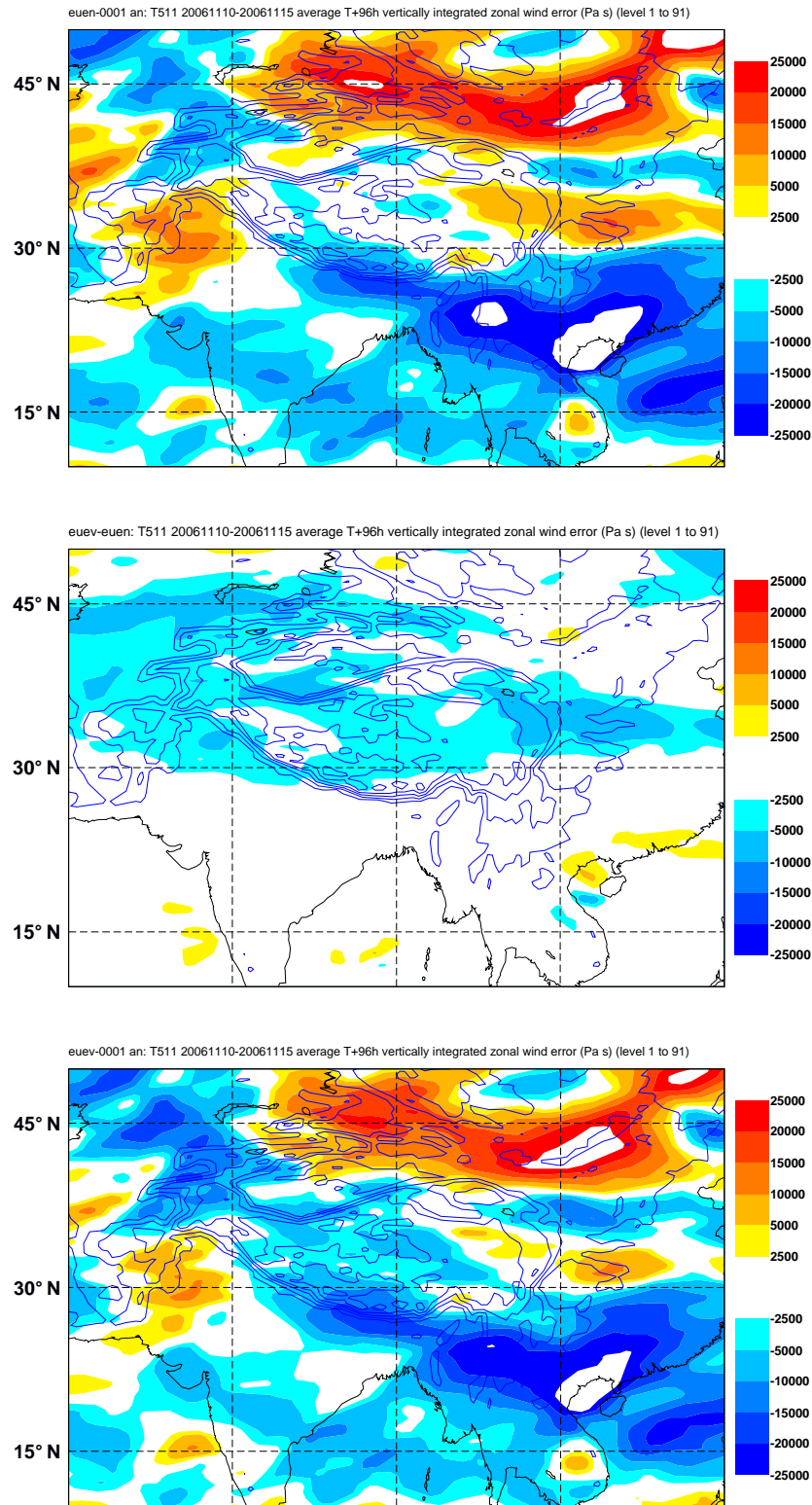
Figure 88: Experiment euev average vertically integrated zonal wind difference fields (Pa s) over the Himalayan region of south-east Asia for 96 hour T511 CY31R1 forecasts from 12Z on each day of 10 to 15 November 2006 using a value $2H_{eff}$. Top panel: control error; middle panel: impact of experiment; bottom panel: experiment error. Also shown are contours of mean (T511) orography height from 1000 to 6000 m with a 1000 m interval.
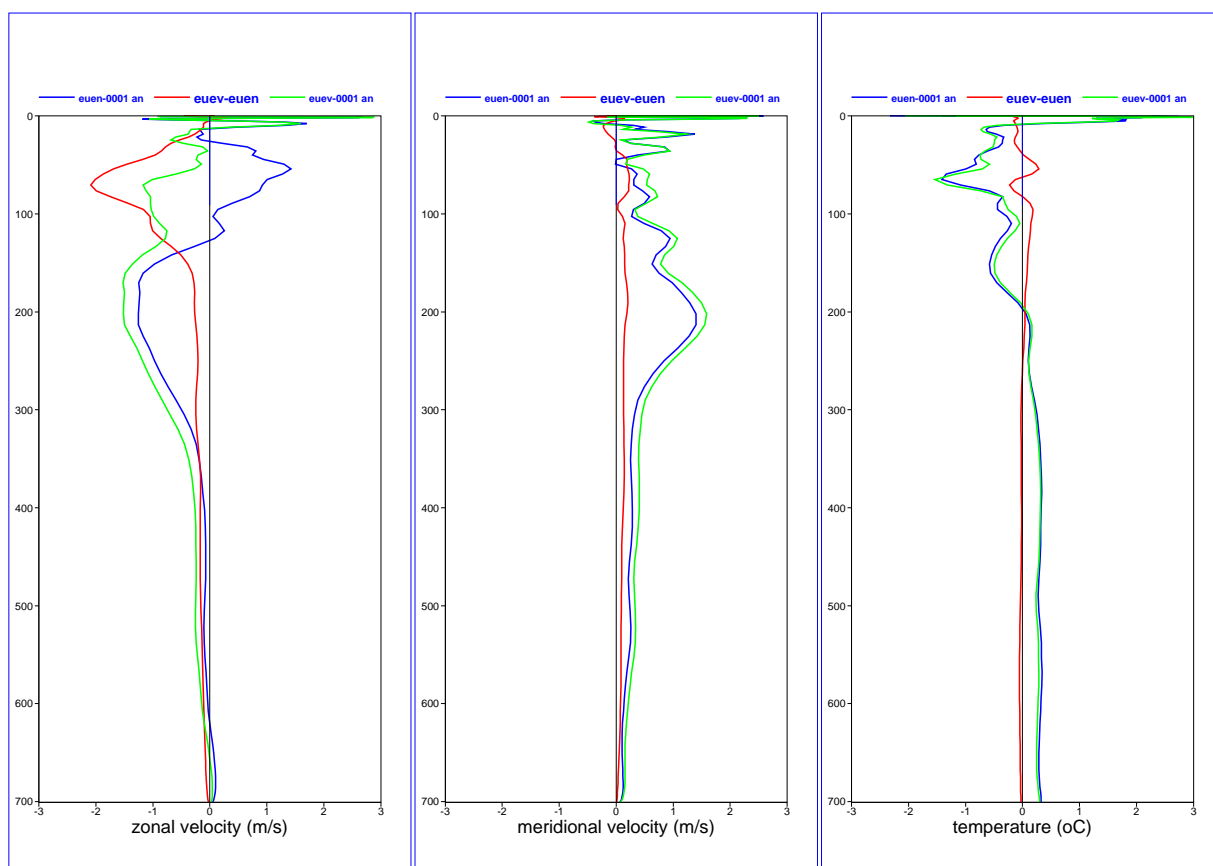
Figure 89: Experiment euev vertical profiles of difference fields averaged over the Himalayas (26ºN to 40ºN and 75ºE to 105ºE) for 96 hour T511 CY31R1 forecasts from 12Z on each day of 10 to 15 November 2006 using a value $2H_{eff}$. Left panel: zonal velocity (m s^{-1}); middle panel: meridional velocity (m s^{-1}); right panel: temperature (K). Blue lines: control error; red lines: impact of experiment; green lines: experiment error.
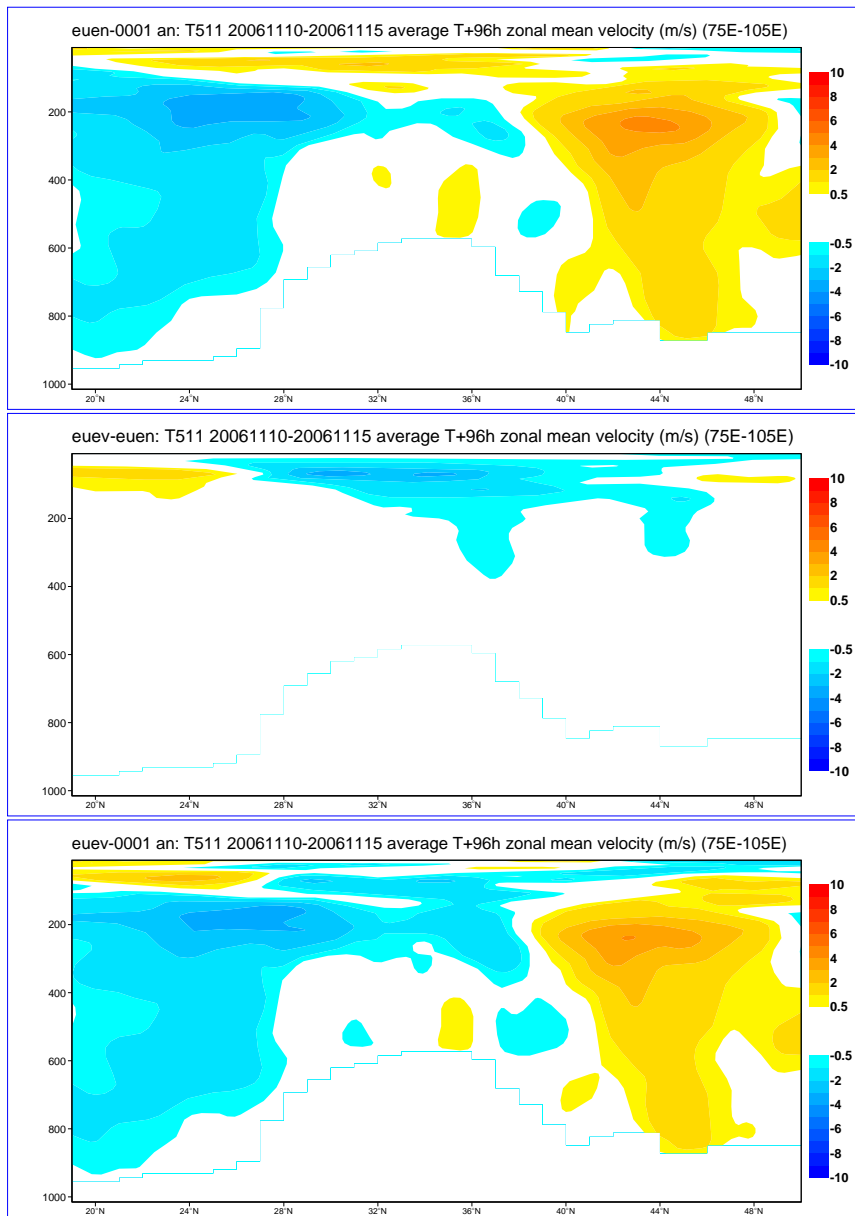
Figure 90: Experiment euev mean zonal wind speed difference field (m s^{-1}) zonally averaged over the Himalayas between 75°E and 105°E for 96 hour T511 CY31R1 forecasts from 12Z on each day of 10 to 15 November 2006 using a value 2H$_{eff}$. Top panel: control error; middle panel: impact of experiment; bottom panel: experiment error.
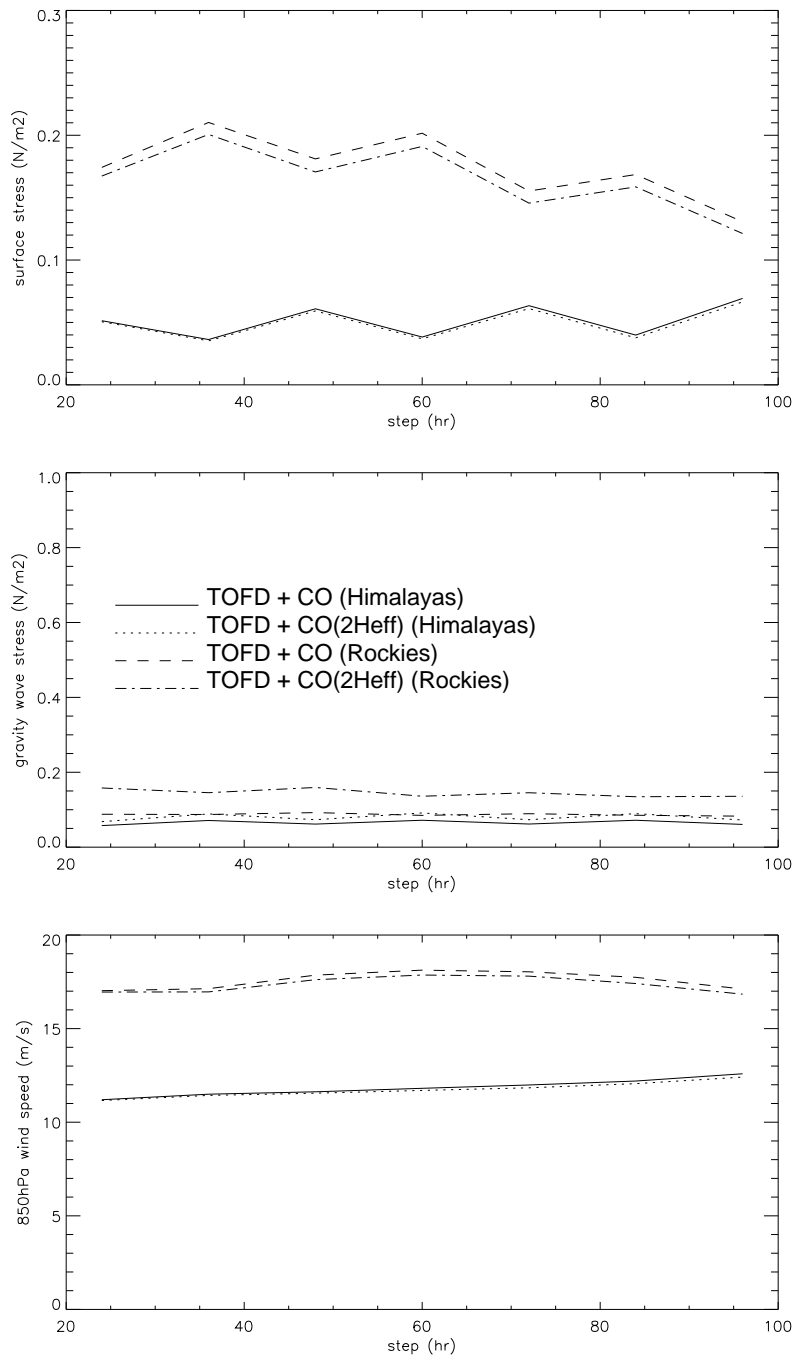
Figure 91: Sensitivity to forecast time of experiment euev (and control euen) surface stress (N m^{-2}; top panel), SSO stress (N m^{-2}; middle panel, labelled 'gravity wave stress'), and 850 hPa wind speed (m s^{-1}; bottom panel) averaged over the Himalayas (26°N to 40°N and 75°E to 105°E) and the Rockies (34°N to 45°N and 112°W to 104°W) for T511 CY31R1 forecasts from 12Z on each day of 10 to 15 November 2006 using a value 2H$_{eff}$.
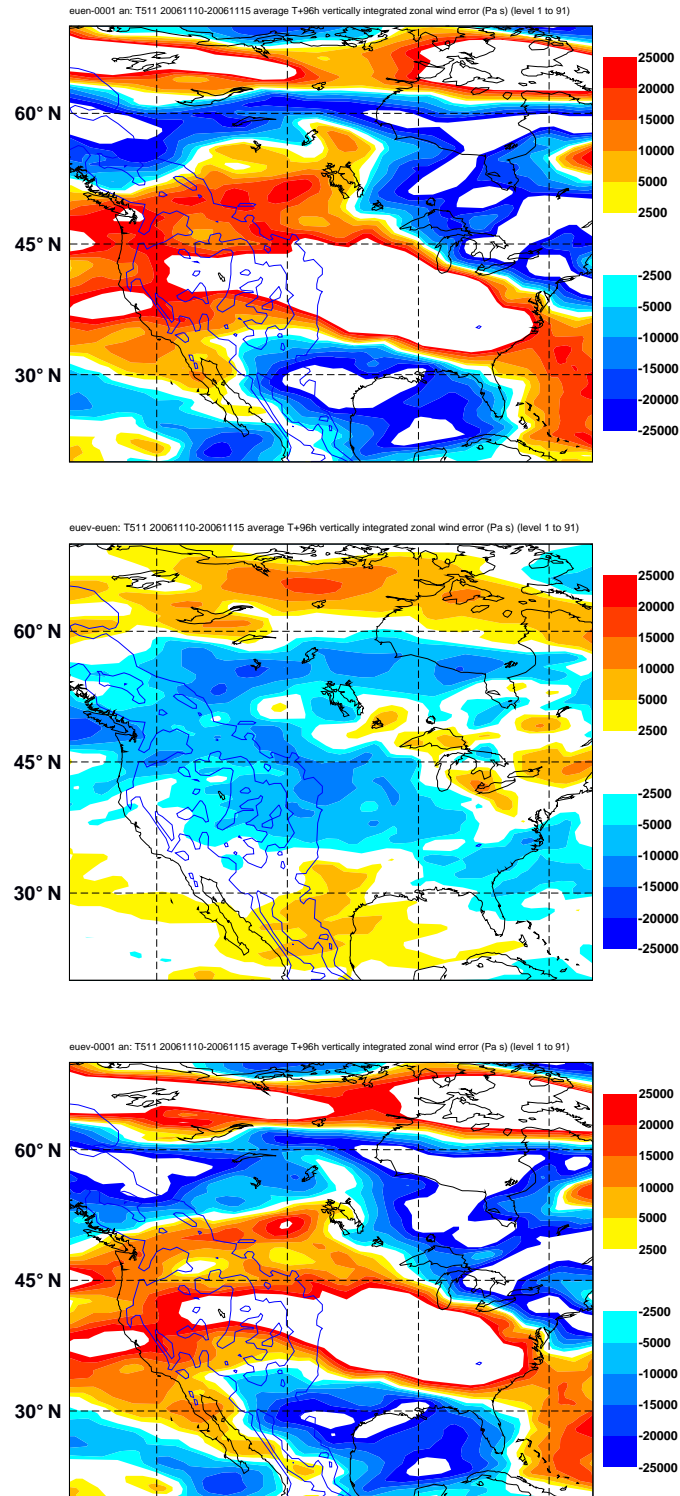
Figure 92: Experiment euev average vertically integrated zonal wind difference fields (Pa s) over North America for 96 hour T511 CY31R1 forecasts from 12Z on each day of 10 to 15 November 2006 using a value $2H_{eff}$. Top panel: control error; middle panel: impact of experiment; bottom panel: experiment error. Also shown are contours of mean (T511) orography height from 1000 to 6000 m with a 1000 m interval.
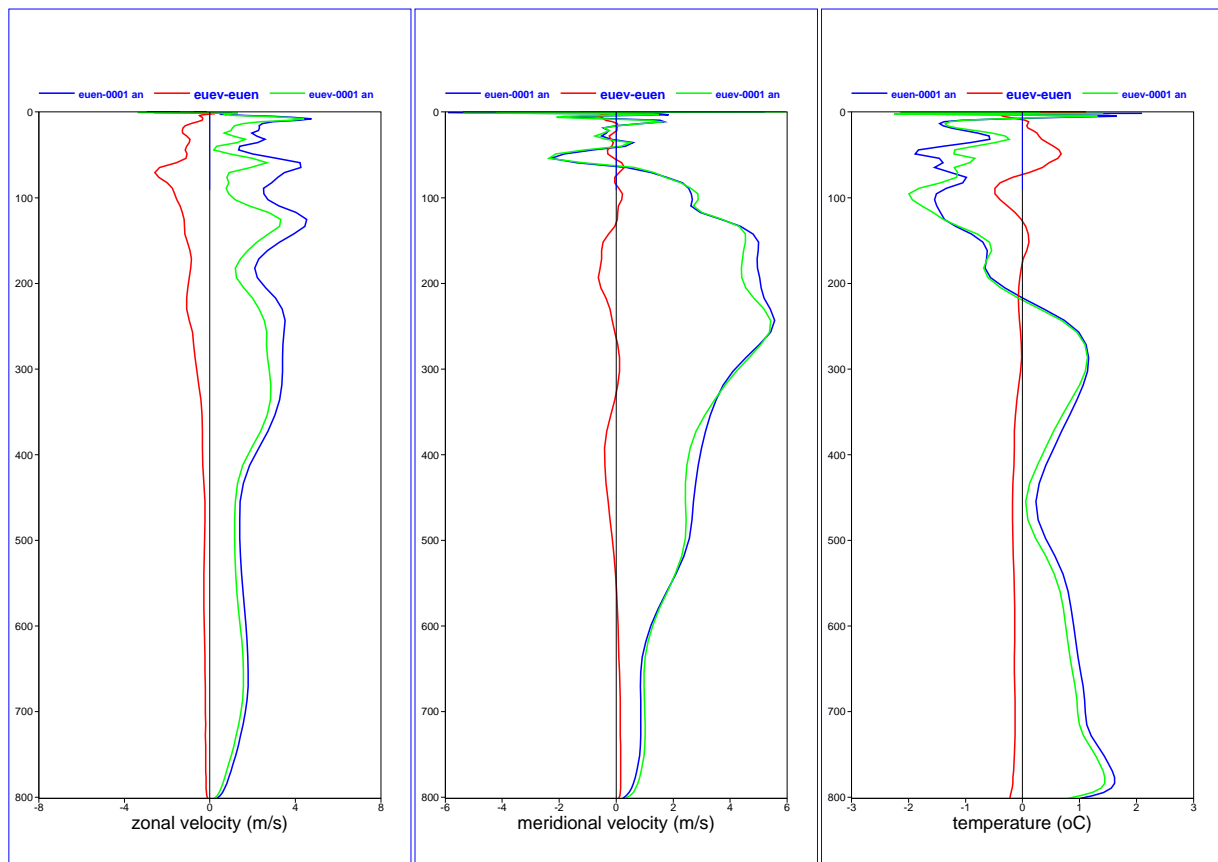
Figure 93: Experiment euev vertical profiles of difference fields averaged over the Rockies (34ºN to 45ºN and 112ºW to 104ºW) for 96 hour T511 CY31R1 forecasts from 12Z on each day of 10 to 15 November 2006 using a value $2H_{eff}$. Left panel: zonal velocity ($m\ s^{-1}$); middle panel: meridional velocity ($m\ s^{-1}$); right panel: temperature (K). Blue lines: control error; red lines: impact of experiment; green lines: experiment error.
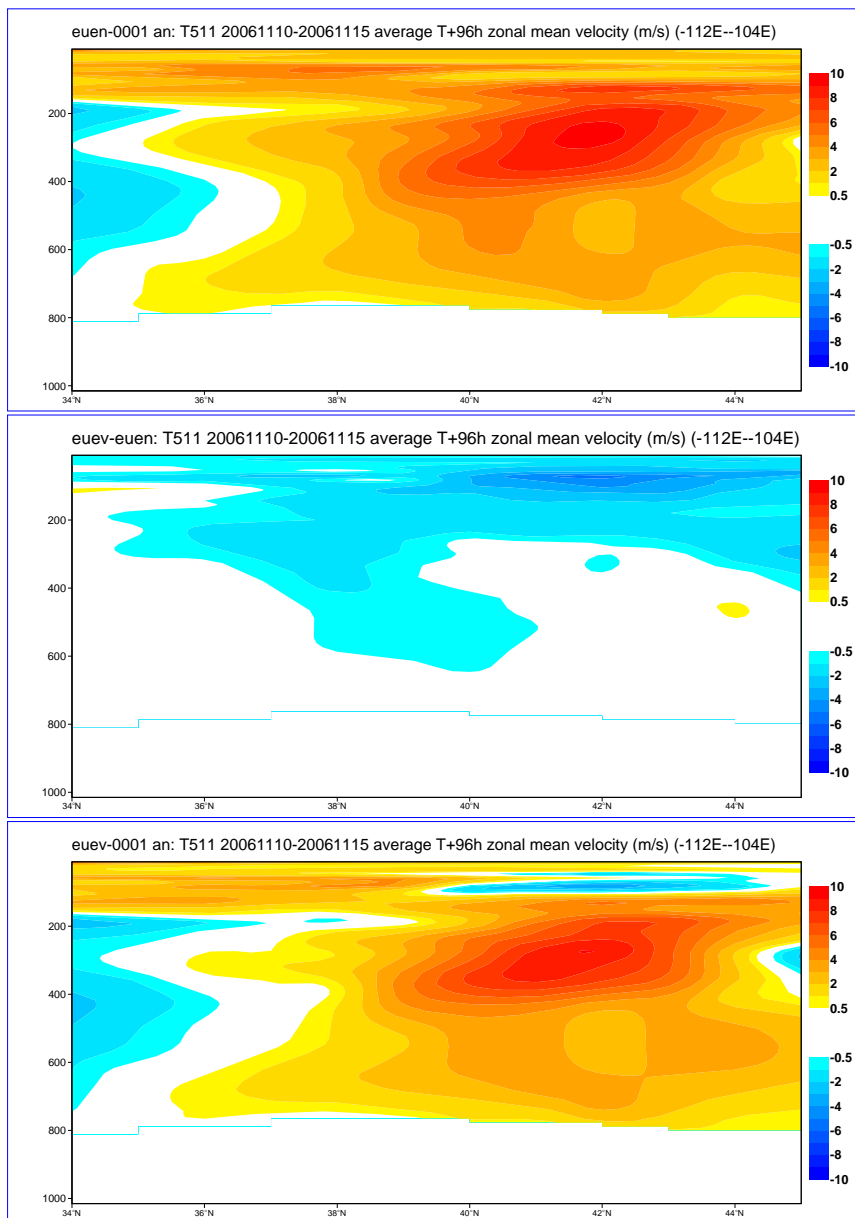
Figure 94: Experiment euev zonal wind speed difference field (m s^{-1}) zonally averaged over the Rockies between 112^oW and 104^oW for 96 hour T511 CY31R1 forecasts from 12Z on each day of 10 to 15 November 2006 using a value $2H_{eff}$. Top panel: control error; middle panel: impact of experiment; bottom panel: experiment error.

7   Summary

Comparing control CY29R1 forecasts with analyses showed that over wintertime the zonal velocity was too slow over orography at levels where parameterised wave breaking from the SSO scheme is important. This was especially apparent at coarse resolution and during winter, and pointed to the gravity wave scheme being too active and excessively decelerating the flow through wave-breaking. This was remedied by adopting a more physically realistic cutoff mountain height in the calculation of gravity wave drag, and was shown to consequently result in a reduction in the velocity deficit over the Himalayas and Rockies, and in general over areas of significant orography.

The cutoff mountain technique in combination with the TOFD scheme was implemented operationally in CY31R1 on 12 September 2006. The TOFD scheme (by vertically distributing the drag) was shown to alter the near-surface wind. Typically, this resulted in an increase in this wind, and as a consequence an increase in gravity wave drag. This results in a reduction of the predominately negative 10 m wind bias over orography (see Table 3). However, over the Himalayas the response was for the surface stress to increase and the near-surface wind to decrease, resulting in a decrease in gravity wave drag. Note that Kiel and Beljaars (2004) found only a slight increase in 10 m wind when coupling the TOFD scheme with the SSO scheme using the full mountain height ($H = 2\mu$).

	Rockies		Andes		Iceland		Himalayas	
	T+24h	T+36h	T+24h	T+36h	T+24h	T+36h	T+24h	T+36h
CY30R1	-1.9	-0.7	-1.7	-0.2	-1.4	-1.3	0.9	-1.4
CY31R1	-1.1	-0.1	-0.8	0.3	-1.4	-1.0	0.9	-1.2

Table 3: Mean 10 m wind bias (m s^{-1}) relative to synop observations averaged over significant orography for CY30R1 (control; operational) and CY31R1 (experiment es2s (see Table 3); cutoff mountain in combination with the TOFD scheme, and using the joint implicit calculation of momentum coefficients) T799 forecasts from 12Z on each day of the period 14 January to 13 February 2006.

It was further shown that by solving the momentum tendency coefficients from the TOFD and SSO scheme in a joint implicit calculation introduced some degree of dependency into these coupled processes, and so reduced the time step sensitivity that existed when each scheme evaluated its tendencies separately. This modification was also implemented operationally in CY31R1.

However, compared to the previous cycle, CY31R1 climate runs showed a large increase in winter positive zonal wind bias at upper levels between 40°N and 80°N, and a corresponding large cold bias developing over the winter pole. This suggested that the reduction in gravity wave drag due to the implementation of the cutoff mountain was excessive at low resolution, which is consistent with the increase in winter positive zonal wind bias developing predominately in climate runs, as opposed to the operational forecasts. In fact, this feature was already apparent in some of the T95 CY29R1 experiment results detailed here, which showed the modifications increasing an already positive wintertime zonal wind bias over the Rockies. While over the Himalayas at upper levels the modification could reverse the negative bias in zonal velocity, to a small positive bias. It was apparent that despite a finer horizontal resolution and thus typically less reliance on parameterised SSO (Smith et al., 2006), the zonal velocity bias in T159 CY31R1 experiments was larger than that of the T95 CY29R1 equivalent. This was particularly evident over the Rockies. However, here the T159 CY31R1 850 hPa zonal wind speed was around double that of the equivalent T95 CY29R1 experiments, meaning a higher effective mountain height (i.e. $H_{eff} \approx UN$ (Lott and Miller, 1997)) and corresponding stronger gravity wave drag and larger possible error.

To remedy this the effective mountain height H_{eff} was doubled, resulting in a increase in gravity wave drag and

reduction of the positive zonal wind bias over the Rockies. This modification was implemented operationally in CY32R2 on 5 June 2007. It was apparent that at T159 the impact of this modification decelerated the flow over the Rockies much more appreciably than over the Himalayas (allowing the strong reduction in zonal wind error achieved over the Himalayas to be maintained). This was evident in the SSO stress, which increased only slightly over the Himalayas as a result of the modification, but by around a third over the Rockies, implying that the Rockies during wintertime have a more sensitive response to gravity wave drag. Indeed, for the period examined (10 to 15 November 2006) the zonal velocity and SSO stress was much stronger over the Rockies than the Himalayas, consistent with the typical winter situation of strong westerlies (through increased storm tracks) incident to the Rockies resulting in a high effective mountain height and corresponding strong gravity wave drag. By contrast, the Himalayas are more sheltered, and here low-level blocking is more important. Surprisingly, the resulting deceleration at T511 as a result of the modification was broadly similar to that at T159. This is despite the increase in SSO stress over the Rockies being more at T159 than at T511. However, there was compensation from the surface stress, which in response decreased more at T159 compared to T511.

Acknowledgments

References

Beljaars, A. C. M., Brown, A. R., and Wood, N., 'A new parameterization of turbulent orographic form drag', *Q. J. R. Meteorol. Soc.*, **130**, pp. 1327-1347, 2004a.

Beljaars, A. C. M., Bechtold, P., Kohler, M., Morcrette, J.-J., Tompkins, A., Viterbo, P. and Wedi, N., 'The numerics of physical parameterization', In *Proc. of ECMWF Seminar on Recent Developments in Numerical Methods for Atmospheric and Ocean Modelling*, ECMWF, Reading, UK, 2004b.

Brown, A. R., 'Test of modifications to the Lott and Miller orographic parameterization', research note, 2004a.

Brown, A. R., 'Resolution dependence of orographic torques', *Q. J. R. Meteorol. Soc.*, **130**, pp. 3029-3046, 2004b.

Holton, J.R., *An Introduction to Dynamic Meteorology*, 3rd Edition. Academic Press, 1992.

IFS CY31R1, 'IFS Documentation - Cy31r1,', Part IV: Physical Processes, ECMWF, 2007.

Keil, C., and Beljaars, A., 'The impact of a new parameterization of turbulent orographic form drag', ECMWF Technical Memorandum 419, 2003.

Lott, F., and Miller, M. J., 'A new subgrid-scale orographic drag parameterization: Its formulation and testing', *Q. J. R. Meteorol. Soc.*, **123**, pp. 101-127, 1997.

Palmer, T. N., Shutts, G. J., and Swinbank, R., 'Alleviation of a systematic westerly bias in general circulation

and numerical weather prediction models through an orographic gravity wave drag parameterization', *Q. J. R. Meteorol. Soc.*, **112**, pp. 1001-1039, 1986.

Rontu, L., 'A study on parameterization of orography-related momentum fluxes in a synoptic-scale NWP model', *Tellus*, **58A**, pp. 69-81, 2006.

Smith, S. A., Doyle, J. D., Brown, A. R., and Webster, S., 'Sensitivity of resolved mountain drag to model resolution for MAP', *Q. J. R. Meteorol. Soc.*, **132**, pp. 1467-1487, 2006.

Wood, N., Brown, A. R., and Hewer, F. E., 'Parameterizing the effects of orography on the boundary layer, an alternative to effective roughness lengths', *Q. J. R. Meteorol. Soc.*, **127**, pp. 759-778, 2001.